FAULT RIDE THROUGH CAPABILITY ANALYSIS OF WIND TURBINE WITH DOUBLY FED INDUCTION GENERATOR

Salem Molla

PGR/19355/12

A Thesis Submitted to
The Department of Electrical Power and Control Engineering
School of Electrical Engineering and Computing

Presented in Partial Fulfilment of the Requirement for the Degree of Master of science in Electrical Power Engineering

Office of Graduate Studies
Adama Science and Technology University

July, 2021

Adama, Ethiopia

FAULT RIDE THROUGH CAPABILITY ANALYSIS OF WIND TURBINE WITH DOUBLY FED INDUCTION GENERATOR

Salem Molla

PGR/19355/12

Advisor: Dr. Milkias Berhanu (PhD)

A Thesis Submitted to
The Department of Electrical Power and Control Engineering
School of Electrical Engineering and Computing

Presented in Partial Fulfilment of the Requirement for the Degree of Master of science in Electrical Power Engineering

Office of Graduate Studies
Adama Science and Technology University

July, 2021

Adama, Ethiopia

APPROVAL PAGE

I, the advisor of the thesis entitled "Fault Ride Through Capability Analysis of Wind Turbine with Doubly Fed Induction Generator" and developed by Salem Molla, hereby certify that the recommendation and suggestions made by the board of examiners are appropriately incorporated into the final version of the thesis.

Advisor	Signature	Date

We, the undersigned, members of the Board of Examiners of the thesis by Salem Molla have read and evaluated the thesis entitled "Fault Ride Through Capability Analysis of Wind Turbine with Doubly Fed Induction Generator" and examined the candidate during the open defense. This is, therefore, to certify that the thesis is accepted for partial fulfillment of the requirement of the degree of Master of Science in Electrical Power Engineering.

Chairperson	Signature	Date
Internal Examiner	Signature	Date
External Examiner	Signature	Date
Department Head	Signature	Date
School Dean	Signature	Date
Office of Postgraduate Studies, Dean	Signature	Date

DECLARATION

I hereby declare that this Master Thesis entitled "Fault Ride Through Capability Analysis of Wind Turbine with Doubly Fed Induction Generator" is my original work and it has not been submitted for the award of any academic degree, diploma, or certificate in any other university. All sources of materials that are used for this thesis have been duly acknowledged through citation.

____________________________	__________________________	__________________
Name of the student	Signature	Date

RECOMMENDATION

I, the advisor of this thesis, hereby certify that I have read the revised version of the thesis entitled “Fault Ride Through Capability Analysis of Wind Turbine with Doubly Fed Induction Generator” prepared under my guidance by Salem Molla, submitted in partial fulfillment of the requirements for the degree of Masters of Science in Electrical Power Engineering. Therefore, I recommend the submission of the revised version of the thesis to the department following the applicable procedures.

__________________________ _______________________ ________________

Advisor Signature Date

ACKNOWLEDGEMENTS

First and foremost, I would like to give all glory and honor to my Almighty God and Savior, Jesus Christ, who has given me the courage, patience, potential, and wisdom to complete my master's thesis. My profound gratitude goes to my advisor, Dr. Milkias, who supported me with all of the necessary professional advice, feedback, and inspiration to ensure that this study is completed successfully. I also like to acknowledge Mr. Mohammod Awol from the Adama-II wind project office, for providing me the necessary data for this study. I would also like to express my heartfelt gratitude to my parents and my sister who have never left my side and have provided me a lot of inspiration and emotional support during this thesis. Last but not least, I would like to appreciate the Electrical Power and Control Engineering Department for allowing me to work on this project.

Thank you all so much.

TABLE OF CONTENTS

LIST OF TABLES

LIST OF FIGURES

ACRONYMS

Abbreviations	Description
AC	Alternating Current
BTB	Back-to-Back
BESS	Battery Energy Storage System
DC	Direct Current
DFIG	Doubly Fed Induction Generator
DPC	Direct Power Control
DTC	Direct Torque Control
DVR	Dynamic Voltage Restorer
ESS	Energy Storage System
FACTs	Flexible AC Transmission
FLC	Fuzzy Logic Control
FOC	Field Oriented Control
FRT	Fault Ride Through
GSC	Grid Side Converter
HCS	Hill-Climb Search
HAWT	Horizontal Axis Wind Turbine
IGBT	Integrated Gate Bipolar Transistor
LVRT	Low Voltage Ride Through
MPPT	Maximum Power Point Tracking
OTC	Optimal Torque Control
PAC	Pitch Angle Control
PCC	Point of Common Coupling
PI	Proportional Integration

PSF	Power Signal Feedback
PU	Per Unit
PWM	Pulse Width Modulation
RSC	Rotor Side Converter
SC	Super Capacitor
SDR	Series Dynamic Resistor
STATCOM	Static Synchronous Compensator
SVC	Static Var Compensator
THD	Total Harmonic Disorder
TSR	Tip Speed Ratio
VAWT	Vertical Axis Wind Turbine
VSC	Voltage Source Converter
WECS	Wind Energy Conversion System
WRIG	Wound Rotor Induction Generator
WT	Wind Turbine

ABSTRACT

The Doubly-fed induction generator (DFIG) based wind turbine is one of the most effective and frequently used wind power generation systems in the wind power industry. It offers several enticing benefits, including consistent output voltage, low cost, high performance, independent control of active and reactive power, and improved power quality. Despite any of the aforementioned advantages of DFIGs, it is precisely impacted by grid interruption because the stator winding of DFIG is directly connected to the grid and the rotor is connected to the grid via a fault-prone power converter. In early times, when a fault occurred, these generators were required to disconnect from the grid to secure the generator and power converters. However, due to the increased penetration of wind turbines into the power system, grid operators demanded that the wind turbines remain connected to the grid, as disconnecting them would further disrupt the grid and have a significant effect on the stability of the grid operation. The ability of a generator to remain connected to the grid under grid fault is known as fault ride-through (FRT) capability. Any sudden appearance of a fault, such as symmetrical or asymmetrical faults, can cause a reduction in stator voltage, oscillations in stator and rotor currents, DC-link overvoltage, and electromagnetic torque pulsations. Such a phenomenon can considerably affect the performance of the DFIG under a transient state if an appropriate protection system is not considered. Thus, in this thesis work, the crowbar protection system is employed for the improvement of the FRT capability of the wind turbine. The performance of the DFIG both under steady-state and transient state conditions is examined with and without this protection scheme. Furthermore, the analysis of the machine is rendered by integrating the crowbar protection system with the Battery Energy Storage System (BESS) for a much effective outcome in enhancing the ability of the machine to drive the fault. Moreover, the MATLAB/Simulink 2015a software is used for modeling and simulation and all system parameters are obtained from ADAMA-II Wind Farm.

Keywords *Battery Energy Storage System, Crowbar, Doubly-Fed Induction Generator, Fault Ride Through Capability, MATLAB-Simulink*

CHAPTER ONE:

INTRODUCTION

1.1. Background

Conventional energy sources such as petroleum, coal, gas, and oil are environmentally hazardous. Excessive use of these energy sources tends to increase emissions of carbon dioxide and other harmful gases to the atmosphere. Because of the spike in toxic emissions, the overall global temperature is rising at an unprecedented rate, resulting in the greenhouse effect. Several countries have undertaken research for scientific advances to use renewable and clean energy sources such as wind, solar, geothermal, hydro, and tidal energy to address this serious environmental disaster. In this regard, among the various renewable energy resources, wind energy is one of the most efficient, clean, and promising ones with the potential to fulfill the world energy demand [1].

Wind turbines (WT) can be categorized as fixed-speed and variable-speed turbines, which can be further defined by four main types [2].

(1) Fixed Speed Wind Turbine- squirrel cage induction generator that is directly connected to the grid is used exclusively. In the Squirrel Cage Induction Generator, the generator had to operate at a fixed wind speed, which is impractical and perceived to be a drawback. In this concept, a capacitor bank or a reactive power compensator is needed to eliminate the demand for reactive power from the turbine generator to the grid.

(2) Partial Speed Wind Turbine with Variable Rotor Resistance- uses wound rotor induction generator (WRIG) connected to the grid through a transformer. The rotor winding of a generator is connected in series with variable resistance, which is used to adjust the torque characteristics and operating speed within a narrow range (0-10% above synchronous speed).

(3) Variable Speed Wind Turbine with Partial Scale Power Converter- The machine is controlled and connected to the power grid through an electronic power converter. Maximum energy conversion efficiency can be achieved over a large range of wind speeds. The turbine will continuously adapt its rotational speed to the wind speed.

(4) Variable Speed Wind Turbine with Full-Scale Power Converter- uses permanent magnet synchronous generator with full-scale converter. Stator phase windings are connected to the grid by a full-scale power converter.

Variable speed wind turbine with partial scale power converter also known as double fed induction generator (DFIG) is essentially a wound rotor induction generator in which the rotor circuit can be controlled by external devices for variable speed operation. The generator stator is connected to the grid via the transformer, while the rotor connected to the grid is connected using the power converters, the harmonic filters, and the transformer. DFIG has two back-to-back connected pulse width modulation (PWM) converters with a DC-link capacitor mounted between them. Owing to these power converters, power can be supplied or absorbed to/from the grid. The DC-link capacitor is located between the two converters, as energy storage, to keep the voltage fluctuation (or ripple) in the DC-link voltage small [3].

The power converter is comprised of rotor side converters (RSC) and grid side converters (GSC). The primary function of a rotor side converter is to adjust the speed and torque of the machine and regulate active and reactive power independently. The grid-side converter, on the other hand, retains the DC-link voltage constant regardless of the size or direction of the rotor [3]. Since these back-to-back power converters could operate in bi-directional mode, depending on the speed of the rotor the DFIG could thus function either in sub-synchronous speed mode (the generator operates below synchronous speed) or super-synchronous speed mode (the generator operates above synchronous speed) [4]. Figure 1.1 depicts the DFIG block diagram.

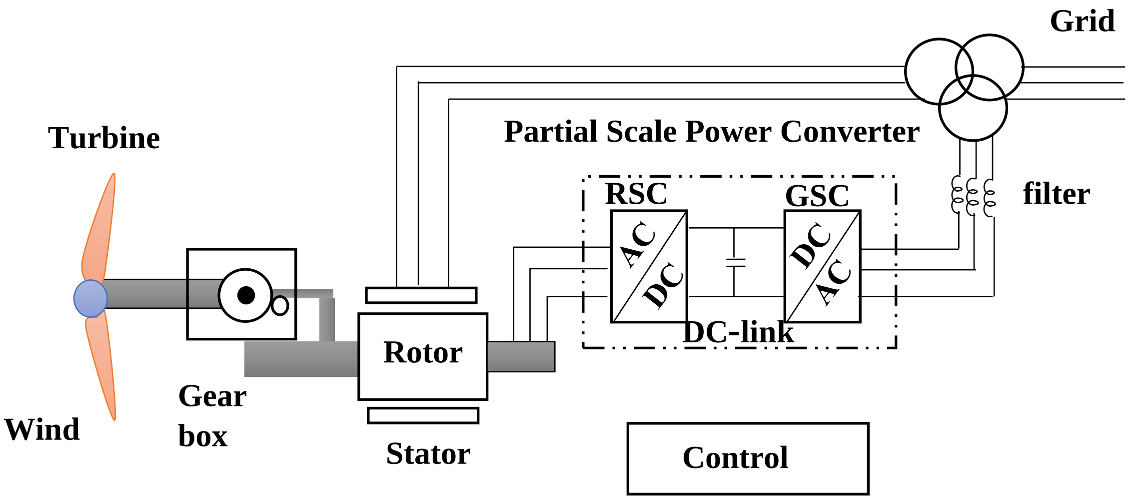

Figure 1.1 General supply configuration of DFIG [4]

The primary benefits of employing DFIGs in association with wind turbines are [4]:

- ➢ The power losses in the converters are lower, leading to the improved overall efficiency

- The mechanical load stresses on wind turbines, which are produced during wind gusts, are reduced.
- Independent control of active and reactive power
- The cost of a DFIG power converter is low, as the power rating of the power converter is typically rated 25% to 30% around the rated power
- Improves power quality, reduces torque pulsations, and eliminates electrical power variations, i.e., fewer flickers.

Although DFIG has the aforementioned advantages, it is vulnerable to grid deterioration. Such that, since the stator winding of the machine is directly attached to the grid, when a failure occurs, the generator and converters are subjected to a high overcurrent caused by high transient stator current. In the occurrence of such a fault, the wind turbine must be isolated from the network to secure the converter. However, in most countries, power grid connection codes mandate wind turbines to remain connected to the grid to ensure reliability throughout and after a short-term outage [5]. Grid transmission and distribution operators have developed rules (grid code) for the generators to stay connected to the grid during instability. The ability of wind turbines to remain connected to the grid during voltage dips is referred to as Fault Ride-Through (FRT) or Low Voltage Ride Through (LVRT) capability. The wind turbine must be fitted with LVRT capabilities, as required by grid operators, to deter the turbine generator from accelerating and compromising mechanical parts due to turbulence, which raises friction and stress on mechanical parts. Thus, these grid code requirements are critical to ensuring that wind turbines do not jeopardize the operation of the power system in terms of supply reliability, performance, and power quality [5].

Two significant issues must be accurately addressed in an attempt to fulfil the LVRT capability of a wind turbine in a fault state. The first is overcurrent, which can occur in rotor and stator circuits, and the second is overvoltage in a DC-link. Both can be attributed to surplus energy causing harm to the power converters [6]. Thus, the main objective of this thesis work is to improve FRT capability under normal and fault conditions by employing a protection system.

1.2. Statement of the Problem

DFIG is extremely susceptible to grid faults. When a short circuit occurs at a grid terminal, the voltage at the Point of Common Coupling (PCC) drops, inducing a stator current oscillation and electromagnetic torque pulsation. Since the stator and rotor are magnetically coupled, the oscillation of the stator current will lead to a high rotor current which may harm the converters. Besides, the variation in electromagnetic torque creates mechanical stress on the wind turbine drive mechanism. Moreover, the voltage drop renders the GSC incapable of transferring power from the rotor to the grid. As a result, the excess energy charges the DC-link capacitor rapidly, resulting in a high DC link voltage. This inrush rotor current and DC-link overvoltage damages both the generator and the converter unless effective protection and control mechanisms are employed. As a consequence, this thesis works highly emphasize protection and control methods to alleviate the aforementioned problems and enhance the generator performance. This brings several benefits in terms of preserving the stability of the power supply and the whole network, as well as ensuring power quality. Furthermore, this research is being conducted on the ADAMA-II wind farm to improve fault ride-through capability by using grid code requirements. However, ADAMA-II Wind Farm is still on the process of establishing grid codes, once the establishment is completed, this analysis would be rather advantageous since the emphasis is on making the wind turbine withstand the fault for some duration of time by applying a protection system and control system.

1.3. Objectives of Thesis

1.3.1. General Objective

The main objective of this study is to improve the FRT associated with DFIGs during both steady-state and transient operations.

1.3.2. Specific Objectives

The specific objectives of this thesis are to:

- Investigate the operation and performance of DFIG under steady-state and transient conditions.
- Model the wind energy conversion system which comprises the electrical generator, the wind turbine and the converter using MATLAB-SIMULINK software.
- Model the crowbar protection scheme and crowbar integrated with Battery Energy Storage System (BESS) and examine how the machine operates under transient conditions.

- Implement the requisite control schemes particularly field-oriented control with the PI regulator to enhance the performance of the machine and improve the fault-ride through capability.
- Analyse the responses and write a conclusion on which one performs better for the enhancement of FRT capability.

1.4. Significant of the Thesis

During a fault, the voltage will drop substantially. Since the stator winding of the machine is directly connected to the grid, it will experience a broad current and the disturbance is further transferred to the rotor side due to magnetic coupling between the stator and rotor windings. Thus, the rotor current is expected to be very strong, which may result in an overcurrent of the rotor side converter. Furthermore, the grid side converter loses the ability to transmit power from the rotor side converter to the grid, however, the WT is still powered by wind energy, so surplus energy is collected in the DC link of the back-to-back electronic converter. This would overcharge the DC capacitor and as a result, the DC bus voltage will be very high. These two problems need to be solved to satisfy the LVRT specifications during voltage sag. Therefore, the relevance of this project is to enhance fault handling by implementing a protection scheme and a control technique to mitigate high rotor current and DC-link overvoltage, which threaten DFIG and power converters.

1.5. Scope and Limitation of the Study

This thesis work aims to examine how the DFIG operates when there is a voltage drop at the grid terminal. MATLAB/Simulink software is utilized for detailed modeling and control of a DFIG-based wind energy conversion system, and all parameters used to simulate the system were obtained from the ADAMA-II wind farm. The emphasis in this study is on improving FRT capabilities through control techniques and protection schemes. Other methods for boosting FRT capabilities, such as the reactive current injection procedure, are beyond the scope of this document. Moreover, the control technique employed is a vector-control technique with a reference frame aligned along the stator flux space vector for RSC and a reference frame aligned along with the grid voltage vector position for GSC.

1.6. Thesis Outline

This thesis is organized into six sections. The current chapter provides an introduction to the DFIG-based WECS, a statement of the problem, the thesis objectives, the significance of the thesis, and the scope of the thesis.

The second chapter includes a literature review for modeling and regulation of DFIG-based WECS linked to the grid, background information on wind turbines, a review of grid code requirements, and various approaches to improving FRT capability. In addition, this chapter demonstrates the aerodynamic conversion scheme with the power curve and power coefficient curve obtained from the simulation analysis.

In the third chapter, a comprehensive overview of the mathematical model of the DFIG-based WT, the mode of operation of the DFIG, and the power converter with the DC-link capacitor are presented. Furthermore, this chapter discusses how the machine performs in steady-state and under grid fault conditions, as well as various approaches used to enhance the performance of the machine under transient conditions.

The fourth chapter discusses the WECS control scheme, which includes the wind turbine control level and the DFIG control level. This chapter gives a clear overview of the control of RSC and GSC with respective inner and outer control loops. Furthermore, the BESS model and its control system are discussed briefly.

In the fifth chapter, the simulation results of DFIG performance under standard operating conditions and grid fault conditions are discussed. Under grid fault conditions, various results have been observed by using the current capacitor bank, crowbar protection system, and crowbar integrated with BESS.

Finally, the sixth chapter presents all about conclusion and recommendation.

CHAPTER TWO:

LITERATURE REVIEW

This section presents a literature review on the FRT capabilities of DFIG and the different approaches employed to improve FRT capabilities. It outlines the previous researches and analysis on a doubly-fed induction generator, as well as the control and protection mechanism and other strategies used to improve FRT capability.

2.1. Literature Survey

According to recent studies, DFIG is gaining a lot of attention as one of the leading technologies for wind power generation. One of its attractive characteristics is that it can provide decoupled active and reactive control of the generator through a variety of control techniques [7]. In DFIG, the winding of the stator is attached directly to the grid while the rotor is connected to the grid by the back-to-back converter. The RSC is used to control both the active and the reactive power as well as the torque and speed of the generator. While the GSC is used to preserve DC-link voltage and deliver reactive power to the grid when necessary. These bidirectional power converters allow power to flow from the grid to the machine and vice versa. Thus, the machine can operate as a generator as well as a motor in both sub-synchronous and super-synchronous modes. However, only the generator mode at both speeds is of great interest in wind power generation. Moreover, the GSC can function as an inverter (when the rotor supplies active power to the grid) or a rectifier, (when the rotor absorbs active power from the grid), depending on the mode of operation [5-7].

The power converter of DFIG can tolerate just 25-30% of the generator capacity, rendering the DFIG WT highly susceptible and vulnerable to grid disturbance. When a grid fault causes a voltage drop, an increase in rotor voltage is expected to compensate for the stator voltage and stabilize the rotor currents. Nevertheless, due to the limited voltage of the converter, when the required rotor voltage exceeds this limit, it is no longer possible to regulate the current. This indicates that a voltage drop will result in a high induced voltage and current in the rotor circuit. Furthermore, the strong current triggers the DC-link voltage to increase [8]. For decades, if such faults existed, generators had to be removed immediately from the grid to protect the generator, power converters, and the dc-link capacitor. However, as wind turbines are gradually being integrated into transmission systems, grid transmission and distribution operators and wind turbine manufacturers have introduced regulations for connecting generators to the grid even during faults [8]. These current grid codes enable the generator to remain connected to the grid even though faults occur. The capability of WT to remain attached to the grid during voltage dips is referred to as low voltage ride through (LVRT) and the key purpose of these standards or requirements is to ensure that the operation of the power grid is not affected by wind farms in terms of protection of supply, reliability, and quality of power. A variety of experiments have been carried out over the past years to enhance the FRT capability of the DFIG wind turbine using different techniques [9].

FRT capability can be improved using three different methods, such as the installation of reactive power injection systems under transient conditions, protection circuits, and the deployment of controllers both under steady-state and transient conditions. Using the protection circuits and various controllers, it is possible to restrict over-current and surplus DC-link voltage produced by the rotor during grid disturbance [8-9]. Besides, the reactive power-injection system exceeds any reactive power deficit to improve the transient output of the DFIG based WT and to automatically align the rotor current and the DC-link voltage [9].

2.1.1. The Reactive Power Injection Method

Reactive power injection using Flexible AC Transmission (FACTs) devices is one of the most important external solutions of FRT capability. During grid fault, the GSC cannot provide adequate reactive power and voltage support to the grid. This is due to the limited rating of its converter, which presents a risk of voltage instability. To solve this issue FACTS devices based on reactive power injection are used to increase FRT capability and the reactive power support offered by the FACTS devices helps to sustain the transitory equilibrium [9-10]. Although several FACT devices are available, Static Var Compensator (SVC), Static Synchronous Compensator (STATCOM), and Dynamic Voltage Restorer (DVR) are widely used for voltage control performance during steady-state and transient conditions at the point of common coupling (PCC) [11]. The SVC enhances voltage stability by providing fast dynamic reactive power compensation that preserves the control of the terminal voltage and the desired transient response. They are linked at the point of common coupling to boost transient and steady-state efficiency. SVC can be a shunt static var compensator and series dynamic voltage restorer. STATCOM will insert maximum reactive current to stabilize the electrical grid in the case of a fault to accelerate the voltage recovery and preserve the voltage stability. Furthermore, it also can generate both lagging and leading reactive power [9]. The DVR consists of a voltage source converter that is positioned between the wind turbine and the grid. DVR can be applied to mitigate sags, swells, and other power quality issues there by improving the FRT mechanism. This approach has the downside of being costly, increasing the device complexity and expense while jeopardizing the reliability of the DFIG system [11].

2.1.2. Protection Circuit Approach

Another strategy for improving fault ride-through capability is to employ a protection system that safeguards the generator and converters. Crowbars, DC-Choppers, Series Dynamic Resistors (SDRs), Super Capacitors (SC), and Energy Storage Systems (ESSs) can be mounted on the rotor side to reduce inrush current and DC-link over voltage [12-14]. According to the authors in [13], the crowbar protection system is one of the most well-known LVRT protection circuits. When a fault occurs and results in a higher rotor current and DC-link over-voltage, the crowbar is activated and a low-resistance path is generated to allow high currents to pass through it. In contrast, the authors in [14] recommend using a crowbar in conjunction with other protection devices like SDR and SC for better enhancement of LVRT capability. The authors stated that when the crowbar is activated inhibiting the RSC for safety purposes, the speed and torque control of the machine is lost. Thus, by utilizing the crowbar with SDR it is possible to maximize the operation time of the RSC, thereby reducing torque fluctuation. SDR can also retain the current during disturbance and reduce the frequent use of crowbar.

The DC link-chopper is another LVRT safety circuit that is discussed in depth in [12]. DC-chopper is a resistance circuit linked in parallel to the DC-link capacitor. This braking resistor, connected in series with the converter is used to maintain the DC-link voltage within acceptable operating voltage. When grid faults occur, the DC-link voltage crosses the acceptable value. In that same situation, the converter should be closed to shorten the connection to the braking resistors which will result in the DC-link voltage being adjusted to an appropriate level. However, after a fault, this method takes a longer time than the crowbar protection system to disengage the converter and return to normal operation.

According to recent research in the renewable energy field, incorporating wind power plants with energy storage systems is another approach to improve fault ride-through capability and quality of power. The authors in [15] claim that the battery energy storage system is critical for sustaining a steady DC-link voltage irrespective of the magnitude and direction of the rotor and stator forces. It is often used to store energy at higher wind speeds when the generated power extracted from the wind system is greater than the average power. Furthermore, when the wind speed is lower and power from the grid is demanded, the battery discharges and provides the required power to the system, thus providing a steady DC-link voltage and resulting in an efficient and stable supply of electrical power to the grid. In this thesis work the crowbar protection system is first employed to observe how the machine performs during a grid fault condition and later on for better enhancement of fault ride-through capability crowbar integrated with the BESS is analyzed.

2.1.3. Control Approach

An alternative approach for enhancement fault ride-through capability both in steady-state and transient state conditions is to implement various control systems. A significant number of researchers have studied different kinds of controllers and categorized control systems of variable speed wind turbines mainly into two control levels, namely the wind turbine control level and the DFIG control level [16].

2.1.3.1. Wind Turbine Control Level

The major aim of the control level of the wind turbine is to achieve full power extraction including active power control and reactive power control at the PCC. Besides, power optimization and power limitation are essential. When the wind speed is above the cut-in speed and below the rated speed, the speed control is essential as it continuously adjusts the speed of the rotor or turbine to maintain the tip speed ratio constant at the level that provides optimum power coefficient and high efficiency. To achieve effective, powerful, and attractive wind energy sources, it is important to obtain maximum energy from wind energy using different Maximum Power Point Tracking (MPPT) control techniques. MPPT controls are used to draw the maximum power from the wind energy conversion system [16]. According to [17] the MPPT control methods are divided into two, the Direct and the Indirect methods. The direct approach does not postulate knowledge of the characteristics of the wind turbine (tip speed ratio and power coefficient). It includes the control of Fuzzy Logic Control (FLC) and Hill-Climb Search (HCS), while the indirect one demands knowledge of the characteristics of wind turbine and entails the control of Optimal Torque Control (OTC) and Power Signal Feedback (PSF). Each controller was described in depth in [17].

Several researchers in [18,19] often use TSR control to gain optimum power by regulating the rotational speed of the turbine to achieve optimum TSR. According to [18], this approach has a fast and robust tracking capability. However, it was in [19], a comparison between two MPPT processes, such as TSR and OTC, has been analyzed, and as a result, the authors concluded that while TSR had the quickest solution to variance in wind speed, it could not provide smooth output power. OTC techniques, on the other hand, have robustness, reliability, and power management capacities and can draw optimum power from the wind independent of the fluctuating wind.

In [17], hill climb search control is another MPPT control system that continuously searches the peak capacity of a wind turbine. Based on the direction of the operating point and the relationship between variations in power and speed, the monitoring algorithm determines the desired optimum signal for the device to achieve the highest power point.

Other researchers in [20] suggested intelligent self-adaptive control and fast hybrid perturb and observe control techniques to overcome the shortcomings of the current perturb and observe MPPT. To effectively adjust the perturbation step-sizes under various environmental conditions, these control strategies depend on estimating the optimal power and rotor speed relationship. Both suggested strategies limit the Maximum Power Point (MPP) search area without splitting the curve into modular operating sectors. However, the authors discovered that the self-adaptive control algorithm performs better in terms of preventing the wrong directionality query, as well as improving the complex efficiency of the WECS by precisely monitoring the MPP with high precision.

When the wind speed is above the nominal value, it will be impossible to regulate the speed of the rotor under the limits due to a lack of electromagnetic torque. This allows the generator and/or converter to overload, in which case the pitch angle control is activated to reduce the mechanical strength extracted from the wind. Various scholars have proposed different methods of pitch angle management, such as PI pitch angle control [21], sensor-less pitch angle control [22], Robust pitch control [23], and Fuzzy Logic control [24]. Proportional-Integral (PI) controllers have been used for industrial process control applications for the past decades, and several researchers have claimed the benefits of PI controllers. In [24], the authors overestimated the benefit of using the PI controller to obtain sufficient and acceptable performance. A contrast of the PI pitch angle controllers with the different control variables was also rendered in [25].

2.1.3.2. Doubly Fed Induction Generator Control Level

Over the years, numerous researchers have suggested various modes of DFIG control methods, such as direct torque control and direct power control [26, 27], field-oriented control [28,29,30], and others [30,31].

For the control of active and reactive power separately, the authors in [26] proposed direct power control on the rotor side converter. The authors have introduced a direct power control system for the control of active and reactive power without the use of a rotor position sensor. The active and reactive power measured in the circuit of the stator will determine the instantaneous switching rate of the RSC. Thus, the evidence illustrates that the DPC eliminates the need for a rotor position sensor. However, measurements carried out at only one terminal of the system will not be reliable because, for certain, when the fault occurs at the terminal, the voltage varies greatly. Besides, the authors did not consider the complexities of regulating the torque and flux at a very low speed with this controller.

The authors in [27] formulated a DTC technique with a new strategy for producing the reference rotor flux as a function of the reference reactive power for regulating the electromagnetic torque and rotor flux generator when controlling the power factor at the stator terminals. The suggested control strategy is based on the selection of an effective rotor voltage vector to be applied to the rotor side converter. However, the authors were met with a challenge that is the phenomenon of some undulations (which are induced by the use of hysteresis controllers) that are often usual in the classic DTC technique.

For the improvement of power flow transfer and dynamic and transient stability, the authors in [28] suggested enhanced field-oriented control (EFOC) technique in rotor side converter of DFIG converter. When grid fault occurs either symmetrically or asymmetrically, STATCOM coordinates the structure to ensure much greater stability and better operation. The authors have reported that with the use of the EFOC controller, it is possible to damp the flux oscillation at the time of the fault and have shown that the current of the stator, which is influenced by the grid fault since it is directly related to it, has decreased to a lower value. In the case of a STATCOM system with additional reactive power support for a DFIG based wind turbine system, the decrease in GSC current was limited to half the value from not being zero during an asymmetrical fault. However, during faults, the high rotor current that could affect the converter did not approach zero in magnitude. Also, the researchers did not take the DC-link over voltage into account when a fault occurred and instead centered on the rotor side converter control system. The outcome would have been satisfactory if the GSC controller had been implemented to restrict the dc-link over-voltage so that the power could flow through it.

In [29], the authors proposed a hybrid field-oriented control (FOC) with a hysteresis current controller using a doubly-fed induction generator, to provide good monitoring of predefined references independent of changing wind speed, and to guarantee a converter with a unit power factor (zero reactive power), which ensures that the grid side converter (GSC) only transfers active power to the grid. However, the use of the PI controller would have shown a better outcome instead of using the hysteresis current controller. Hysteresis current controller delivers more distortion or high THD due to low-level harmonics and variable switching frequency, which makes it unacceptable and the authors had to handle that as well.

The authors in [30,31] investigated the comparison of FOC with other controllers. The authors in [31] claimed that FOC is very sensitive to machine parameter variation and that this makes it a less desirable control system; on the other hand, DPC has a robust response to parameter variation and does not use a rotor current control loop. However even though FOC relays electrical parameters of the system, it delivers excellent control efficiency in terms of robustness, transitory and steady-state response, and installation specification. In this thesis work, both the Flux-oriented FOC (for rotor side converter) and voltage-oriented FOC (for Grid side converter) is implemented.

2.2. Wind Energy Conversion System

In a wind energy conversion system (WECS), the transfer of wind energy takes place in two phases. The extracting device, named the wind turbine rotor, rotates under the motion of the wind speed, thereby extracting mechanical electricity. The rotating electrical machine, the generator, converts the mechanical power from the turbine to electricity. Wind speed plays a crucial role in many aspects of the conversion process, especially concerning the maximum power output [24, 32].

2.2.1. Types of Wind Turbine

The wind turbine is known to transform kinetic energy to mechanical energy through a blade mounted on a rotor hub. The two major types of wind turbines are the Horizontal Axis Wind Turbine (HAWT) and the Vertical Axis Wind Turbine (VAWT), all of which have their pros and cons. HAWT is the most popular choice of wind turbine and has received more funding for research and development since it offers a significant advantage over VAWT [32].

Horizontal Axis Wind Turbine (HAWT)

HAWT is the most widely used design configuration for wind turbines with rotors identical to aircraft rotors. It consists of blades that extract wind energy on a horizontal axis and are parallel to the ground. By facing the wind movement perpendicularly, the blades operate and turn due to the aerodynamic lift. HAWT has a higher efficiency than VAWT when extracting energy from the wind force due to its nature to extract energy through the maximum rotation of the blades when put under a constant wind flow [32]. While HAWT is ideally suited for the use of more wind energy, it has a significant drawback, which is that it must always be directed in the wind direction to function efficiently. With an unforeseeable wind direction, an extra mechanism is required to ensure that the blades still face the wind direction to extract the optimum power output [33].

Figure 2.1 Horizontal axis wind turbine **[**34]

Vertical Axis Wind Turbine (VAWT)

VAWT blades spin along their longitudinal poles perpendicular to the ground. This type of turbine uses either drag or lift or a combination of the two turbines to operate. One of the reasons VAWT varies from HAWT is that it can catch wind from any direction, and its heavy machinery is on the ground. Since the machine is mounted on the ground, it simplifies the construction and creation of the wind tower and therefore reduces the cost of the turbine. The downside of VAWT is that it is ineffective in the high-speed wind environment as it has very poor starting torques and dynamic stability problems. Which makes it vulnerable to backtracking since the blade travels in the same direction to the wind and so the blades need to travel back towards the wind flow before being pushed back around [33].

Figure 2.2.(a) Giromill (lift), (b) Darrieus, (c) Savonius [34]

2.2.2. Components of Wind Turbine

The main components of a wind turbine are as follow:

Blade: - A significant component of the wind turbine which is mounted on the rotor hub and used to extract energy from the wind.

Pitch Mechanism: - It allows the blade to rotate on its longitudinal axis. It can alter the angle of attack of the blade concerning the wind from which the aerodynamic circuit of the blade can be adjusted. This allows a degree of control over the capture power to increase performance. When the wind speed is at or below the rated value, the angle is held to the optimum value and the turbine captures the full power output. When the wind speed reaches the rated value, the pitch function is enabled to regulate and restrict the output power and Whenever the wind speed increases further and approaches the peak of the turbine, the blade is pitched out and no power is captured [35].

Gear Box: - It is used to adopt the low rotational speed of the turbine rotor to the high rotational speed of the generator. Through the gear box, the kinetic energy is transferred from low speed to high-speed rotating shaft

Brakes: - During high wind speed, a brake is used to assist aerodynamic power regulation to stop the turbine or to lock the turbine in the maintenance parking mode. Two separate brakes are applied to the low-speed shaft and the high-speed shaft of the rotor. The low-speed shaft is operated by hydraulic while the high-speed shaft is self-adjusted and the spring is loaded.

Nacelle: - The nacelle houses the generator, the gearbox, the hydraulic system, and yawing mechanism.

Yaw Mechanism: -Maximizes the captured wind energy by keeping the turbine facing the wind. It consists of one electric drive, yaw gear, yaw rim, and bearing.

Wind Sensor (Anemometer): –. It is a device used to measure wind speed and direction. Wind turbines need to be steered towards the wind, with blades regulated according to wind strength to ensure optimum performance. To achieve this, an anemometer is mounted at the top of each wind turbine, providing a main control feature for the wind turbine [35].

Generator: - The conversion of mechanical power of wind turbine into the electrical power can be accomplished by one of the following types of the electrical machine

1. Synchronous machine
2. Induction machine

Tower: - Towers are made from tubular steel, concrete, or steel lattice. Because wind speed is getting higher with the height, taller towers enable turbines to capture more energy and this way generates more electricity.

2.2.3. Operating Region of the Wind Turbine

The power curve in Figure 2.3 describes the power output of a wind turbine at various wind speeds by illustrating the operating region of a variable-speed variable-pitch wind turbine [34].

1. Cut-in Wind Speed

   The point at which the wind turbine began to produce power or the lowest wind speed at which the machine will deliver usable power.

2. Rated Wind Speed

   Wind speed at which the turbine achieves the maximum "rated" power output. Rated power is the maximum power output of the electrical generator.

3. Cut-out (Cut-off) Wind Speed

   It is a maximum wind speed at which the turbine is allowed to deliver power but is shut down before it reaches the danger zone by a brake or blade pitching mechanism. The main objective of the controller is to maintain the rated power of the wind turbine.

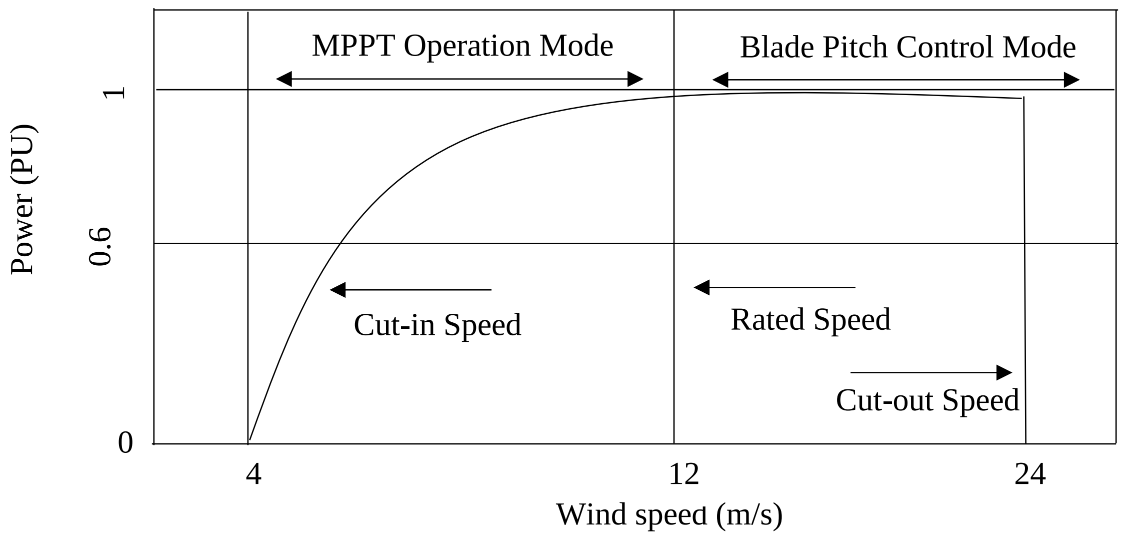

Figure 2.3 Power curve of a variable speed wind turbine [34]

2.2.4. Wind Distribution

The annual average wind speed is an incredibly critical consideration for the output power of the wind turbine. The average wind speed on a shorter time basis is also based on the distribution, aside from the annual wind speed. The most widely used probability density function to describe wind speed is the Weibull function [36]. The Weibull distribution is described by the probability density function as:

$$f[\omega] = \frac{k}{c}(\omega / c)^{(k-1)} e^{-(\omega/c)k} \tag{2.1}$$

Where, k is a shape parameter, c is a scale parameter, and ω is the wind speed. As a consequence, average wind speed (or estimated wind speed) ω_{avg} can be calculated from

$$\omega_{avg} = \int_0^\infty \omega_f(\omega) d\omega \tag{2.2}$$

$$\omega_{avg} = \frac{c}{k}\Gamma(\frac{1}{k}) \tag{2.3}$$

Where, Γ is Euler's gamma function which is expressed as

$$\Gamma(z) = \int_0^a t^{2-1} e^{-t} dt \tag{2.4}$$

If the shape parameter equals 2, the Weibull distribution is known as the Rayleigh distribution.

2.2.5. Aerodynamic Control in Wind Turbine

Wind turbines are designed to deliver maximum output at wind speeds of about 12m/s. In the event of stronger winds, much of the surplus energy of the wind must be wasted to prevent destroying the wind turbine. Therefore, all wind turbines are equipped with a power control called aerodynamic power control [36-37]. The three methods of aerodynamic power control are described in detail as follows:

Pitch Controlled Wind Turbines

The pitch controller of the turbine monitors the power output of the turbine multiple times per second on a pitch-controlled wind turbine. If the wind speed approaches the rated value and the power output is too high, it sends a signal to the blade pitch system, which automatically pushes the rotor blades out of the wind. Conversely, the blades are turned back towards the wind if the wind drops down again [36].

Passive Stall Controlled Wind Turbines

Passive stall-controlled wind turbines are bolted to the hub by rotor blades at a rated (optimal) angle of attack. When the wind speed is at or below the rated value, the turbine blade with a rated angle of attack captures the maximum possible wind power [37]. The stall controller utilizes the geometry of the rotor blade to limit the lifting force while the wind speed is above the rated value by causing vibration behind the rotor blade. In this controller, no pitch mechanism is required.

Active Stall Controlled Wind Turbines

At low wind speed, to produce comparatively high torque, the turbines would typically be designed to pitch their blades much like a pitch-controlled machine and if the generator is going to be overloaded, the machine will turn its blades in the opposite direction than what the pitch-controlled machine does. In other words, the angle of attack of the rotor blades would increase to make the blades go into a deeper stall, thereby losing the extra energy in the wind [37]. One benefit of an active stall is that it manages the output power more precisely to prevent overshooting the rated power of the system at the start of the wind gust. The machine will even operate at almost perfectly rated power at all high wind speeds.

2.2.6. Aerodynamic Conversion

The wind turbine rotor absorbs the available power from the wind and transforms it into mechanical power operating on the rotor shaft of the wind speed.

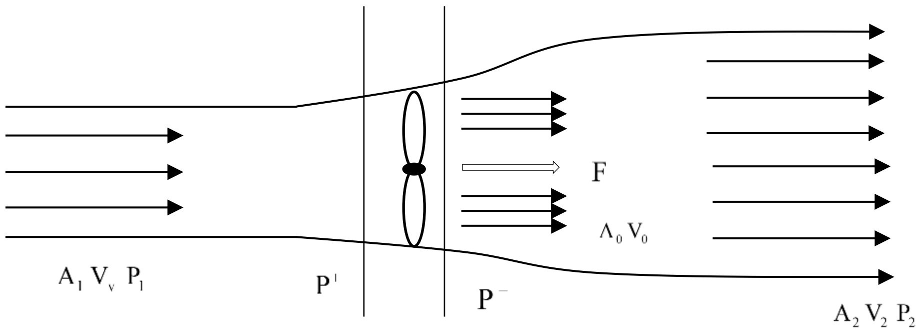

Figure 2.4 Schematic of fluid flow through a disk-shaped actuator [37]

The magnitude of power that is contained in the form of kinetic energy in the wind crossing at a speed v_v, surface A1, is expressed by

$$P_\omega = \frac{1}{2}\rho\pi R^2 v_\omega{}^3 \qquad (2.5)$$

Where, P_ω is the power extracted from the wind, ρ is the air density, R is the radius of the turbine rotor, and v_ω is the velocity of the wind.

The turbine rotor then converts the power obtained from wind speed into mechanical power. The mechanical power is expressed as:

$$P_{mec} = \frac{1}{2}\rho\pi R^2 v_\omega{}^3 C_p(\lambda,\beta) \qquad (2.6)$$

Where, P_{mec} is the mechanical power, R is the radius of the wind turbine, and Cp is the power coefficient.

From Equation 2.6, it is shown that the power coefficient is the function of the wind speed, the speed of rotation of the wind turbine, and the pitch angle. Albert Betz, a German physicist, has calculated the theoretical optimum for mechanical wind power generation by demonstrating that the maximum energy output is attained when Cp = 16/27 or 59.3%, and that percentage is known as the Betz Limit [36]. Nevertheless, such value is indeed not achievable with real turbines and its maximum value is normally around 0.5. The performance coefficient can be estimated by using three alternative techniques. These are the Blade Element Method, $C_p(\lambda,\beta)$ Look-Up Table, and Analytical Calculation Method [36]. In this thesis work, the analytical approximation method is used since it offers a detailed and reliable result. The representation of power coefficient through analytical expression as a function of tip speed ratio (λ) and pitch angle (β) is given as

$$C_p = C_1\left(\frac{C_2}{\lambda_i} - C_3\beta - C_4\right)\left(e^{-C_5/\lambda_i}\right) + C_6\lambda_i \tag{2.7}$$

$$\lambda_i = \frac{1}{\lambda + 0.08\beta} - \frac{0.035}{\beta^3 + 1} \tag{2.8}$$

Where, C_1= 0.5176, C_2=116, C_3=0.4, C_4=5, C_5 =21, C_6 =0.0068

Tip Speed Ratio (λ)

TSR for wind turbines is the ratio between the tangential speed of the tip of a blade and the actual speed of the wind. The tip-speed ratio is related to efficiency, with the optimum varying with blade design. Higher tip speeds result in higher noise levels and require stronger blades due to larger centrifugal forces [36].

$$\lambda = \frac{\omega x R}{v} \tag{2.9}$$

Where, ω is the rotational speed of the rotor in radians/second, R is the rotor radius in meters and V is wind speed.

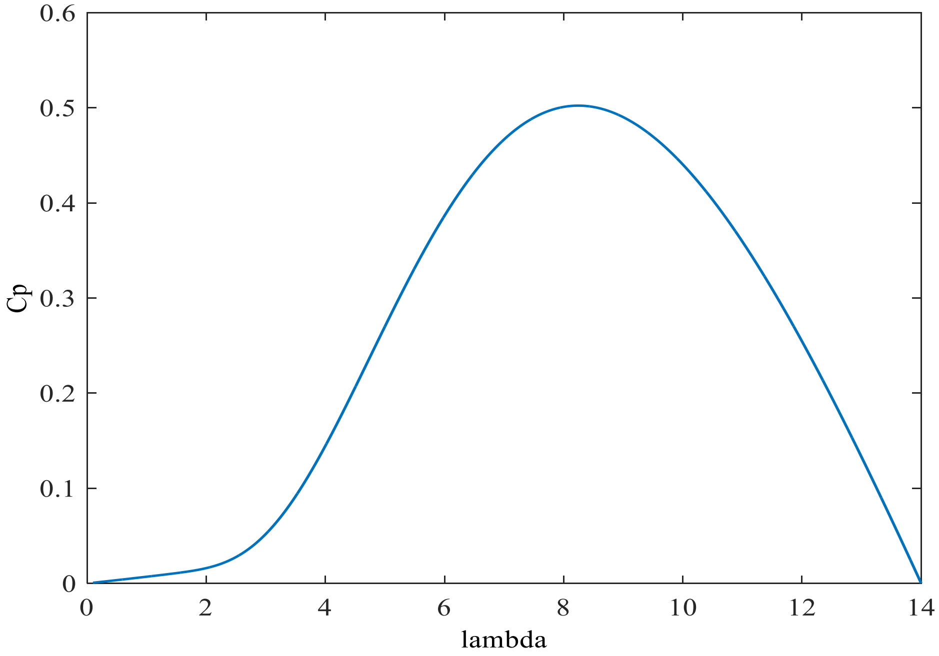

Figure 2.5 The typical curves of Cp versus TSR for pitch angle 0°

As demonstrated in Equation 2.5, the amount of power available from the wind depends on the velocity of the wind cubed. Thus, even a slight rise in wind speed would lead to an exponential increase in available power. Power at a given wind speed is optimal at a certain value of the speed of the rotor called optimum wind speed. This is the speed that leads to the optimal TSR (λopt). The turbine should always run at the optimal tip speed ratio to provide maximum power. This is possible by adjusting the rotational speed of the rotor such that it constantly rotates at the optimum rotational speed. For a given wind turbine, the power coefficient depends on both the TSR and the pitch angle of the rotor. Figure 2.5 elucidates the power coefficient concerning the TSR (λ) and the blade pitch angle at 0º. When the blade angle is 0º the maximum value of the power coefficient is 0.4865 corresponding to an optimum TSR of 8.1.

The relationship between wind speed and power is determined by the power curve that represents the power delivered by the wind turbine. For variable speed wind turbine, this relationship can be expressed as follows:

$$p(v) = \begin{cases} 0 & v<v_{ci} \text{ or } v>v_{ci} \\ q(v) & v_{ci} \leq v < v_r \\ p_r & v_r \leq v < v_{co} \\ 0 & v_{co} \leq v \end{cases} \quad (2.10)$$

Where, $p(v)$ is the electric power, v_{ci} is the cut-in wind speed, v_{co} is the cut-out wind speed, v_r is the rated wind speed, p_r is the rated power and $q(v)$ is the non-linear relationship between power and wind speed and a point at which a control approach is vital to extract maximum power from the wind.

In this study, the power curve is derived from ADAMA-II wind power generation, which employs 1.5MW DFIG wind turbines. The power curve of a wind turbine is determined by the cut-in wind speed, the rated speed, and the cut-out speed. According to ADAMA-II wind power generation, the cut-in speed is 3.5m/s and the cut-out speed is 25m/s.

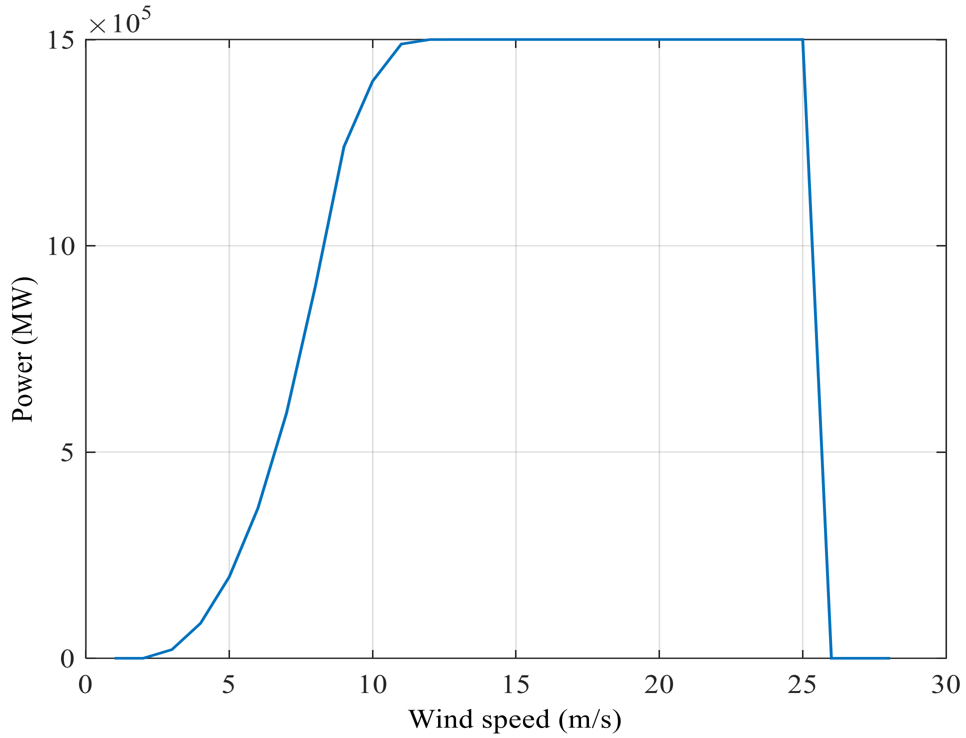

Figure 2.6 Mechanical power as a function of wind speed

Figure 2.6 indicates that when the wind speed is below the cut-in speed (3.5m/s), the wind turbine preserves shut down as the speed of the wind is too low to generate usable energy. Then once in operation, the power output increases following a broadly cubic relationship with wind speed until rated wind speed is attained. Remark that as long as the speed of the rotor persists below its rated speed, the performance coefficient is retained at the optimum, and the maximum power is obtained. Here, the turbine achieves full power (1.5MW) at a wind speed of approximately 12m/s and operates at 1.5MW until it reaches cut-off wind speed. When the wind speed is above the rated wind speed, the aerodynamic rotor is designed to restrict the mechanical power generated from the wind and thereby reduce the mechanical loads on the drive train. The turbine is then shut down at very high wind speeds (cut-off speed).

2.3. Wind Energy Conversion System Configurations

The wind energy system consists of two major components, a wind turbine system and an electrical generator. The essential objective of the wind turbine is to transform kinetic energy to mechanical energy, while the electrical generator converts mechanical energy from the wind turbine, which functions as a prime mover, to electrical energy which is then transmitted to the electrical grid. Over the year, numerous types of wind turbines have been developed. A wind turbine can operate at fixed or variable speeds. For fixed-speed wind turbines, the generator is directly attached to the grid and the speed of the wind turbine is almost fixed and uncontrollable. Where, as in the variable speed wind turbine, the generator is connected to the grid through power converters and thus the speed of the rotor can be controlled [36-38]. Various types of generators used in wind turbines are listed and described in detail below.

2.3.1. Fixed Speed Wind Turbines

Squirrel cage induction generator, which is directly connected to the grid, is used primarily in fixed-speed wind turbines. In the squirrel cage induction generator, the stator winding is normally attached to the load/excitation source where the rotor is provided with a short-circuited cage winding, which is very sturdy. Maintenance is usually limited to bearing lubrication, which makes it very prominent for wind power. The operational speed of the SCIG is a steady rotational speed of the rotor because it runs at a slip of around 1% [38]. This strategy represents a capacitor bank or a reactive power compensator to eradicate the demand for reactive power from the turbine generator to the grid. It is typically achieved by continuously swapping capacitor banks following a transition in power generation [38].

The key limitations to this concept are

- It does not support any regulation of speed
- Reduces the efficiency of energy conversion
- Wind fluctuation is transformed to mechanical fluctuation and, in turn, to electrical fluctuation, which induces voltage fluctuation in the event of a weak grid, thus causing grid disruption.

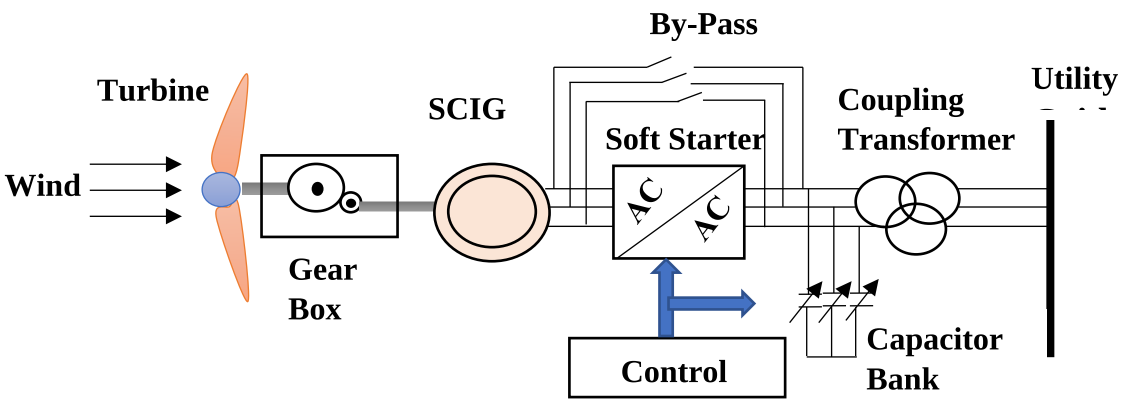

Figure 2.7 Fixed speed wind turbine squirrel cage induction generator [38]

2.3.2. Partial Variable Speed Wind Turbine with Variable Rotor Resistance

In this type of wind turbine, the wound rotor induction generator is directly attached to the grid. The regulated resistances are linked in series with the rotor phase winding of the generator. The total rotor resistances can thus be monitored, and the slip and output power can be managed. Usually, the speed adjustment range is restricted to about 10% above the synchronous speed of the generator. The capacitor bank, as shown in Figure 2.8 performs a reactive power compensation and a smooth grid connection exists via a soft starter. The soft starter is used to minimize inrush and reactive power [37-38].

The downsides of this configuration are

- Energy losses in the rotor resistance
- High cost compared to squirrel cage induction generator
- The speed range is limited
- Poor control of active and reactive power
- The slip power is dissipated in the variable resistance

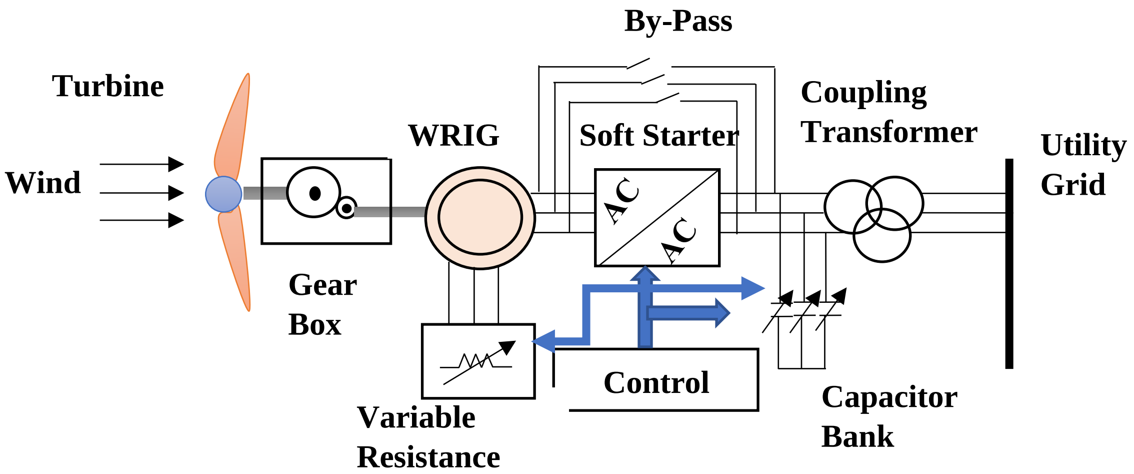

Figure 2.8 Partial variable-speed configurations with variable rotor resistance [38]

2.3.3. Variable Speed Wind Turbine with Partial-Scale Frequency Converter

This configuration is known as the Doubly-Fed Induction Generator (DFIG) concept, which is similar to the WRIG method. In DFIG, the stator is directly connected to the grid while the rotor is connected to the grid via a partial scale power converter. These converters are capable of maintaining both the rotor frequency and the rotor speed. Besides, they compensate for the reactive power and smooth the grid connection. One of the benefits of DFIG as opposed to WRIG is that the speed control range of the rotor is wider [38]. DFIG has a reduced converter cost relative to wind energy systems using full-capacity converters. The power rating of the partial-scale frequency converter determines the speed range (usually within ±30% of the synchronous speed). The major weakness of this design is its slip rings and gearboxes, which require constant maintenance, its restriction of fault ride-through capability, which necessitates a protection mechanism, and its dynamic control scheme.

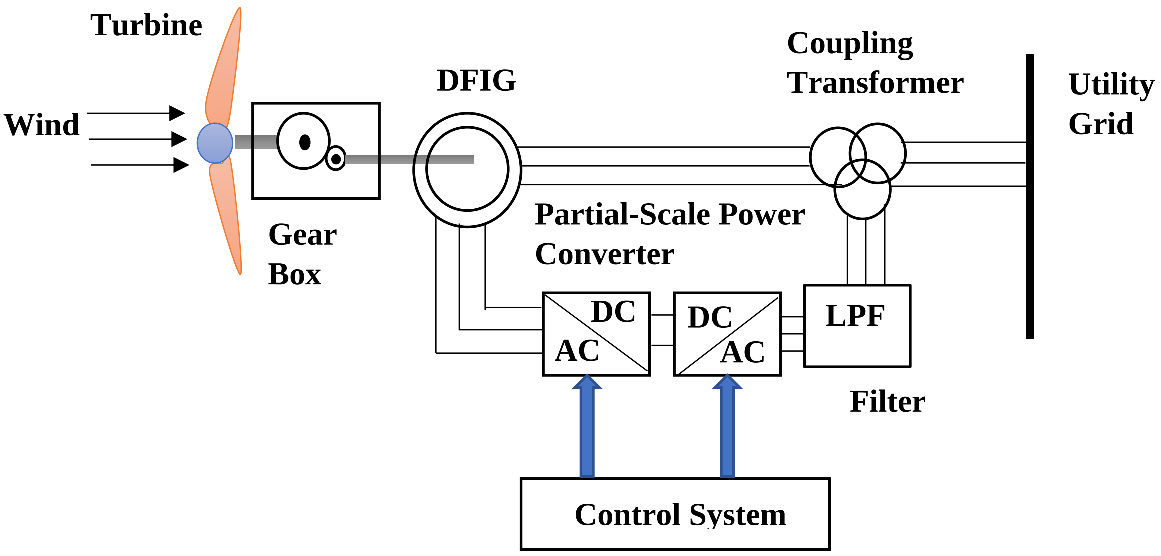

Figure 2.9 Variable-speed configurations with reduced-capacity converters [38]

2.3.4. Variable Speed Wind Turbine with Full-Scale Power Converter

In this configuration, the generator is connected to the grid through a full-scale power converter and the power rating of the converter is normally the same as that of the generator. Any of these types of wind turbines have a gearless configuration, which implies that using a low-speed synchronous generator with a large number of poles, the wind energy system can work without the need for a gearbox. Elimination of the gearbox boosts the performance of the machine and reduces the initial costs and maintenance which can be taken as one of its strengths [36]. The frequency converter performs a reactive power compensation and a smooth grid connection for the whole speed range. Figure 2.10 displays the variable speed wind turbine with a full-scale converter. Another advantage of this type is the ability to independently control real and reactive power. However, owing to its high generator and installation costs, this turbine also has a drawback. The PMSG-based power converters have a full-scale power rating that will cause high losses and generate high harmonic parts [35].

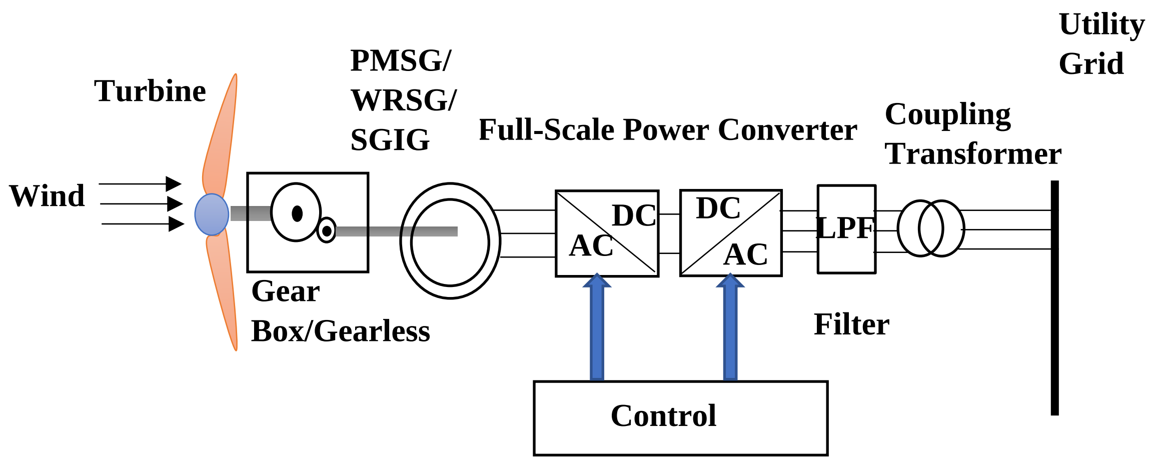

Figure 2.10 Variable Speed Wind Turbine with Full-scale Power Converter [38]

2.4. Review on Grid Codes Requirement

The transmission and distribution network operators define the Grid codes to outline the rights and responsibilities of all generation units/consumers connected to the transmission system. In previous years, the grid codes did not include any regulations for large WPPs, as the degree of penetration of wind power was comparatively limited relative to conventional generation systems. However, recent growth in the production of wind power has reached a degree where the impact of the wind farm on the reliability of the power grid can no longer be ignored. In recognition of this obstacle, power grid providers have placed standards on massive wind farms attempting to link to their transmission networks [39-41].

The existence of the technological requirements in the grid codes and associated documentation varies between the power grids. The following are standard specifications for most grid codes

- ✓ Frequency and voltage tolerance
- ✓ Fault ride-through (FRT)
- ✓ Reactive power and voltage control capability
- ✓ Active power control
- ✓ Power quality

2.4.1. Frequency and Voltage Operating Range

The Grid operators require the frequency to be kept within acceptable limits. Since the power system frequency is an indicator of the equilibrium between power generation and loads any sudden rise in load leads to a decrease in the frequency of the voltage generated. The unexpected generation loss and changes can result in the incidence of under frequency and over frequency, respectively [39]. Anticipating this problem, grid codes require wind farms to be able to function continuously within the range of voltage and frequency variations encountered under normal operating conditions. It must have the capability to operate within the typical frequency range to ensure the security of supply, prevent overloading of electrical equipment and comply with the standard power quality. The frequency operating range of the power grid varies from country to country. For instance, the Italy grid code requires the wind turbine to operate between 47.5Hz–51.5 and the UK grid code requires the wind turbine to operate consistently between 47.5 Hz and 52 Hz and at least 20 seconds between 47 Hz and 47.5 Hz. Operation with a significant frequency deviation above these limits would harm the generating plants and lead to a loss of power that would lead to a blackout [39,41].

2.4.2. Fault Ride Through (FRT)

Wind power connection codes in most countries enable the wind turbine to remain connected to the grid to preserve reliability and stability throughout and after a short-term fault. Over the decades, the wind turbine coupled to the asynchronous squirrel-cage was very susceptible to grid faults, and even during mild disruptions, the safety mechanism disconnects the turbine. At present, the wind turbine continues to work as it is attached to the power system at all times, including with grid failure [39]. One of the most frequent faults likely to occur in the power system is the drop in voltage at the grid terminal. Depending on the location of the fault, the depth of the voltage dip can vary. Some faults can be single-phase ground, three-phase ground, line-to-line fault, etc. In the case of DFIG, the stator is attached directly to the grid, causing the generator vulnerable to grid disruption. A short circuit within the grid can generate 5-8 times the rated DFIG stator current resulting in a high inrush rotor current, which is likely to cause tension on the mechanical drive and shaft, damage to the RSC and DC bus overvoltage [40]. Various protection and control mechanisms must be set to prevent this harm and enhance the ability to drive faults.

2.4.3. Active and Reactive Power Control Capability

The Grid code requires the current and voltage of wind turbine power to be within the acceptable harmonic range and the wind turbine to support active and reactive power for the grid to share the demanded load. The prerequisite of the grid code for the active power regulation of the wind farm is to be able to manage its active power output at a specified level and at a defined ramp rate and perhaps to engage in the energy supply as conventional power stations and to avoid overloading of the lines. The goal of these criteria is to ensure a consistent frequency in the system [40].

On request from the network operator, most grid codes demand active power reduction at the defined set-point. This is achieved either by disconnecting the wind turbines or by regulating the pitch angle of the blades to restrict wind power. Some grid codes also limit the rate of change in active power, with maximum and minimum ramp-up and ramp-down rates. The most demanding criteria for both ramp-up and ramp-down rates under standard conditions are in Denmark, where wind farms must still be able to adjust their active ramp rates from 10% to 100% of nominal power per minute. These limitations aim to suppress high-frequency fluctuations caused by intense wind conditions and to prevent high voltage and in-rush currents during the start-up and shutdown of the wind farm. To control the voltage level at the point of common coupling (PCC), the wind turbine is often needed to generate or absorb a constant particular amount of reactive power. Under regular operation, the PCC voltage can be increased by introducing reactive power into the grid and can be lowered by absorbing the reactive power. Wind farms should have reactive power capability to sustain the grid voltage during voltage fluctuations and to help offset the reactive power demand in the system [41].

2.5. Comparison of the Grid Code Requirements

This section illustrates the relevant aspects of the latest grid code specifications for the integration of wind power in a variety of countries. The different requirements are compared, and the most demanding ones are highlighted. The grid code requirements for reactive power management and voltage regulation, active power, and frequency control, power factor control, LVRT, HVRT, regulation of active and reactive power following faults are explained and compared in detail in [39,40]. In this segment, however, only the low voltage ride-through, one of the most critical criteria for the dynamic output of wind turbines during network failures, is considered in detail.

2.5.1. Low Voltage Ride Through

The most critical and recently updated grid code prerequisite for wind farm service is low voltage ride-through capability. LVRT is vital for the stable and reliable operation of power supply networks, especially in regions with high penetration of wind power generation. This phenomenon indicates the ability of massive wind turbines to remain attached for a brief period during fault and voltage dip events. This implies that there is no lack of wind production for widely cleared faults.

The grid code of Denmark states that the wind generator shall be removed from the grid for a period of 100ms if the system voltage is below 20% and the wind power plant restores 75% of the system voltage at 750ms after the voltage dip. The Ireland grid code allows the wind power plant to operate through symmetrical and asymmetrical sags with a voltage of 0.15 at 0.625s, followed by a voltage restore of 0.9 PU at 3s [39]. The grid code requirement for Spain allows the wind farm to tolerate three-phase and one-phase voltage faults down to 0.2 PU for 0.5 s, followed by a linear voltage restore to 0.8 PU for the next 0.5 s. For two-phase faults, on the other hand, continuous activity of wind power plant is needed for voltage sags with a retaining voltage of 0.6 PU and a maximum period of 0.8 s. Wind farm must remain connected under symmetrical and asymmetrical sags with a voltage drop to zero for 140 ms and 400 ms, respectively and the supply voltage must then be restored to 0.7 PU in 2 s and 0.8 PU in 10 s, based on the Australian grid code standard. In practical applications, German LVRT grid requirements are often favored over other GCRs. They enable the wind turbines to remain connected to the grid for at least 150ms after performance degradation with a voltage drop of 0.1pu and the voltage should recover to 90% of its rated voltage within 1500ms after fault clearance [39]. Table 2-1 lists international grid code requirements of LVRT capability [40].

Table 2-1 LVRT capability requirement in international grid codes

Country	During fault condition		After fault condition	
	V_{min} (pu)	T_{max} (s)	V_{min} (pu)	T_{max} (s)
Australia	0.00	0.10	0.70	2.00
Canada	0.00	0.15	0.85	1.00
Denmark	0.20	0.50	0.90	1.50
Germany	0.10	0.15	0.9	1.50
India	0.15	0.30	0.85	3.00
Ireland	0.15	0.625	0.90	3.00
New Zealand	0.00	0.20	0.60	1.00

CHAPTER THREE:

METHODOLOGY AND SYSTEM DESCRIPTION

3.1. Introduction

In this chapter, the general methodologies employed to achieve the objectives of this thesis work along with the detail model of DFIG and the power converters are discussed. The Flowchart of the methods followed to accomplish the thesis work is presented in Figure 3.1

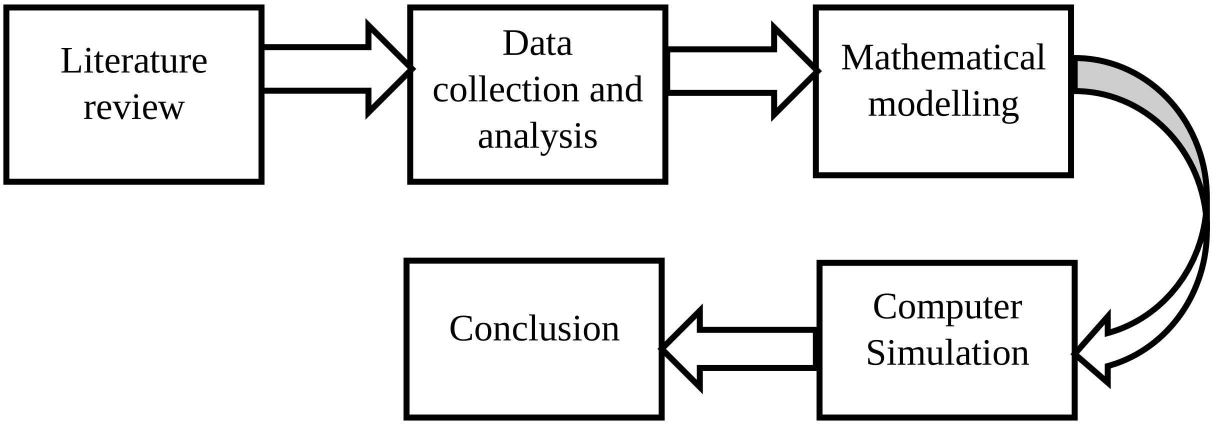

Figure 3.1 Flowchart of the proposed system

Literature review

First, a review of the literatures on the examination of DFIG-based wind turbines is undertaken from journals, articles, dissertation and available books. Theoretical descriptions of wind turbine types and components, as well as models of doubly fed induction generators and power converters, are investigated. Furthermore, several control and protection approaches employed by previous researchers to enhance FRT capability have been explored. This assists in gathering important information and adopting different concepts and approaches as required.

Data collection and analysis

The second method adopted to carry out this thesis work is data collection. Various input data required for the model were gathered from the Adama-II wind farm project office, which is located on the wind farm site. The data is collected through physical observation in the wind farm and from the recorded data and equipment specifications. The generator parameters, wind speed and power curve, and the converters specification are all obtained for modelling, simulation and analysis of the entire system.

Mathematical modelling

Modeling of doubly fed induction generator as well as power converters have been realized based on the data obtained. When modelling the machine, reference frame transformation has been employed to transform the three phase DFIM in to two-phase to eradicate the complexity of the model. The purpose of modelling and controlling the DFIG-based WECS connected to the power grid is to fully understand how the machine performs in steady state and transient conditions. To improve the performance of the machine, crowbar protection system and crowbar integrated with BESS are modeled. The MATLAB/SIMULINK software is used for modeling the system. Simulink is a multi-domain simulation and model-based design block diagram environment. It includes a graphical editor, block libraries that can be customized, and algorithms for modeling and simulating dynamic systems.

Computer simulation

This approach is adopted after the modeling has been completed. The simulation will be carried out using MATLAB/SIMULINK 2015a to assess how the machine operates in normal and fault conditions. In this thesis work, four distinct simulation is carried out to have a better understanding of the DFIG. The performance of the DFIG is first assessed under normal conditions, and then the operation of the machine under a fault scenario is assessed utilizing the three approaches. These approaches are as follows:

- Existing capacitor bank
- Crowbar protection scheme
- Crowbar integrated with BESS

Finally, a comparison of the existing capacitor bank, crowbar protection system, and crowbar combined with BESS is performed to determine which method performs best in terms of enhancing fault ride through capabilities.

Conclusion

Lastly, based on detailed analysis and simulation results, as well as from the comparative analysis a conclusion is reached.

3.2. Modelling of Doubly Fed Induction Generator

The DFIG is tremendously acknowledged in the modern wind power industry due to its high reliability, increasing power efficiency, reducing mechanical stress on wind turbines, and comparatively low cost. The DFIG comprises a stator winding and a rotor winding equipped with a slip ring. The stator is supplied with three-phase insulated windings that form the desired pole configuration and is connected to the grid through a three-phase transformer. Whereas, the rotor is fed to the grid via a variable frequency converter, which only demands to accommodate a fraction (25-30%) of the overall power to achieve maximum generator control. The variable speed converter (VSC) consists of two PWM converters that are linked back-to-back by a DC-link capacitor, namely, a rotor side converter (RSC) and a grid-side converter (GSC) [42].

The essential feature of the grid side converter is to regulate the dc-link voltage such that it remains almost constant during regular and irregular activity. Also, it tends to couple the rotor winding with the non-ideal grid. Conversely, the rotor-side converter is directly connected to the windings of the rotor and thus regulates the frequency and magnitude of the rotor voltages supplied to the machine. The frequency of the windings of the rotor deviates from the fundamental frequency of the grid. Likewise, the entire machine will run on all 4-quadrants by the appropriate tuning of the frequency converter. This is certainly an asset of vital significance since the generator will either supply or deliver reactive power to/from the grid [43].

It is crucial to recognize the models for the DFIG wind power systems, including the steady-state and dynamic model, for the design of the regulation of the wind power systems. This model represents the operating relationship of the variables in the DFIG power system [44]. The subsequent sections demonstrate the steady-state model, which tends to focus on the behavior of the machine in steady-state conditions, and the dynamic model, which reflects on the transition behavior of the machine and its response to changes in the DFIG network equivalent circuit.

3.2.1. Steady-State Equivalent Circuit of DFIG

The doubly-fed induction machine can be depicted in the basic form of an electrical transformer connected to a balanced three-phase source [44]. The steady-state equivalent electrical circuit of DFIG should preferably be streamlined, with the following assumptions:

- Both the stator and the rotor are connected in the configuration of the star.
- The stator is supplied by the grid at constant and balanced three-phase voltage amplitude and frequency.
- The rotor is often supplied at steady and balanced AC voltage amplitude and frequency, regardless of the stator, for instance, by a back-to-back voltage source converter.

Figure 3.2 demonstrates the equivalent steady-state circuit of DFIM. On account of the symmetry of the machine, only one phase of the stator and rotor is represented. the other two phases are modeled as essentially identical.

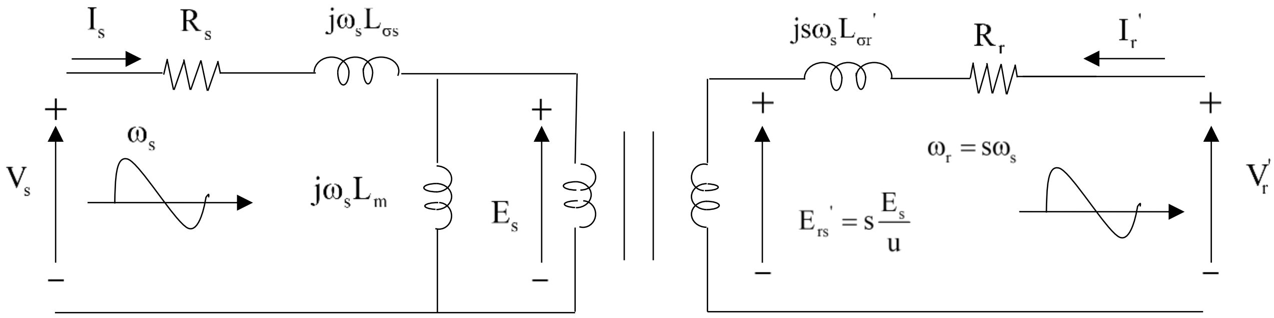

Figure 3.2 One-phase steady-state equivalent electric circuit of the DFIG [43]

The frequency of the stator and the rotor circuit is distinct in such a way that the frequency of the stator (f_s) is constant when the stator is attached directly to the grid, whereas the frequency of the rotor voltages and currents is variable (f_r) and depends on the speed of the machine.

Analyzing the stator and rotor independently, the steady-state model of electrical equations can be derived as follows:

$$\begin{aligned} V_s - E_s &= (R_s + X_{\sigma s})I_s \text{ at } f_s \\ V_r' - E_{rs}' &= (R_r' + X_{\sigma r}')I_r' \text{ at } f_r \end{aligned} \tag{3.1}$$

Where, V_s and V_r' are supplied stator and rotor voltage, E_s and E_{rs}' are induced emf in stator and rotor, R_s and R_r are the stator and rotor resistance, I_s and I_r are induced stator and rotor current with frequency f_s and f_r respectively, $x_{\sigma s} \rightarrow j\omega_s L_{\sigma s}$ and $x_{\sigma r} \rightarrow j\omega_r L_{\sigma r}$ are the stator leakage impedance and rotor leakage impedance

It is not practical for the stator and rotor circuit to operate at different frequencies. Thus, it is advisable to transform the stator and rotor equivalent circuits to a circuit in which both rotor and stator currents and voltages function at the same frequency [43]. The effect of the u-factor, a coefficient that indicates the relationship between the stator and the rotor, must first be taken into consideration before considering the difference in frequencies between the rotor and the stator.

$$u = \frac{N_s}{N_r} \tag{3.2}$$

The induced electromagnetic field in the stator and rotor is therefore determined by:

$$E_{rs}' = \frac{E_s}{u} s \tag{3.3}$$

As stated above, a rotor and a stator circuit having a different frequency are not practical. Hence both the stator and the rotor circuits must be susceptible to the same frequency to simplify the equivalent circuit analysis.

$$V_r - sE_s = (R_r + j_s\omega_s L_{\sigma r})I_r \rightarrow \frac{V_r}{s} - E_s = (\frac{R_r}{s} + j\omega L_{\sigma r})I_r \tag{3.4}$$

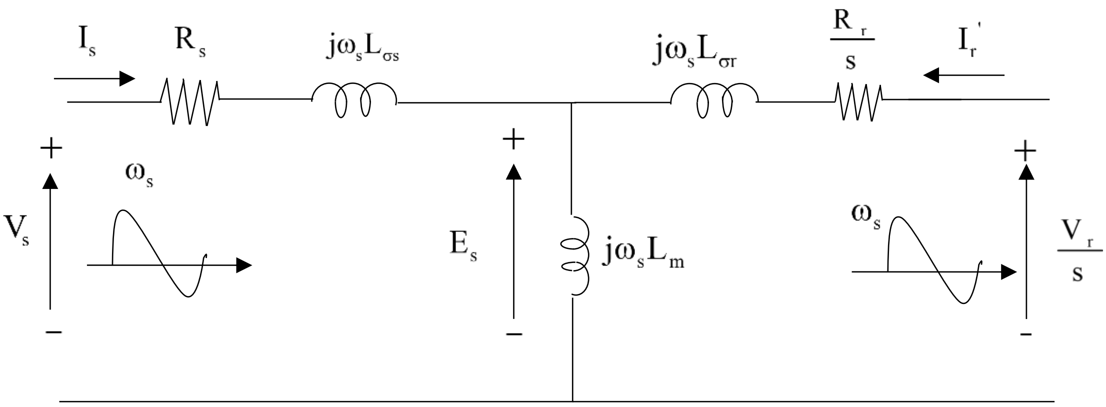

Figure 3.3 Steady-state equivalent circuit of the DFIG referred to stator [43]

It is possible to deduce the phasor diagram by using the model equations of the machine. Equation 3.5 elucidates the stator and rotor fluxes attained from the stator and rotor currents.

$$\begin{aligned} \psi_s &= L_m(I_s + I_r) + L_{\sigma s} I_s = L_s I_s + L_m I_r \\ \psi_r &= L_m(I_s + I_r) + L_{\sigma r} I_r = L_m I_r + L_r I_r \end{aligned} \tag{3.5}$$

Where, L_s, L_r, L_m are the stator, rotor, and mutual inductances:

$$\begin{aligned} L_s &= L_m + L_{\sigma s} \\ L_r &= L_m + L_{\sigma r} \end{aligned} \tag{3.6}$$

The voltage is obtained by substituting the fluxes in equation 3.5 in 3.1

$$\begin{aligned} V_s &= R_s I_s + j\omega_s L_{\sigma s} I_s + j\omega_s L_m (I_s + I_r) \\ \frac{V_s}{s} &= \frac{R_r I_r}{s} + j\omega_s L_{\sigma r} I_r + j\omega_s L_m (I_s + I_r) \end{aligned} \tag{3.7}$$

3.2.2. Dynamic Model of Doubly Fed Induction Generator

A steady-state analysis that tends to concentrate solely on the behavior of the machine in steady-state situations would not be adequate to obtain a satisfactory degree of machine understanding during dynamic and transient conditions. The dynamic and transient behavior of the DFIG must therefore be analyzed for modeling purposes, and even more precisely for the implementation of the subsequent machine control. Through dynamic behavior, which is analyzed by a "dynamic model," it is possible to know the behavior of the system in both the transition state and the steady state. A dynamic model can provide the continuous performance of the variables of the machine, such as torque, currents, and fluxes, under certain voltage supply conditions. That way it is possible to identify dangerous behaviors, such as volatility or strong transient currents by identifying the transition from one state to another. Besides, the dynamic model provides extra information on the system during steady-state operation, such as dynamic oscillations and torque or current ripple [43,44].

DFIG is a high-order, nonlinear, and time-varying machine [44]. As a consequence, the following assumption is added to simplify the complex analysis:

- The magnetic saturation of the stator and the rotor core is neglected
- Iron degradation of both the stator and the rotor core is ignored
- The parasitic resistance of the stator and rotor does not change with temperature and frequency
- Sustained air gap reluctance
- Stator and rotor windings of the DFIG are assumed symmetrically

The mathematical model of the three-phase machines is indeed complicated. It is therefore fundamental to transform it into two-phase stationery, rotor, and synchronous reference frame. Space vector notation is essential for this task. Space vector notation is an extensively studied technique that can be used in AC machines to represent flux, voltage, and current magnitude in a feasible manner. Details on the state space notation and reference frame transformation can be found in Appendix B.

3.2.2.1. α,β Model

DFIG can be characterized by three different reference frames such as the stator reference frame (stationary frame), the rotor reference frame (DQ) which rotates at ω_m , and the synchronous frame (d-q) which rotates at ω_s . The figure below illustrates these reference frames.

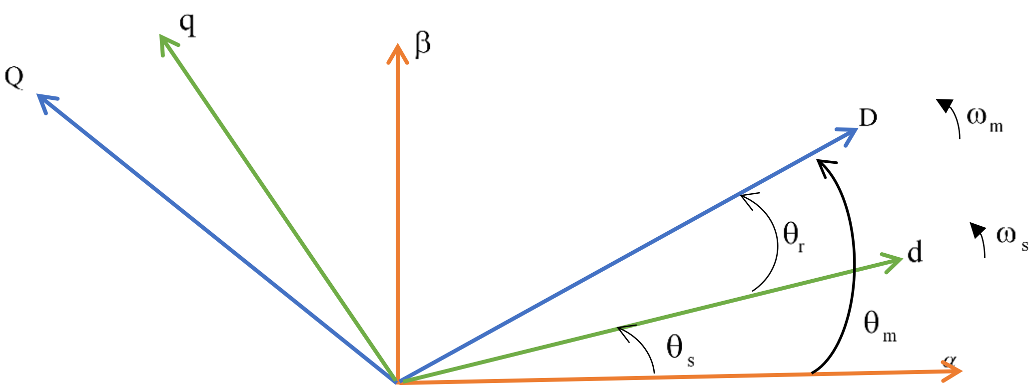

Figure 3.4 Different reference frames to represent space vectors of the DFIM [45]

Space vector theory is used to represent the three coils of the stator and rotor independently by two stationary coils (α,β) for the stator and two rotating coils DQ for the rotor [45]. The stator and rotor voltage and magnetic flux equations of the DFIG in the stationary reference (α,β) frame are as follows:

Stator and rotor voltage in (α,β)

$$v_{\alpha s} = R_s i_{\alpha s} + \frac{d\psi_{\alpha s}}{dt}$$
$$v_{\beta s} = R_s i_{\beta s} + \frac{d\psi_{\beta s}}{dt} \tag{3.8}$$

$$v_{\alpha r} = R_r i_{\alpha r} + \frac{d\psi_{\alpha r}}{dt} + \omega_m \psi_{\beta r}$$
$$v_{\beta r} = R_r i_{\beta r} + \frac{d\psi_{\beta r}}{dt} - \omega_m \psi_{\alpha r} \tag{3.9}$$

The expressions of the stator and rotor flux in the form of space vector in the stationary reference frame are:

Stator and rotor flux in (α,β)

$$\begin{aligned}\psi_{\alpha s} &= L_s i_{\alpha s} + L_m i_{\alpha s} \\ \psi_{\beta s} &= L_s i_{\beta s} + L_m i_{\beta s}\end{aligned} \tag{3.10}$$

$$\begin{aligned}\psi_{\alpha r} &= L_m i_{\alpha r} + L_r i_{\alpha r} \\ \psi_{\beta r} &= L_m i_{\beta r} + L_r i_{\beta r}\end{aligned} \tag{3.11}$$

Where, $V_{\alpha s}, V_{\alpha r}, V_{\beta s}, V_{\beta r}$, $i_{\alpha s}, i_{\alpha r}, i_{\beta s}, i_{\beta r}$ and $\psi_{\alpha s}, \psi_{\alpha r}, \psi_{\beta s}, \psi_{\beta r}$ are voltages [V], currents [A] and flux linkages [Wb] of the stator and rotor in α, β axis, R_s and R_r are the stator and rotor resistance [Ω], L_s, L_r and L_m are the stator, rotor, and mutual inductance [H] respectively, ω_m and ω_s are the rotor electrical speed and the stator frequency [rad/s].

The active and reactive power of the stator and rotor in the (α, β) frame is calculated as follows:

$$\begin{aligned}P_s &= 1.5(v_{\alpha s} i_{\alpha s} + v_{\beta s} i_{\beta s}) \\ Q_s &= 1.5(v_{\beta s} i_{\alpha s} - v_{\alpha s} i_{\beta s})\end{aligned} \tag{3.12}$$

$$\begin{aligned}P_r &= 1.5(v_{\alpha r} i_{\alpha r} + v_{\beta r} i_{\beta r}) \\ Q_r &= 1.5(v_{\beta r} i_{\alpha r} - v_{\alpha r} i_{\beta r})\end{aligned} \tag{3.13}$$

Where, P_s, P_r, Q_s and Q_r are the active and reactive power of the stator and rotor in the (α, β) frame.

The electromagnetic torque of the machine can be determined using the following equivalent expressions:

$$T_{em} = 1.5\left(\frac{L_m}{\sigma L_r L_s}\right) p \operatorname{Im}\{\psi_r . \psi_s\} \tag{3.14}$$

Where, p is the pole pair of the machine and $\sigma = 1 - L_m^2 / (L_s . L_r)$ is the leakage coefficient

The equivalent circuit of the dynamic model in the (α, β) reference frame is demonstrated in Figure 3.5 and Figure 3.6.

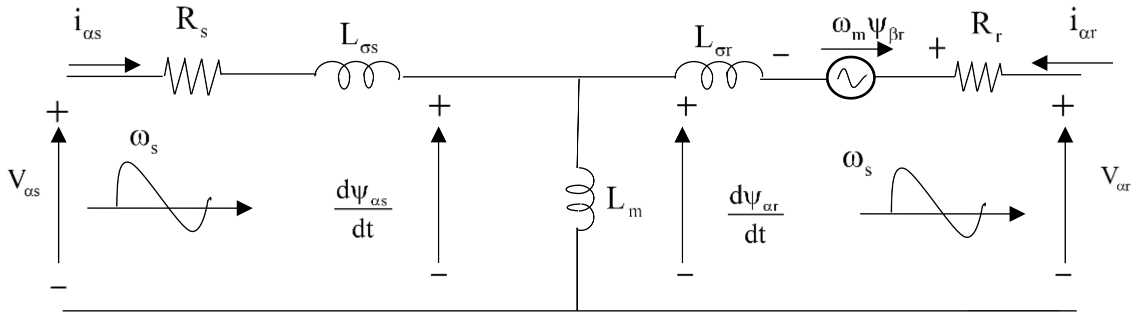

Figure 3.5 Model of the DFIM in the α, β reference frame (α -axis) [43]

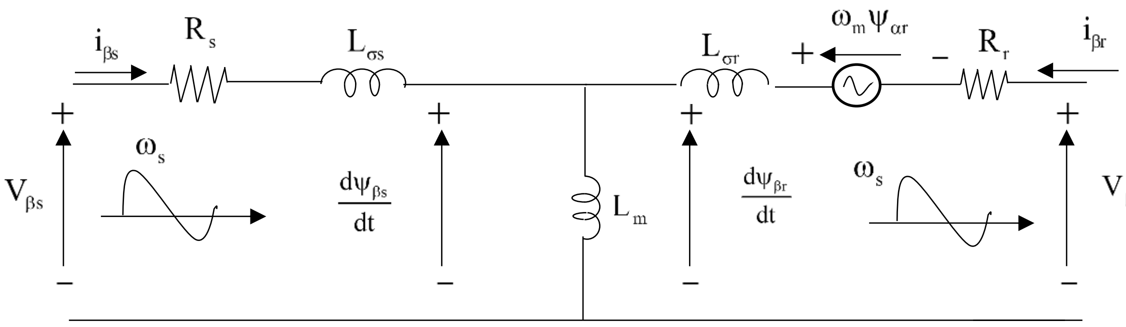

Figure 3.6 Model of the DFIM in the α, β reference frame (β -axis) [43]

3.2.2.2. d-q Model

The d-q model of induction machine is the most widely used, which provides numerous advantages in terms of induction machine control. The transformation of the three-phase induction machine model to a two-phase (d-q) equivalent circuit results in the eradication of time-varying inductances in the voltage equations. This implies that the time-varying variables of the three-phase system become constant when referred to as the two-phase system. This would eliminate the computational nightmare as all the inductances in the transformed model would be time-invariant and can be efficiently resolved using conventional numerical techniques [42].

The dynamic equation of a three-phase DFIG in a two-phase direct-quadrature (d-q) reference frame is expressed as:

The stator and rotor voltage in the d-q reference frame

$$\begin{aligned} v_{ds} &= R_s i_{ds} + \frac{d\psi_{ds}}{dt} - \omega_s \psi_{qs} \\ v_{qs} &= R_s i_{qs} + \frac{d\psi_{qs}}{dt} + \omega_s \psi_{ds} \end{aligned} \tag{3.15}$$

$$\begin{aligned} v_{dr} &= R_r i_{dr} + \frac{d\psi_{dr}}{dt} - \omega_r \psi_{qr} \\ v_{qr} &= R_r i_{qr} + \frac{d\psi_{qr}}{dt} + \omega_r \psi_{dr} \end{aligned} \tag{3.16}$$

The stator and rotor flux in the d-q reference frame

$$\begin{aligned} \psi_{ds} &= L_s i_{ds} + L_m i_{dr} \\ \psi_{qs} &= L_s i_{qs} + L_m i_{qr} \end{aligned} \tag{3.17}$$

$$\psi_{dr} = L_r i_{dr} + L_m i_{ds}$$
$$\psi_{qr} = L_r i_{qr} + L_m i_{qs} \tag{3.18}$$

Where, $V_{ds}, V_{dr}, V_{qs}, V_{qr}$, $i_{ds}, i_{dr}, i_{qs}, i_{qr}$ and $\psi_{ds}, \psi_{dr}, \psi_{qs}, \psi_{qr}$ are voltages [V], currents [A], and flux linkages [Wb] of the stator and rotor in the d-q axis. The torque and power expressions in the d-q reference frame are identical to the torque and power expression in α, β reference frame.

The equivalent dynamic circuit in the d-q reference frame is derived from the above equation as indicated in Figure 3.7 and Figure 3.8 respectively [43].

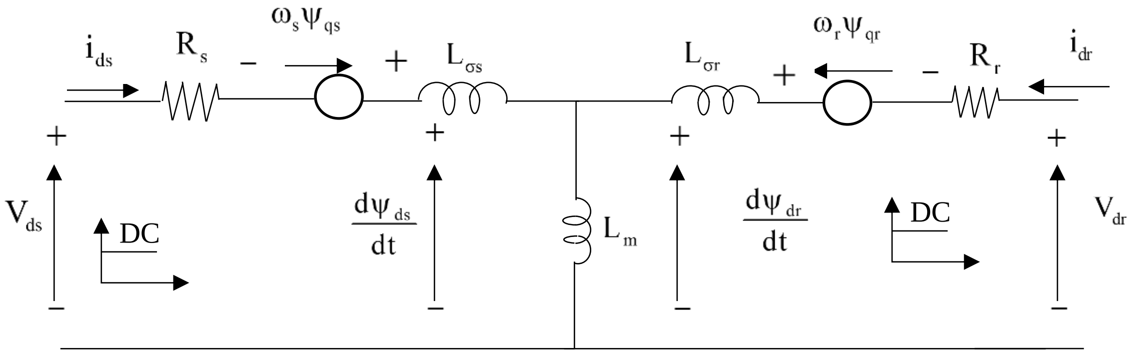

Figure 3.7 d-q equivalent circuit of DFIG (d-axis circuit)

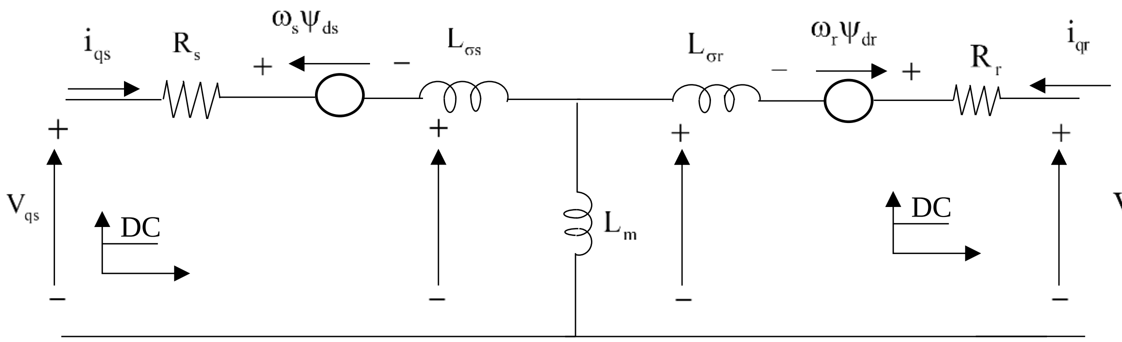

Figure 3.8 d-q equivalent circuit of DFIG (q-axis circuit)

3.3. Power Relation in Doubly Fed Induction Generator

Analysing the power relations of DFIG is fundamental for identifying the different modes of operation of such machines. The flow of electrical current in the machine coils generates active and reactive power in the DFIG stator and rotor windings. This machine can either supply or consume these powers from the respective terminals. Thus, depending on the sign of these powers, the operation of the machine can be described as a motor or a generator. This signifies that the positive value of P_s and P_r is construed as the power absorbed by the machine and the negative value of P_s and P_r is perceived as the power supplied to the grid [46].

3.3.1. Active Power Balance

The active power which is fed to the DFIG via the stator and the rotor circuit must first be examined to determine the power flow of the DFIG system. The stator and the rotor active power is expressed as:

$$\begin{aligned} P_s &= 3\,\mathrm{Re}\{v_s.I_s^*\} \\ P_r &= 3\,\mathrm{Re}\{v_r.I_r^*\} \end{aligned} \tag{3.19}$$

Active power can also be represented as dependent on the parameters, currents, and slip of the machine by substituting the stator and rotor voltage from equation (3.1) in (3.19):

$$\begin{aligned} P_s &= 3R_s\,|I_s|^2 + 3\omega_s L_m\,\mathrm{Im}\{I_s.I_r^*\} \\ P_r &= 3R_r\,|I_r|^2 - 3s\omega_s L_m\,\mathrm{Im}\{I_s.I_r^*\} \end{aligned} \tag{3.20}$$

The mechanical power, the power transmitted through the electric circuit to the mechanical shaft, is expressed as:

$$P_{mec} = P_s + P_r - P_{cu\_s} - P_{cu\_r} \tag{3.21}$$

Where, P_{cu_s} and P_{cu_r} are the copper losses in the stator and rotor and is expressed as:

$$\begin{aligned} P_{cu\_s} &= 3R_s\,|I_s|^2 \\ P_{cu\_r} &= 3R_r\,|I_r|^2 \end{aligned} \tag{3.22}$$

By substituting equation (3.20) and (3.22) in equation (3.21) the final expression of mechanical power is obtained:

$$P_{mec} = 3\omega_m L_m.\mathrm{Im}\{I_r^*.I_s\} \tag{3.23}$$

As previously stated, the operation of the machine is characterized by a sign of mechanical power, which implies that if $P_{mec} > 0$ then the machine delivers mechanical power through the shaft (motor operation mode). Whereas, if $P_{mec} < 0$ then the machine is consuming power through shaft (generator operation mode) [45]. The efficiency (η) of the machine-specific to the operation of the motor or generator can therefore be determined according to the following equations:

$$\eta = \frac{P_m}{P_s + P_r} \quad \text{if } P_m > 0$$
$$\eta = \frac{P_s + P_r}{P_m} \quad \text{if } P_m < 0 \tag{3.24}$$

The resistive and magnetizing losses have been neglected for the approximations of stator and rotor powers. The relation between stator and rotor power is indicated as:

$$P_r \cong -sP_s \tag{3.25}$$

The stator and rotor power in terms of mechanical power is given as:

$$P_s = \frac{P_{mec}}{(1-s)}$$
$$P_r = \frac{-sP_{mec}}{(1-s)} \tag{3.26}$$

Then, by dividing P_{mec} with mechanical rotor speed ($\Omega_m = \omega_m / p$), the produced electromechanical torque can be obtained.

$$T_{em} = P_{em} \cdot \frac{p}{\omega_m} \tag{3.27}$$

3.3.2. Reactive Power Balance

Reactive power is used to maintain the electrical and magnetic fields required by the alternating current equipment. In the occurrence of a grid fault, reactive power support is required to assist the grid voltage. This can be achieved by enhancing the reactive current supplied to the grid. DFIG supplies reactive power during transient conditions irrespective of the active power generation [44,45]. It acts as a capacitor and supplies reactive power to the grid when the voltage at point of common coupling (PCC) is below a specific range. On the other hand, as the voltage increases above a given level, it serves as an inductor and absorbs the reactive power from the grid.

The expression of stator and rotor reactive power can be written as:

$$Q_s = 3\,\mathrm{Im}\{v_s . I_s^*\}$$
$$Q_r = 3\,\mathrm{Im}\{v_r . I_r^*\} \tag{3.28}$$

Corresponding to active power, by substituting the stator and rotor voltage from Equation (3.1) in (3.19), the reactive power dependent on the parameters, currents, and slip of the machine can be obtained.

$$Q_s = 3\omega_s L_s |I_s|^2 + 3\omega_s L_m \, \mathrm{Re}\{I_r . I_s^*\}$$
$$Q_r = 3s\omega_s L_r |I_r|^2 + 3s\omega_s L_m \, \mathrm{Re}\{I_s . I_r^*\} \quad (3.29)$$

3.4. Mode of Operation of Doubly Fed Induction Machine

Doubly Fed Induction Machine (DFIM) has both the stator and the rotor windings that are connected to the grid and is capable of supplying power from both the stator and the rotor [39]. The significance of DFIG is that irrespective of the speed of the wind turbine rotor, it can sustain constant amplitude and constant frequency of output voltage at the grid value. Owing to this, the double-fed induction generator can be directly be connected to the AC power grid and can always be coordinated. Adjusting the frequency of AC voltage and current that is fed to the winding of the rotor is critical for regulating the speed of the rotor to resolve the distinction of wind speed.

The primary aspect of the double-fed induction generator is the versatility of its dual armature, by which the regulation of the power flow can conveniently be rendered between the machine and the grid. As a result, depending on the speed of the rotor and the power supply, DFIG is likely to work in the motor or generator, inducing four characteristic modes of operation. The power flow in the rotor of the double-fed induction generator has three components. These are a) the electromagnetic power exchanged between the stator and the rotor through the air gap regarded as the P_s air gap. (b) the mechanical power and P_m conveyed between the rotor and the shaft. (c) slip power P_r, which is transmitted between the rotor and some external source or load via the rotor slip rings. The rotor circuit will receive or deliver power to or from the grid based on whether the slip is positive or negative [46].

3.4.1. Sub-Synchronous Motor Mode

At a time when DFIM operates like a motor at sub-synchronous speed, the power (P_r) is provided to the grid via the rotor. Figure 3.9 demonstrates explicitly that the stator power is entering the machine while the rotor and the mechanical power are exiting the machine implying that the machine is receiving the stator power and supplying the rotor and mechanical power to the grid [44].

Note that depending on the sign of these powers, the operation of the machine can be described as a motor or a generator

- $s > 0, \quad \omega_m < \omega_s$
- $P_{mec} > 0$ (machine delivers mechanical power)
- $P_r < 0$ (machine delivers power via rotor)
- $P_s > 0$ (machine receives power via stator)

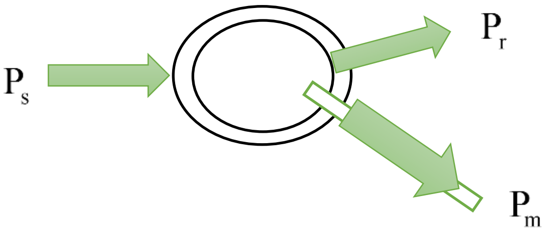

Figure 3.9 Power flow in sub-synchronous motor mode [45]

3.4.2. Super Synchronous Motor Mode

When DFIM performs like a motor at a super-synchronous speed, the power (P_r) is consumed by the machine. Figure 3.10 illustrates explicitly that the stator and rotor power is entering the machine, indicating that the machine absorbs both stator and rotor powers [44]. On the other side, mechanical power exits the machine suggesting that the machine delivers mechanical power to the grid.

- $s < 0, \quad \omega_m > \omega_s$
- $P_{mec} > 0$ (machine delivers mechanical power),
- $P_s > 0$ (machine receives power via stator)
- $P_r > 0$ (machine receives power via rotor)

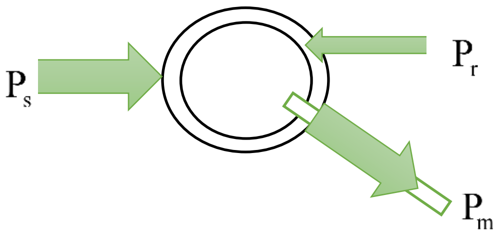

Figure 3.10 Power flow in super-synchronous motor mode [45]

3.4.3. Sub-Synchronous Generator Mode

Whenever the speed is below the synchronous speed, the generator functions at sub-synchronous mode with a positive slip. The sub-synchronous mode would allow the use of wind power at a lower wind speed. In this mode of operation, the power (P_r) is delivered to the machine.

Figure 3.11 elucidates the following:

- $s > 0, \quad \omega_m < \omega_s$
- $P_{mec} < 0$ (machine receives mechanical power)
- $P_r > 0$ (machine receives power via rotor)
- $P_s < 0$ (machine delivers power via stator)

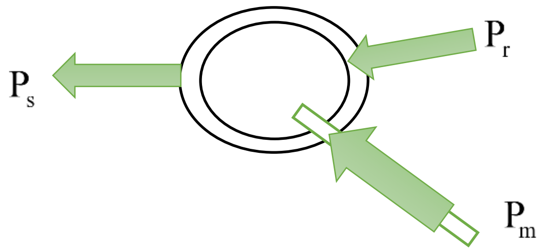

Figure 3.11 Power flow in sub-synchronous generator mode [45]

3.4.4. Super Synchronous Generator Mode

If the slip is a negative value, the system operates above the synchronous speed in the direction of the rotating field. Figure 3.12 indicates that whenever the speed is increased for a generator to operate in super-synchronous mode, the power changes direction and the rotor has a possible recovery power [45]. In this case, the power (P_s and P_r) is delivered to the grid through a stator and a rotor, and the slip power is converted to AC power through an inverter-converter combination

This mode of operation indicates

- $s < 0, \quad \omega_m > \omega_s$
- $P_{mec} < 0$ (machine receives mechanical power)
- $P_r < 0$ (machine delivers power via rotor)
- $P_s < 0$ (machine delivers power via stator)

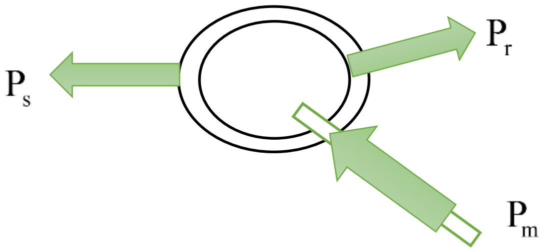

Figure 3.12 Power flow in super-synchronous generator mode

Remark, although DFIG can be operated as a generator and motor at both sub-synchronous and super-synchronous speeds, only generator mode at both speeds, is of particular relevance in wind power generation.

3.5. Power Converters

In wind power conversion systems, power converters are extensively used. These converters are used in variable-speed WECS to regulate both the speed/torque of the generator and the active/reactive power of the grid. The back-to-back voltage source converter with insulated-gate bipolar transistors is the most prevalent converter topology exploited in variable-speed wind turbines. These power converters are usually composed of a back-to-back (BTB) two-level PWM voltage fed current regulator converter that enables a bidirectional power flow and comprises of two VSC namely Rotor side converter (RSC) and grid side converter (GSC) [46].

These two converters are affiliated back-to-back, with a DC-link capacitor mounted between them as an energy storage system, to keep the voltage in the DC-link as small as possible and to provide the energy buffer demanded between the generator and the grid. One of the benefits of two-level back-to-back converters is their full power controllability (four-quadrant operation) with a simple structure and fewer components that lead to both efficient performance and low cost. Furthermore, it regulates the rotor current of the machine to accumulate the stator voltage to match the amplitude, frequency, and phase with the grid. To preserve a steady DC-link voltage, the power flow of the grid side converter must be regulated. on the other hand, the generator side control must be set to follow the magnetization requirements and the reference speed [46].

3.5.1. Rotor Side Converter (RSC)

The rotor side converter, which is connected to the grid side converter by a DC-link capacitor, regulates the active power and torque produced by the generator. It also can control the reactive power produced by the generator side of the stator by regulating the rotor current. The additional objective of the rotor-side converter is to control rotor currents in such a way that the rotor-side flux position is optimally aligned with the stator flux such that the desired torque is achieved at the shaft of the machine. It is also possible to control the speed of the generator and the power factor at the stator terminals [46-47] When the wind speed is low, the rotor-side converter uses an indirect speed controller to regulate the wind turbine output power by extracting maximum power. This converter operates in a stator flux d-q reference frame [46]. A very fast inner control loop regulates the direct and the quadrature component of the rotor current. The current setpoints are defined by the slower outer control loop regulating the active and reactive power.

3.5.2. Grid Side Converter (GSC)

The PWM converter, used as the grid side converter for wind power applications, has been extensively developed and validated in recent years due to its potential for almost instantaneous reversal of power flow, power factor management, and reduction of input/output harmonic distortion. The ultimate goal of the PWM grid (line) side converter is to maintain constant DC-link voltage, transmit the active power to the grid and facilitate the reactive power exchange between the grid and the converter as specified by the application requirements [47].

Though GSC transfers voltage and currents from DC to AC, the power exchange can be in all directions from AC to DC (rectifier mode) and from DC to AC (inverter mode). Whether it serves as an inverter or a rectifier, the power flow in the converter circuit is bidirectional: the power can flow from its DC side to the AC side, and vice versa [46]. The DC side voltage is shared with RSC on the contrary the AC side of GSC is connected to the power grid.

The GSC can absorb or deliver active power based on the DFIG mode of operation. Active power is supplied from the grid to the rotor side of DFIG through a back-to-back converter in sub-synchronous mode. During these circumstances, the GSC absorbs power from the grid and serves as a rectifier while the RSC extracts power from the GSC and transmits it to the AC for the rotor winding. In super-synchronous mode, the DFIG rotor delivers active power to the grid via the BTB converter. In this case, RSC derives input from the rotor while the GSC provides power to the grid and acts as an inverter [44,47].

The power rating of the GSC is mostly determined by the overall slip power, as it frequently functions at a unity power factor to eliminate losses in the converter. The reactive power support for the grid, which the DFIG wind power system is expected to provide, can be generated from the stator side of the DFIG through the control of RSC. The grid side converter can be utilized to increase the efficiency of the power grid. However, the capacity of the GSC is typically only $\pm 30\%$ of the capacity of the DFIG, which means that it requires a higher converter rating and, for this purpose, its reactive power output is restricted [44].

3.5.3. DC-Link Model

The DC-link capacitor is the connection between the grid side and the rotor side converters. It serves as a source of reactive power making it achievable to supply magnetizing current partially or entirely from the rotor side so that the stator side power factor can be regulated. The voltage in the DC-link capacitor must be adjusted so that power can be supplied from the rotor to the grid at constant voltage magnitude and frequency. An endeavor to store more active power in the capacitor will increase the voltage level of the capacitor. This DC-link capacitor is thus used to mitigate power variations to preserve a steady voltage in the terminals of the grid side converter [48]. The DC-link model also specifies the deviation of DC-link capacitor voltage as a function of the input power to the DC-link.

The amount of energy incorporated in the DC-link capacitor is as follow:

$$E_c = \int P dt = \frac{1}{2} C V_{dc}^{\ 2} \tag{3.30}$$

Where, P is the net power flow into the capacitor and is equal to $P_r - P_L$ (The rotor power inflow and the grid power outflow respectively), C is the DC-link capacitor, and V_{dc} is the capacitor voltage or the DC-link voltage. Figure 3.13 displays the blocked diagram of the dc-link system comprises of the line side (grid side), rotor side converters, and the dc-link capacitor [48].

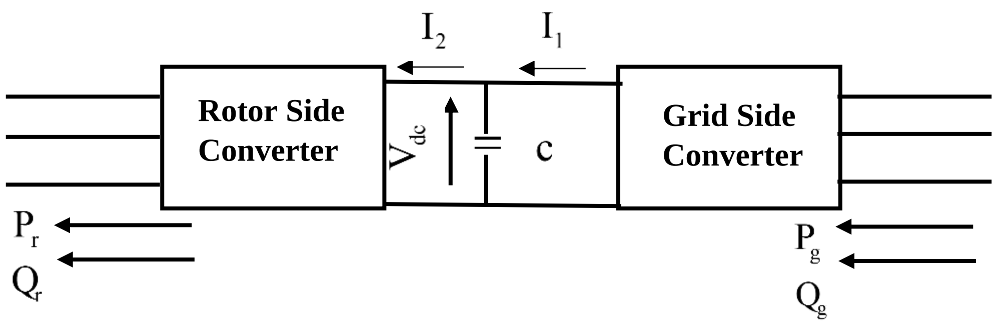

Figure 3.13 Power flow through the dc-link element

3.6. DFIG Under Normal Operating Condition

The stator and rotor windings of the DFIG are closely linked to the grid. The stator winding is directly linked to the grid whereas the rotor is connected to the grid via power converters. In normal operation, the RSC governs the speed of a generator to maximize energy extraction, whereas the GSC regulates the DC-link voltage to maintain a constant value. However, the maximum energy is captured only when the wind speed is less than the rated speed. If the wind speed exceeds the nominal, the blade pitch angle is controlled to restrict the energy captured from the wind so that it does not surpass the nominal characteristic of the generator, and the rotor side converter (RSC) controls the speed of the generator to a fixed point [49].

The controller implemented in this thesis work is vector control with a synchronous rotating reference frame. During the steady-state condition, the RSC controller regulates the stator active power/torque and reactive power via the d-axis and q-axis rotor current components. In this case, the control objectives are met by taking the stator flux-oriented reference frame into account. The primary goal of the GSC controller is to retain a steady dc-link voltage irrespective of the direction of rotor power flow [49]. To accomplish this, a vector control approach with a reference frame oriented along the stator voltage vector position is engaged. In this control technique, the direct axis (d-axis) and quadrature axis (q-axis) rotor currents are controlled to keep the DC-link voltage constant and to regulate the reactive power flow between the grid side converter and the grid. In this vector control system, all voltage and current quantities are converted to a reference frame that rotates at the same rate as the source voltage, with the direct axis (d-axis) reference frame aligned to the supply voltage vector [50].

3.7. DFIG Under Grid Fault Condition

Grid faults are characterized as deviations from the nominal operational state of the grid. Faults on the grid side terminal are known as open circuits or short circuits. A temporary short circuit can be distinguished from a permanent short circuit. Temporary type results in brief interruptions, such as an insulator flashover, which are cleared by tripping one or more circuit breakers. Permanent faults, on the other hand, are caused by a prolonged disturbance, such as falling debris on the grid, such as a tree, or snowfall, triggering a short circuit among the phases. A short circuit fault can be both symmetrical and asymmetrical [39, 50]

Symmetrical faults, also known as three-phase balanced faults, are power system faults in which the three phases are adversely affected. Insulation failure may occur as a consequence of device over-voltage or under-voltage caused by lighting or switching spikes, insulation contamination, or other physical causes. Asymmetrical faults, on the other hand, are unbalanced faults between one or two of the three phases that are typically caused by mechanical contact as a result of weathering on the transmission line [39]. Several studies on voltage swell caused by both symmetrical and asymmetrical faults have been conducted, but they are beyond the scope of this thesis. This thesis work is based on voltage dips induced by symmetrical and asymmetrical faults, with a greater emphasis on symmetrical faults.

DFIG has increased in popularity since it employs a lightweight and low-cost power converter. These machines are controlled by a converter connected to the rotor, with a power that is only a small fraction of the stator power, approximately equal to the slip. As a consequence of these considerations, the properties of DFIG are relevant for wind turbines. Nonetheless, as the penetration of wind energy expanded, the downside of standard DFIG became more evident. As a short circuit occurs, the voltage at the terminal decreases and the stator and rotor fluxes of the generator is decreased, enabling the generator to demagnetize. As a result, the active power and electromagnetic torque are diminished. The reduction in electromagnetic torque would place mechanical tension on the drive train, causing it to act like a bent torsion spring. Moreover, if the voltage dip is not rapidly compensated by the rotor voltage, a high current transient emerges at the stator, and the stator disruption is transferred to the rotor due to magnetic coupling between the stator and rotor winding. The high rotor current can damage the converters if no protection is used. The voltage drop, on the other hand, prohibits the GSC from transmitting the whole power from the rotor to the grid. As a result, the excess energy will quickly charge the dc-bus capacitor, resulting in a high DC bus voltage [50].

The rotor side converter can be utilized to compensate for rotor current changes by increasing the rotor voltage reference, to preserve the flux linkage within the rotor winding constant. The generator, on the other hand, has a rotor voltage limit, which means that the converter supplying the rotor will only provide 30% of the supply voltage. Because of this constraint, the converter approaches its limit quickly and, as a result, loses the ability to control the generator during a fault [50]. As a consequence, a protection strategy known as crowbar and

BESS is employed in this thesis work to protect the converters from high stator and rotor current and to maintain DC-link voltage constant, thereby, enhancing FRT capability.

3.8. FRT Capability Enhancement Methods

Grid operators, who are in charge of maintaining power system reliability and stable power supply, have established grid integration standards for wind power generation. According to the German Grid code, when a short circuit fault occurs at a grid terminal, the grid voltage should be restored quickly without disconnecting the generator from the grid. Similar requirements can be found in different country specifications such as Italy, Denmark, Spain, and the Netherlands [39].

This grid requirement was enforced by the grid operators because demanding the generator to be disconnected during different types of fault conditions could result in extreme voltage instability at network locations with high penetration levels. This ensures that when failures in the transmission infrastructure occur, such as short-duration voltage sags, all grid-connected renewable energy sources must ride through such a situation to guarantee the consistency and reliability of transmitting a high degree of wind power into the network [50]. Fault ride-through refers to the capability of the generator to stay attached to the grid during voltage dips and swells. Various researches have been conducted on both low voltage ride through and high voltage ride through. However, since this thesis work focuses on voltage dip rather than voltage swell, fault ride through implies only to low voltage ride through (LVRT). When a transient failure incident occurs, LVRT provisions mandate generation facilities to maintain contact to the grid network to provide post fault voltage [50]. Taking all of the preceding into account, this section describes the two FRT schemes used in this thesis work to improve the transient response of DFIGs-based wind turbines.

3.8.1. Crowbar Protection

The DFIG based wind power plants are extremely sensitive to grid disruptions, particularly voltage dips. As faults occur and cause voltage dips, control is briefly lost, enabling the current flowing through the power converter to rise. During this situation, crowbar protection is activated to protect the system from over-currents caused by loss of control. The crowbar creates a low resistance path, isolating the RSC and ensuring that the entire rotor currents circulate through it as shown in Figure 3.14 [51]. Once the stator and rotor currents decay and the power converters gain control of the machine, the crowbar is deactivated.

The timing of the deactivating crowbar and the value of the series resistor in commercial DFIG exhibit critical effects on converter safety and system recovery. This indicates that early removal of the crowbar does not fulfill the purpose of converter protection, whereas delayed removal results in higher absorption of reactive power from the grid [52]. Crowbar resistance has a major effect as well, with a high value causing a large peak of electromagnetic torque and a low value causing large currents during a voltage dip. As a result, the acceptable value of crowbar resistance is considered appropriate as a balance between certain objectives based on DFIG efficiency and grid code enforcement. The main concern with this protection method is that prolonged use of the rotor crowbar results in loss of torque control and the DFIG to operate as a squirrel cage induction machine and draw stator side magnetization. This results in a high-slip reactive power demand, which degrades stator voltage.

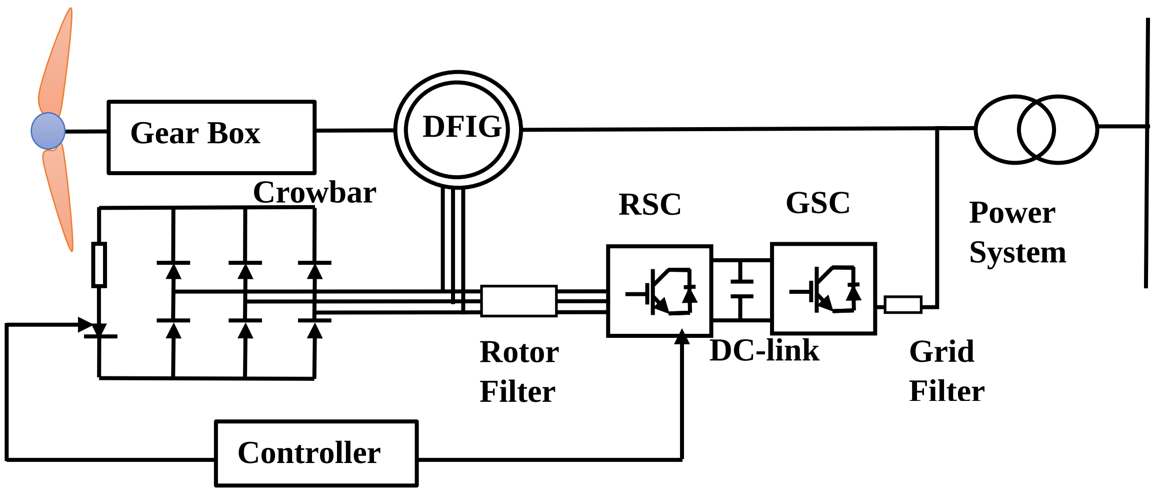

Figure 3.14 Crowbar protection system

3.8.2. Battery Energy Storage System

According to recent research in the renewable energy field, incorporating wind power plants with energy storage systems is an approach to strengthen the technological performance of wind power plants as well as increasing the revenue of these systems [53]. Energy storage technologies may control power output, thus mitigating the detrimental impact of renewable energy indeterminacy. A research work of [54] compares various forms of Energy Storage System (ESSs) technologies. Among the many emerging energy storage systems, such as a flywheel, pump hydro, capacitor, super-capacitor, and compressed air energy storage, BESS provides greater versatility in terms of power, siting facility, and quick response to accommodate the expectations of storage device applications. Several researchers have also proposed that a battery energy storage device is an appropriate option for merging with wind turbines to enhance efficiency [53]. Battery energy storage systems (BESS) are being implemented in cooperation with DFIG to increase efficiency and thus encounter energy demand, resulting in a significant increase in the capabilities of wind power systems to provide ancillary services such as DC-link voltage control.

Under normal operating conditions, the rotor of the DFIG delivers power to the grid through the converter when the rotational speed is greater than the wind speed. Even so, at higher wind speed, the output power produced is greater than the average power. As a result, the extra power is stored in the battery, allowing it to charge. When the rotational speed is lower than the wind speed, the rotor side of the DFIG receives active power from the grid through the BTB converter, with the GSC acquiring power from the grid and functioning as a rectifier. However, with the implementation of BESS, this situation could be improved in such a manner that when the wind speed is low, the battery discharges, releasing power to the rotor side of the machine to sustain the average power feed to the grid. As a result, it is possible to guarantee that the electricity supplied to the grid side is still consistent, contributing to an efficient and stable supply of electrical power to the grid [55].

During a fault, a voltage dip at the grid terminal prohibits the grid side converter from transferring power to the grid. Thus, excess energy is deposited in the DC-link capacitor, resulting in DC-link overvoltage. To prevent this issue, BESS is integrated with a crowbar to maintain a DC-link voltage constant. Furthermore, as mentioned in previous sections, the main drawback of the crowbar system is that, while it protects the RSC by ensuring that high currents circulate through it, machine control is lost due to RSC inhibition, and the DFIG operates like a squirrel cage induction generator, only absorbing reactive power from the grid, resulting in grid voltage degradation. As a result, integrating BESS with crowbar protection is crucial since during a failure, the stored energy in the battery discharges, supplying power to the GSC [55].

CHAPTER FOUR:

CONTROL SYSTEM FOR DOUBLY FED INDUCTION GENERATOR

4.1. Introduction

Wind turbine technology is well recognized for its variable wind speed. Wind speed variations may cause torque to fluctuate, resulting in mechanical stress in the drive train if an effective control mechanism is not applied. As a result, in a wind energy conversion device, adequate control properties are crucial for optimizing machine performance [42,50]. The overall variable speed wind turbine control approach is divided into two main control levels: wind turbine control level and DFIG control level. In this chapter, the control of wind turbines, doubly-fed induction generators, and principles associated with back-to-back converters are investigated, with an emphasis on rotor side and grid side controllers, as well as DC-link voltage control. Moreover, the model and control of the battery energy storage system are extensively discussed [43].

4.2. Wind Turbine Control

Various scholars studied the wind turbine control level as explained in detail in Chapter Two. The goal of the wind turbine control level is to optimize and limit power. This is accomplished through the use of two cross-connected controls, speed control, and a power controller. By adapting the generator speed by a rotor magnetizing current with the wind speed/reference speed, the speed controller achieves the optimum energy. The power controller, on the other hand, aims to restrict the generator power at rated power and above wind speeds. This is achieved by altering the angle of pitch based on the actual power generated [56].

4.2.1. Pitch Angle Control

Differences in blade pitch concerning the wind direction or rotation plane are substantially influencing the power coefficient. Slight variation in the pitch angle, the angle between the chord line of the blade and the plane of rotation, can have a dramatic effect on the output power. The turbine should produce the maximum power in low to moderate wind speeds with the help of speed control, such that the pitch angle does not generally have to be varied. To produce maximum power, the angle of a pitch should be at its optimum value. However, in the case of wind speed operating beyond a rated value, the electrical torque cannot increase more than a certain value since it results in overload on the converters or generators. Thus, there ought to be an approach to restrict the extracted power from the wind, and this is conceivable through adjustment of pitch angle. Pitch control offers a compelling method for managing the streamlined force and loads delivered by the rotor so it does not surpass as far as possible. Also, this controller allows independent control of each propeller usually through hydraulic actuators. This permits the reduction of the tension generated in the entire system [56].

4.2.2. Maximum Power Point Tracking Control

At the point when the wind speed is over the cut-in speed and below the rated speed, the speed control is fundamental as it ceaselessly adjusts the speed of the rotor to sustain the tip speed ratio steady at the level that provides ideal power coefficient and high proficiency. It is essential to acquire the greatest energy from wind energy utilizing distinctive maximum power point tracking (MPPT) control strategies to accomplish viable, compelling, remarkable, and powerful wind energy sources. MPPT controls are utilized to draw the maximum power from the wind energy conversion system employing a combination of generators. The rotor rotational speed fluctuates relatively with the wind speed. Thus, to extract maximum power, the rotational speed must always rotate at optimum speed. Maximum power point tracking is employed for the purpose to extract maximum power by maintaining the rotor rotational speed with the adjustment in wind speed, to maintain the tip speed ratio at its optimal value. Thus, the wind turbine is controlled at the ideal turbine rotational speed by the regulator, concerning the current wind speed. Additionally, a few strategies are utilizing the relationship between the electromagnetic torque and the maximum power to indirectly adjust the rotor speed to the optimal value under different wind speeds [56].

The speed control strategy used in this thesis work is indirect speed control. In the indirect speed control strategy, the behavior of rotational speed depends on the mechanical coupling, and the mechanical coupling dynamics are not canceled out, inciting a fixed soft response of the system. The indirect speed control relies upon the association between the electromagnetic torque and the angular velocity, nonetheless, the relationship between the electromagnetic torque and the angular velocity does not have a direct dynamic relation due to the inertia involved. This controller moreover modifies the d-q frame currents to command the back-to-back converters allowing controllability of slip angle which also affects the speed and the torque of the generator [56].

4.3. Doubly Fed Induction Generator Control

When generating energy from a wind turbine, a control system is essential for maintaining the magnitude of the generator, as well as magnitudes related to the grid side converter for the proper and efficient generation of energy. The control of DFIG and power converters is used both in balanced and unbalanced grid voltage conditions. In this thesis work, vector control of DFIG in the synchronous reference frame is employed. Among the control strategies for grid-connected converters, this control technique is widely adopted. It has high accuracy, simple implementation parameters, a good dynamic response under normal and faulty operating conditions, and a fixed switching frequency [57-58]. The presence of a fault in the grid terminal creates a voltage disruption, which leads to a high inrush current, which could endanger the converters if appropriate countermeasures are not applied. Consequently, for this purpose, this controller is essential to control the high current of the rotor and the stator as well as the active and reactive power. Based on the characteristics of the power grid, such grid voltage fluctuations can be of a diverse range of nature, such as voltage dips, voltage swells, imbalances, and harmonics [58]. However, the most hazardous and regularly occurring disturbance, often resulting in the disconnection of wind turbines, is the voltage dip.

4.3.1. Rotor Side Control

The main role of the RSC control is to regulate the active and reactive power separately by controlling the quadrature and the direct axis rotor current. It is also capable of providing fundamental magnetization power to the generator via the rotor circuit [57]. For the intention of decoupling the rotor quantity power, the standardized expressions for the DFIG can be streamlined by availing a reference frame associated with the stator flux (i.e., $\psi_{ds} = |\overrightarrow{\psi_s}|, \ \psi_{qs} = 0$).

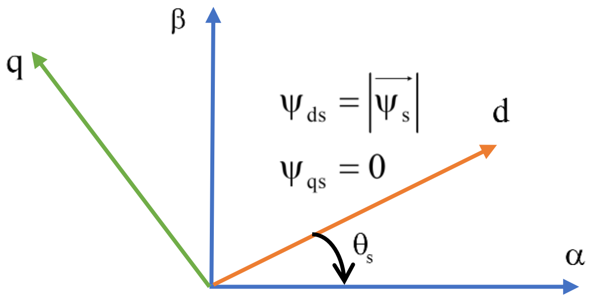

Figure 4.1 Vector control of the d-q reference aligned with stator flux space vector [58]

Considering stator flux orientation, the relationship between the current and the fluxes can be expressed as follow:

$$\begin{aligned} \psi_{ds} &= \psi_s = i_{ds}L_s + i_{dr}L_m \\ 0 &= i_{qs}L_s + i_{qr}L_m \end{aligned} \quad (4.1)$$

From the above equation, the relation between stator and rotor current is obtained

$$\begin{aligned} i_{ds} &= \frac{1}{L_s}(\psi_s - L_m i_{dr}) \\ i_{qs} &= -\frac{L_m}{L_s} i_{qr} \end{aligned} \quad (4.2)$$

The correlation between the rotor flux and currents is

$$\begin{aligned} \psi_{dr} &= \frac{L_m}{L_s}\psi_{ds} + \sigma L_r i_{dr} \\ \psi_{qr} &= \sigma L_r i_{qr} \end{aligned} \quad (4.3)$$

Where, σ is $(1-\frac{L_m^2}{L_s})$

In the absence of a small drop in stator resistance, the voltage of the stator and the relationship between the voltage of the rotor and the current can be expressed as follows:

$$\begin{aligned} v_{ds} &= 0 \\ v_{qs} &= v_g = \omega_s \psi_s \end{aligned} \quad (4.4)$$

$$\begin{aligned} v_{dr} &= R_r i_{dr} - \omega_r \sigma L_r i_{qr} + \sigma L_r \frac{d}{dt} i_{dr} \\ v_{qr} &= R_r i_{qr} + \omega_r \sigma L_r i_{dr} + \sigma L_r \frac{d}{dt} i_{qr} \end{aligned} \quad (4.5)$$

The equations below demonstrate that, under the stator flux orientation, the independent control of the active and reactive powers is possible through the direct and quadrature rotor currents. The active and reactive power of the stator as well as the electromagnetic torque, which is governed directly by the quadrature current, can be formulated as:

$$P_s = -\frac{3L_m}{2L_s}(v_{qs} i_{qr}) \tag{4.6}$$

$$Q_s = \frac{3v_{qs}}{2L_s}(\psi_{ds} - L_m i_{dr}) \tag{4.7}$$

$$T_e = -\frac{3}{2} p \frac{L_m}{L_m}(\psi_{ds} i_{qr}) \tag{4.8}$$

The RSC control comprises two cascaded control systems, namely the inner control loop and the outer control loop. The inner current control loops are used for controlling the d axis and q-axis rotor currents and the outer control loops are used to control the active and reactive power on the stator. To achieve reasonable control over the RSC, both these controllers must be designed and tuned with considerable accuracy [57]. The subsequent sections discuss the inner and outer loop control systems in depth.

4.3.1.1. Inner Loop Control

The inner control loop has a significant advantage for the protection of the DFIG. It can naturally protect the system from over-current since current limiters can easily be inserted into the control system. For controlling the inner loop different controllers might be used. However due to its simplicity, the most widely used is the proportional-integral (PI) controller.

The PI controller is adopted in the rotor circuit of DFIG for effective control of the direct and quadrature rotor currents as well as adequate control of both the damping and the bandwidth of the inner loop. One of the benefits of the PI controller is it increases the speed of response eliminating the steady-state error and converges to a solution in a shorter time. A comparison of different controllers with PI controllers can be found in [59]. The PID controller, when compared with the PI controller, has a poor performance for an integral process and a large time delay process. Moreover, it cannot incorporate ramp-type setpoint change and slow disturbance. If the sampling time is small, the PID controller severely fluctuates shortening the life of the actuator. Because of the aforementioned reasons, the proportional-integral (PI) controller which is usually adopted with stator flux orientation is analyzed.

The relationship between the rotor voltage and the rotor currents in equation 4.9 is used to calculate the PI regulator parameters

$$\begin{aligned} v_{dr} &= R_r i_{dr} - \omega_r \sigma L_r i_{qr} + \sigma L_r \frac{d}{dt} i_{dr} \\ v_{qr} &= R_r i_{qr} + \omega_r \sigma L_r i_{dr} + \sigma L_r \frac{d}{dt} i_{qr} \end{aligned} \tag{4.9}$$

From equation 4.9, if it is assumed that:

$$\begin{aligned} e_1 &= -\omega_r \sigma L_r i_{qr} \\ e_2 &= \omega_r \sigma L_r i_{dr} \end{aligned} \tag{4.10}$$

Then the voltage equation in equation 4.9 can be written as:

$$\begin{aligned} v_{dr} &= R_r i_{dr} + \sigma L_r \frac{d}{dt} i_{dr} + e_1 \\ v_{qr} &= R_r i_{qr} + \sigma L_r \frac{d}{dt} i_{qr} + e_2 \end{aligned} \tag{4.11}$$

From equations 3.46 and 3.47, the plant model includes the voltage drop in the transitory inductance σL_r, cross-coupling from the orthogonal loop, and the emf induced by the stator flux.

By simplifying the above equations and expressing them in their current form:

$$\begin{aligned} i_{dr} &= \frac{(v_{dr} - e_1)}{R_r + s\sigma L_r} \\ i_{qr} &= \frac{(v_{qr} - e_2)}{R_r + s\sigma L_r} \end{aligned} \tag{4.12}$$

Furthermore, the plant for the current control loop is written as:

$$N(s) = \frac{i_{dr}}{v_{dr}} = \frac{i_{qr}}{v_{qr}} = \frac{1}{R_r + s\sigma L_r} \tag{4.13}$$

The following are the direct and quadrature rotor current control loop forms:

$$\begin{aligned} v_{dr} &= (R_r + \sigma s L_r) i_{dr} = (K_{pI} + \frac{K_{iI}}{s})(i_{dr}^* - i_{dr}) \\ v_{qr} &= (R_r + \sigma s L_r) i_{qr} = (K_{pI} + \frac{K_{iI}}{s})(i_{qr}^* - i_{qr}) \end{aligned} \tag{4.14}$$

The transfer function between the reference and real currents is written as follows:

$$\frac{i_{dr}}{i_{dr}^{*}} = \frac{i_{qr}}{i_{qr}^{*}} = \frac{sK_{pI} + K_{iI}}{s^2 + \frac{s(R_r + K_{pI})}{\sigma L_r} + \frac{K_{iI}}{\sigma L_r}} \quad (4.15)$$

As a result of equating the transfer function denominators to the second-order standard denominator of classical control theories, the constant PI controllers can be obtained.

$$s^2 + \frac{s(R_r + K_{pI})}{\sigma L_r} + \frac{K_{iI}}{\sigma L_r} = s^2 + 2\xi\omega_n s + \omega_n^{\,2} \quad (4.16)$$

The value of K_{pI} and K_{iI} will be:

$$K_{pI} = 2\omega_n * \sigma L_r - R_r$$
$$K_{iI} = \omega_n^{\,2}\sigma L_r \quad (4.17)$$

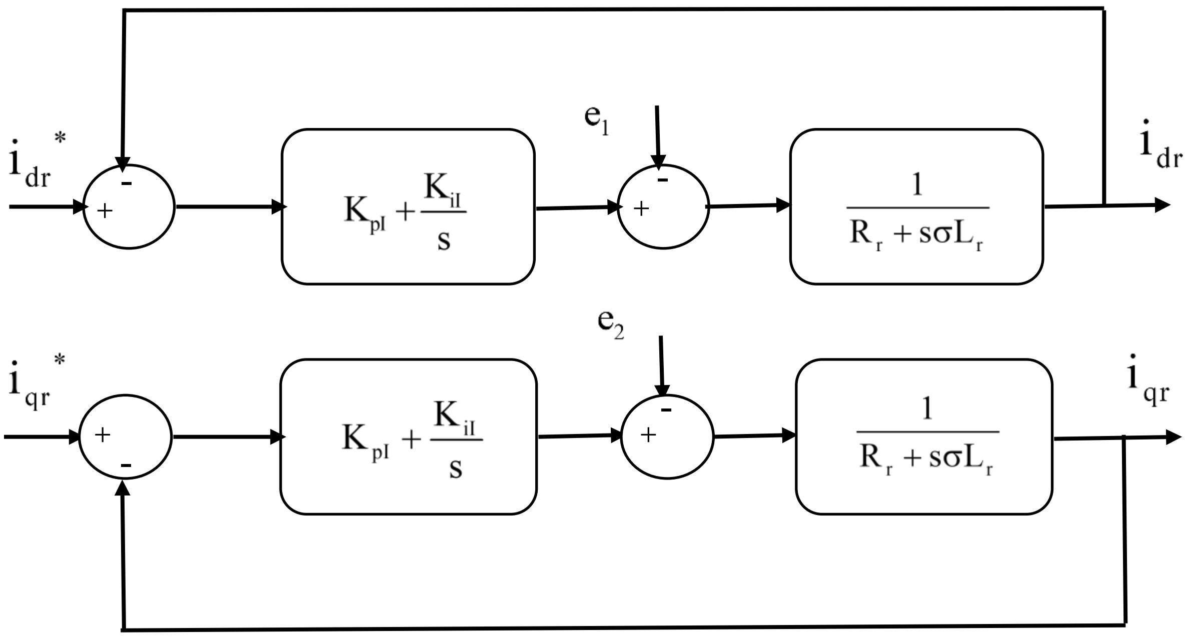

Figure 4.2 Inner loop current control [58]

4.3.1.2. Outer Loop Control

In contrast to the squirrel cage induction machine, which utilizes the rotor-oriented reference frame, the DFIG employs a stator flux-oriented reference frame. This indicates that the direct component is aligned to the flux of the stator (Ψ_{qs} = 0 and V_{ds} = 0). The stator flux of DFIG can be assumed to be a constant provided by the grid voltage because the stator winding of the machine is directly integrated into the grid [57-58].

As a function of stator flux and rotor current, the torque expression is given as

$$T_{em} = -\frac{3}{2} p \frac{L_m}{L_s} \left| \overrightarrow{\psi_s} \right| i_{qr} \\ = K_{opt} i_{qr} \tag{4.18}$$

Where, K_{opt} is the optimal constant-coefficient which is set to boost the extracted power. According to the equation above, the q component of rotor current is proportional to torque, implying that the torque and thus the speed can be regulated by controlling i_{qr}.

The dynamic equation for the rotor speed of the machine is:

$$\frac{d}{dt}\omega_m = \frac{p}{Js}(T_m - T_e - c_f \omega_m) \tag{4.19}$$

The equation can be written as follows if the power coefficient (c_f) is ignored and the PI regulator is used:

$$\frac{Js}{p}\frac{d}{dt}\omega_m = (T_m - T_e) = K_{p\omega m} + \frac{K_{i\omega m}}{s}(\omega_m{}^* - \omega_m) \tag{4.20}$$

The transfer function between the reference rotor speed and the actual rotor speed is given in the same way as the inner loop rotor currents:

$$\frac{\omega_m}{\omega_m{}^*} = \frac{sK_{p\omega m} + K_{i\omega m}}{(J/p)s^2 + sK_{p\omega m} + K_{i\omega m}} \tag{4.21}$$

The value of $K_{p\omega m}$ and $K_{i\omega m}$ is PI control parameters of the rotor speed which is achieved by equating the transfer functions denominators to the second-order standard denominator of classic control theories:

$$(J/p)s^2 + sK_{p\omega m} + K_{i\omega m} = s^2 + 2\xi\omega_n s + \omega_n{}^2 \tag{4.22}$$

The value of $K_{p\omega m}$ and $K_{i\omega m}$ is:

$$K_{i\omega m} = \omega_n{}^2 * \frac{J}{p} \\ K_{p\omega m} = 2\omega_n * \frac{J}{p} \tag{4.23}$$

The stator reactive power expression in d-q is:

$$Q_s = \frac{3}{2}(v_{qs}I_{ds} - v_{ds}I_{qs}) = \frac{3}{2}v_{qs}I_{ds} \tag{4.24}$$

As noted earlier, the direct component of voltage will be equal to zero due to the alignment of the direct component to the stator flux. This is mostly due to a 90^0 shift in voltage and flux.

By substituting the voltage and current equation from equation 3.16 and 3.17 to 4.24, assuming the stator flux as constant and neglecting losses in the stator resistance

The stator reactive power is expressed as:

$$Q_s = \frac{3}{2}\frac{\omega_s}{\sigma L_s}\left(\psi_{ds}{}^2 - \frac{L_m}{L_r}\psi_{ds}\psi_{dr}\right) \tag{4.25}$$

By differentiating equation 4.25 with respect to time

$$\frac{d}{dt}Q_s = -\frac{3}{2}\frac{\omega_s}{\sigma L_s}\frac{L_m}{L_r}\psi_{ds}\frac{d}{dt}\psi_{dr} \tag{4.26}$$

Solving the above equation in terms of $\frac{d}{dt}\psi_{dr}$

$$\frac{d}{dt}Q_s = -\frac{3\omega_s L_m \psi_{ds}}{2\sigma L_s L_r}\left(v_{dr} - R_r i_{dr} - \sigma L_r(\omega_m) i_{qr}\right) \tag{4.27}$$

Rewriting the above equation

$$\frac{2\sigma L_s L_r}{3\omega_s L_m \psi_{ds}}\frac{d}{dt}Q_s = -\left(v_{dr} - R_r i_{dr} - \sigma L_r(\omega_m) i_{qr}\right) \tag{4.28}$$

Let $\frac{2\sigma L_s L_r}{3\omega_s L_m \psi_{ds}} = N$

By incorporating a PI controller

$$N\frac{d}{dt}Q_s = \left(K_{pQ} + \frac{K_{iQ}}{s}\right)\left(Q_s^* - Q_s\right) \tag{4.29}$$

The transfer function between the reference and real currents is written as follows:

$$\frac{Q_s}{Q_s^*} = \frac{1/N(sK_{pQ} + K_{iQ})}{s^2 + 1/N(sK_{pQ} + K_{iQ})} \tag{4.30}$$

Where, K_{pQ} and K_{iQ} are the controller parameters for PI controller for controlling the stator reactive power and is obtained by equating the denominator of the transfer function to the second-order standard denominator of classical control theories.

$$K_{pQ} = 2\omega_n N$$
$$K_{iQ} = \omega_n{}^2 N \tag{4.31}$$

The d-axis and q-axis rotor currents are used to control the active power/torque and reactive power exchange with the grid. The d-axis rotor current is used to regulate reactive power exchange with the grid, which is set to zero in normal operation. When the measured d-axis rotor current is compared to the reference value, an error is generated and sent to the PI controller. The PI controller eliminates steady-state error and provides a reference value for the d component voltage. The q-axis rotor current, on the other hand, is used to regulate the speed/torque using MPPT strategies. The indirect speed control system provides the torque reference value, which is then divided by K_{opt} to generate the q-axis rotor current reference value. The actual and reference rotor current values are compared, and the difference is sent to another PI controller, which determines the reference voltage for the q components [57]. This d-q reference voltage is converted to a two-phase stationary reference frame using a suitable vector transformation $e^{j(\theta s - \theta r)}$.

Where, θ_s and θ_r are the positions of the stator and rotor voltage space vectors, respectively. It is necessary to achieve θ_r for reference frame transformation. So, first, 90^0 is subtracted from the estimated angle to get the angle of the stator voltage space vector.

$$\theta_v = \tan^{-1}\left(\frac{v_\beta}{v_\alpha}\right)$$
$$\theta_s = \theta_v - 90^0 \tag{4.32}$$
$$\theta_r = \theta_s - (p.\theta_m)_{elec}$$

The rotor angle can therefore be calculated in this manner. The voltage is then transformed back to the three-phase using a suitable vector transformation known as the park transformation.

4.3.2. Grid Side Control

The purpose of GSC is to maintain a constant DC-link voltage for the RSC and, if necessary, to provide reactive support to the grid. The GSC controls the DC bus voltage, which is shared with the RSC. The alternating current (AC) of the GSC is connected to the power grid. Depending on the DFIG operating mode, GSC may receive or deliver active power. As a result, the GSC is in charge of both coordinating the power flow between the GSC and the grid and adjusting the DC-link voltage for the RSC [44].

A vector-control technique with a reference frame oriented along the grid voltage vector position is used, allowing autonomous control of the active and reactive power flowing between the grid and the grid-side converter. The d-axis current is used to regulate the DC-link voltage and the q-axis current is used to regulate the reactive power in the PWM voltage source converter. The inverter is attached to the grid through an RL filter; it is placed after the DC bus and has two fundamental functions: to maintain constant DC bus voltage regardless of the magnitude and direction of power flow through it and to ensure a sustainable power factor at the power grid connection point [58].

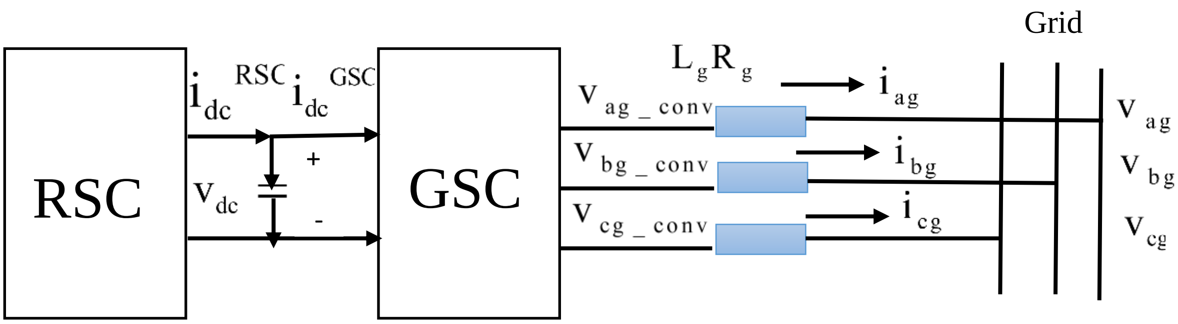

Figure 4.3 The grid system [58]

An optimum three-phase balanced voltage model is used to represent grid voltage. To model the three-phase system, three autonomous but similar single-phase systems can be used. As a result, the balance across the inductor is as follows:

$$\begin{bmatrix} v_{ag} \\ v_{bg} \\ v_{cg} \end{bmatrix} = R_g \begin{bmatrix} i_{ag} \\ i_{bg} \\ i_{cg} \end{bmatrix} + L_g \frac{d}{dt} \begin{bmatrix} i_{ag} \\ i_{bg} \\ i_{cg} \end{bmatrix} + \begin{bmatrix} v_{ag\_conv} \\ v_{bg\_conv} \\ v_{cg\_conv} \end{bmatrix} \tag{4.33}$$

Where, i_{ag}, i_{bg}, i_{cg} indicates the three-phase grid-side converter currents [A], v_{ag}, v_{bg}, v_{cg} are the three-phase grid voltages [V], $v_{ag\_conv}, v_{bg\_conv}, v_{cg\_conv}$ are the three-phase grid-side converter voltages [V], R_g and L_g are the inductor resistance [Ω] and inductance [H] respectively.

By using Clark transformation, the above equation can be expressed in a two-phase stationary reference frame (α, β).

$$v_{\alpha g} = R_g i_{\alpha g} + L_g \frac{di_{\alpha g}}{dt} + v_{\alpha g\_conv}$$
$$v_{\beta g} = R_g i_{\beta g} + L_g \frac{di_{\beta g}}{dt} + v_{\beta g\_conv} \quad (4.34)$$

The corresponding equation is obtained through Park transformation (α, β to d-q)

$$v_{dg} = R_g i_{dg} + L_g \frac{di_{dg}}{dt} - \omega_e L_g i_{qg} + v_{dg\_conv}$$
$$v_{qg} = R_g i_{qg} + L_g \frac{di_{qg}}{dt} + \omega_e L_g i_{dg} + v_{qg\_conv} \quad (4.35)$$

Where, v_{dg}, v_{qg} are the grid voltages [V] in d-q axis, v_{dg_conv}, v_{qg_conv} are the grid-side converter voltages [V] in d-q axis, i_{dg}, i_{qg} are the grid-side converter currents [A] in d-q axis, ω_e is the electrical angular velocity of the grid voltage [rad/s].

The active and reactive power flow between the grid and the grid side converter is denoted as:

$$P_g = 1.5\left(v_{dg} i_{dg} + v_{qg} i_{qg}\right)$$
$$Q_g = 1.5\left(v_{qg} i_{dg} - v_{dg} i_{qg}\right) \quad (4.36)$$

The angle of the grid voltage is required for voltage and current coordinate transformations. The angular position of the supply voltage is computed as follows:

$$\theta_e = \int \omega_e dt = \tan^{-1}\left[\frac{v_{\beta g}}{v_{\alpha g}}\right] \quad (4.37)$$

4.3.2.1. Inner Control Loop

The vector control with reference frame aligned along the grid voltage vector position is depicted in Figure 4.4 [58]. In this alignment, the quadrature component of grid voltage is zero, and the direct component of grid voltage is constant.

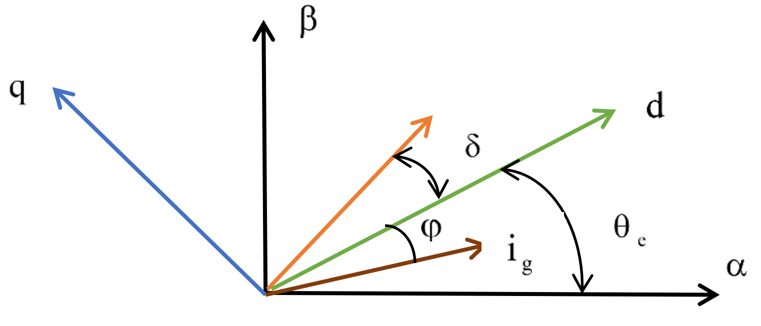

Figure 4.4 d-q reference frame aligned with the grid voltage

The system equations, based on the alignment of the reference frame along with the grid voltage, is represented as:

The active and reactive power

$$
\begin{aligned}
P_g &= 1.5\left(v_{dg}.i_{dg}\right) \\
Q_g &= -1.5\left(v_{dg}.i_{qg}\right)
\end{aligned} \tag{4.38}
$$

The grid voltage equation is obtained in a quite similar way as the RSC control

$$
\begin{aligned}
v_{dg} &= \left(R_g + L_g \frac{d}{dt}\right) i_{dg} \\
v_{qg} &= \left(R_g + L_g \frac{d}{dt}\right) i_{qg}
\end{aligned} \tag{4.39}
$$

For the current control loops, the plant model is given by:

$$
\frac{i_{dg}}{v_{dg}} = \frac{i_{qg}}{v_{qg}} = \frac{1}{R_g + L_g s} \tag{4.40}
$$

As a consequence, using a PI controller, it is possible to design a feedback loop and PI controller to produce the reference value of voltage in the current control regulatory formula as follows:

$$
\begin{aligned}
v_{dg} &= \left(R_g + L_g s\right)\left(K_{p\_Ig} + \frac{K_{i\_Ig}}{s}\right)\left(i_{dg}{}^{err}\right) \\
v_{qg} &= \left(R_g + L_g s\right)\left(K_{p\_Ig} + \frac{K_{i\_Ig}}{s}\right)\left(i_{qg}{}^{err}\right)
\end{aligned} \tag{4.41}
$$

Where, $i_{dg}{}^{err} = i_{dg}{}^{*} - i_{dg}$ and $i_{qg}{}^{err} = i_{qg}{}^{*} - i_{qg}$

The grid side converter closed-loop transfer function with PI controller is as regards:

$$
\frac{i_{dg}}{i_{dg}{}^{*}} = \frac{i_{qg}}{i_{qg}{}^{*}} = \frac{\left(\dfrac{1}{L_g}\right)\left(sK_{p\_Ig} + K_{i\_Ig}\right)}{s^2 + s\left(\dfrac{K_{p\_Ig} + R_g}{L_g}\right) + \dfrac{K_{i\_Ig}}{L_g}} \tag{4.42}
$$

Where, K_{p_Ig} and K_{i_Ig} are the controller parameters for the PI controller for controlling the grid current and is achieved by equating the denominator of the transfer function to the second-order standard denominator of classical control theories.

$$
\begin{aligned}
K_{p\_Ig} &= 2\omega_{n\_Ig} L_g - R_g \\
K_{i\_Ig} &= (\omega_{n\_Ig})^2 L_g
\end{aligned} \tag{4.43}
$$

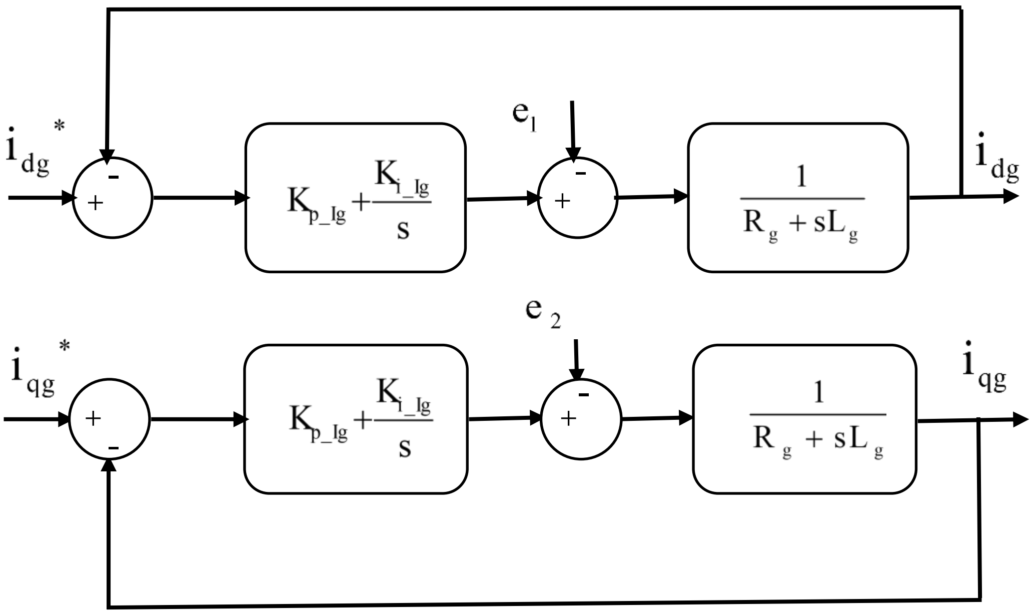

Figure 4.5 Grid side inner loop control [58]

4.3.2.2. Outer Control Loop

The control of the power exchanged by the converter is used to adjust the DC-link voltage. The DC-link voltage level is increased or reduced by drawing more or less power from the grid concerning what the DC link requires, thereby varying the value of the reference for the AC inner current control loops. The outer loop of the GSC is the DC-link voltage loop, and the inner loop is the current control loop. Because the primary goals of the outer loop are optimum regulation and stability, the outer loop may be intended to be slightly slower. Inner loops, on the other hand, are designed to accomplish quick settling times [50,58].

The DC-link voltage, as shown in Figure 3.13 which is dependent on the current flowing through the capacitor, is computed as:

$$v_{dc} = \frac{1}{c_{dc}} \int i_c dt \tag{4.44}$$

The power and current equations of DC-link are:

$$\begin{aligned} i_{dc} &= c\frac{dv_{dc}}{dt} = i_{dc}{}^{RSC} - i_{dc}{}^{GSC} \\ cv_{dc}\frac{dv_{dc}}{dt} &= P^{RSC} - P^{GSC} \end{aligned} \tag{4.45}$$

The transfer function for grid side converter DC bus voltage is regulated in the same way as GSC inner loop control.

$$cs\ v_{dc} = \left(K_{p\_vdc} + \frac{K_{i\_vdc}}{s}\right)\left(v_{dc}^{*} - v_{dc}\right) \tag{4.46}$$

$$v_{dc}\left(cs + \left(K_{p\_vdc} + \frac{K_{i\_vdc}}{s}\right)\right) = \left(K_{p\_vdc} + \frac{K_{i\_vdc}}{s}\right)v_{dc}^{*} \tag{4.47}$$

Finally, the outer loop transfer function is

$$\frac{v_{dc}}{v_{dc}^{*}} = \frac{sK_{p\_vdc} + K_{i\_vdc}}{s^2c + sK_{p\_vdc} + K_{i\_vdc}} \tag{4.48}$$

Where, K_{p_vdc} and K_{i_vdc} are the controller parameters for the PI controller for controlling the DC bus voltage.

These parameters are obtained by equating the denominator of the transfer function to the second-order standard denominator of classical control theories.

$$\begin{aligned} K_{p\_vdc} &= 2\omega_n.c \\ K_{p\_vdc} &= (\omega_n)^2.c \end{aligned} \tag{4.49}$$

4.4. Battery Model

The battery has become one of the most relevant researched elements in recent years given the enormous role in power system engineering, especially in renewable energy plants such as wind power. Different types of batteries are clarified and contrasted in [54]. In this study, a Lithium-ion battery is used since it has a low density and a broad standard electrode potential, culminating in batteries with low weight and a high operating voltage. This battery has low self-discharge, no memory effect, and long life for deep cycle applications. These properties have also proved to be beneficial for electric vehicle traction, power tools, and the conservation of intermittently available renewable energy [54]. A standard BESS arrangement includes battery banks and a DC/AC power conversion device. The storage device/battery bank is critical for regulating frequency and voltage. The storage device is made up of a series and parallel connection of batteries. Figure 4.6 depicts the battery equivalent circuit [15].

Where, v_b is the battery terminal voltage, E_{oc} is the open-circuit voltage which is directly related to the state of charge and R_s is the equivalent resistance of series/parallel-coupled batteries, the value of which depends on the attachment conditions and the number of batteries.

The R_b and C_b parallel circuit is used to define the stored energy and voltage during charging and discharging. R_b is paired in parallel with C_b to simulate a self-discharging of battery. Since the battery is an energy storage device, its energy is estimated in kWh. When a capacitor is used to model a battery cell, the capacitance can be calculated using the following equation.

$$C_b = \frac{(Kwh).3600x10^3}{0.5(v_{oc\_max}{}^2 - v_{oc\_min}{}^2)} \tag{4.50}$$

Where, v_{oc_max} and v_{oc_min} are the maximum and minimum voltage across battery capacitance, respectively.

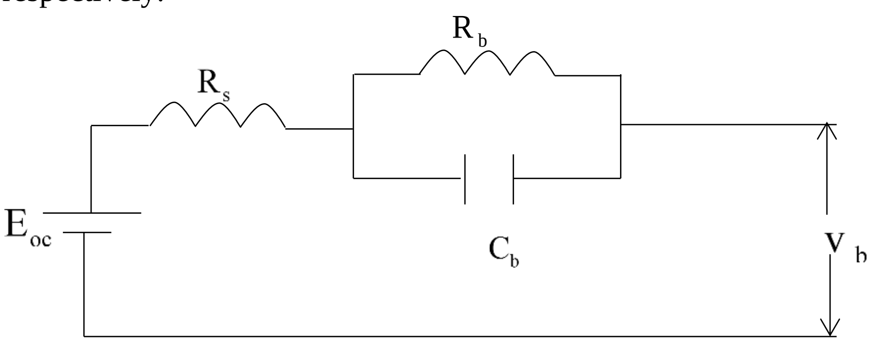

Figure 4.6 Thevenin equivalent circuit of BESS

When modeling the battery, two important factors need to be considered: the state of charge and the depth of discharge. It is advised that the battery never be discharged to less than 50% of its capacity. The battery is the most commonly used unit for energy storage in a variety of applications since it retains energy in an electrochemical form. The characteristics of the rechargeable battery are given by:

$$v_b = E_{oc} - r_b i_b - k\frac{Q}{Q - \int i_b dt} + A\exp(-B\int i_b dt) \tag{4.51}$$

$$SOC = 100\left(1 - \frac{\int i_b dt}{Q}\right) \tag{4.52}$$

Where, E_{oc} is the open circuit potential (V), K is the polarization voltage (V), Q is the battery capacity (Ah), r_b is the internal resistance of the battery, A is the exponential voltage (V), and B is the exponential capacity (Ah).

The direction of power flow signifies BESS power output which indicates that the battery is discharging if i_b is positive and charging if i_b is negative.

4.5. Battery Energy Storage System Control

Transient frequency stabilization, increased reliability, peak shaving, transmission congestion management, performance power leveling, ramp rate monitoring are all potential BESS services. By controlling BESS active power production, it is possible to enhance output power fluctuation control, frequency control, and peak shaving. Governing BESS reactive power production, on the other hand, allows for reactive power reinforcement, voltage modulation, and low voltage ride-through [60].. The core objective of this segment is to provide a thorough overview of BESS applications as a storage element in renewable energy integrated power systems for retaining constant DC bus voltage and enhancing low voltage ride-through capability.

4.5.1. Frequency Control

Energy storage systems (ESS) are widely used to assist renewable energy system such that they can be used as a buffer to offset the power imbalance between sources and loads to counteract the impacts of voltage, power, and frequency volatility and minimize the detrimental influence of intermittent sources [55-60]. As the grid frequency deviates from the nominal value, frequency regulation is enabled. The frequency deviation is:

$$\Delta f = f_{ref} - f_{grid} \tag{4.53}$$

Frequency management can be aided by the installation of active power from a battery energy storage system, which enables wind systems to become more effective in high wind conditions or low power demand circumstances by retaining surplus energy. In the occurrence of frequency drop caused by grid disconnection, the kinetic energy of the wind turbine, along with the power from the BESS, is delivered to the system via the DFIG converters [55]. To prevent BESS activity during minor frequency changes and to comply with grid code the dead band is used.

When a frequency variation occurs, the response of a generating unit to this variation is characterized by its droop. Droop is a percentage that relates the active power output and change in frequency and is obtained from Equation:

$$\text{Droop} = 100\left(\frac{\Delta f}{\Delta p}\right) = R \tag{4.54}$$

The operation of the droop control in the case of DFIG for frequency control is rendered by adjustments in the active output power during the disturbance. As the power grid is disrupted, the frequency variation reduces the DFIG rotor speed and releases the kinetic energy contained in the rotary mass, reducing the generator power output. The power needed by droop control is derived from the BESS power, which is then injected into the electrical system by the GSC. The value of R governs the power value injected by the BESS [55].

4.5.2. DC Link Voltage Control

During the steady and transient states of the DFIG wind energy conversion system, the battery energy storage system supports the DC-link capacitor. The battery, following a power converter, aids in maintaining a steady DC-link voltage. The converter is in charge of regulating the DC-link by controlling the battery current. During an interruption, as the strong stator current triggers the DC-link voltage to rise, all of the extra energy in the DC-link capacitor will be deposited in the battery, and it begins to charge. When the crowbar safety is triggered, causing the DFIG to consume power from the battery, the BESS discharges, guaranteeing that the grid has a reliable supply of electric power. In general, as the DC-link voltage rises, the battery begins to charge, and when the DC bus voltage falls, the battery provides power [62].

4.5.3. Active and Reactive Power Control

The Simulink Model for BESS regulation is illustrated in Appendix D. The active and reactive power control involves comparing the actual value of active and reactive power at the BESS output terminal to the active and reactive power reference obtained from the frequency and voltage controller [62].

The resultant active power difference is paired with the signal id, which is the difference between the charge controller input and the output current on the d-axis and fed to a PI controller. A PI controller then generates the active current reference on the d-axis. The difference between the reference voltage value and the voltage at the BESS connection stage is fed into another PI controller, which produces a reactive current reference on the q-axis. In the PQ controller, the difference between the charge controller input and the output current on the q-axis is applied to the reactive power difference. Nevertheless, since the primary objective of this study is to obtain constant DC-link voltage, active power is prioritized over reactive power by the dead band and lower gain for reactive power activation [62].

4.5.4. Charge Control

Based on the available state-of-charge of the battery and the incoming current reference value of the d-axis, the charge controller produces a charging/discharging signal [61-62]. The control mechanism will first track the wind speed through the DFIG rotor speed and will intervene when the minimum rotational speed needed to maintain the system stabilized is surpassed. The control is enabled whenever the rotational speed of DFIG exceeds the optimum wind speed required to generate power. The control first requests the battery state of charge (SOC), If SOC is less than SOCmax, the monitor checks to see if the DFIG is in super synchronous mode ($\omega_r > \omega_s$). If the response is valid, the battery begins charging using the power that flows through the converter. When the DFIG is in sub-synchronous mode ($\omega_r < \omega_s$), the battery discharges to retain a steady DC-link voltage without consuming grid power. The battery cannot be charged if the SOC is higher than the SOCmax and cannot be discharged if the SOC is less than the SOCmin. If SOC = SOCmax, power from the machine is injected into the grid [55,62].

CHAPTER FIVE:

RESULT AND DISSCUSION

5.1. Introduction

In this chapter, simulation analysis is carried out using MATLAB/SIMULINK software to examine the performance of DFIG based WT during the normal and fault conditions. Furthermore, during a fault state, simulation results are evaluated using the existing capacitor bank, crowbar protection circuit, and crowbar protection integrated with BESS to improve the operating performance of the machine and fulfill grid code specifications. The parameters used to model the machine are listed in Appendix A.

5.2. Model Description

In this section, the simulation models of DFIG are presented. The simulation models are designed using MATLAB/SIMULINK 2015a. The model shown in Figure 5.1 contains the generator, power converters, wind turbine, transformer, crowbar, BESS, and so on. The type of wind turbine employed is a variable-speed wind turbine with partial-scale power converters commonly known as the Doubly Fed Induction Generator. The specification of the generator (with a rated power of 1.5MW) used to run the model is obtained from the ADAMA-II wind farm. DFIG has an AC/DC/AC Insulated-Gate Bipolar Transistor (IGBT)-based Pulse Width Modulation (PWM) converter with a switching frequency of 4Khz. The modulation index, which is the ratio of the amplitude of modulated sinewave to the amplitude of triangular carrier wave, is less than one. This will mitigate harmonic distortion from occurring in the output waveform. The stator winding is connected directly to the 50 Hz grid while the rotor is connected to the grid through the AC/DC/AC converter. The back-to-back two-level PWM converter has two converters, one is connected to the rotor side (RSC) and another is connected to the grid side (GSC). With a vector control method implemented the RSC is used to control the active and reactive power while the GSC is used to maintain a constant DC-link voltage. This model additionally incorporates a crowbar protection system as well as BESS for improving FRT capabilities or machine performance in transient conditions.

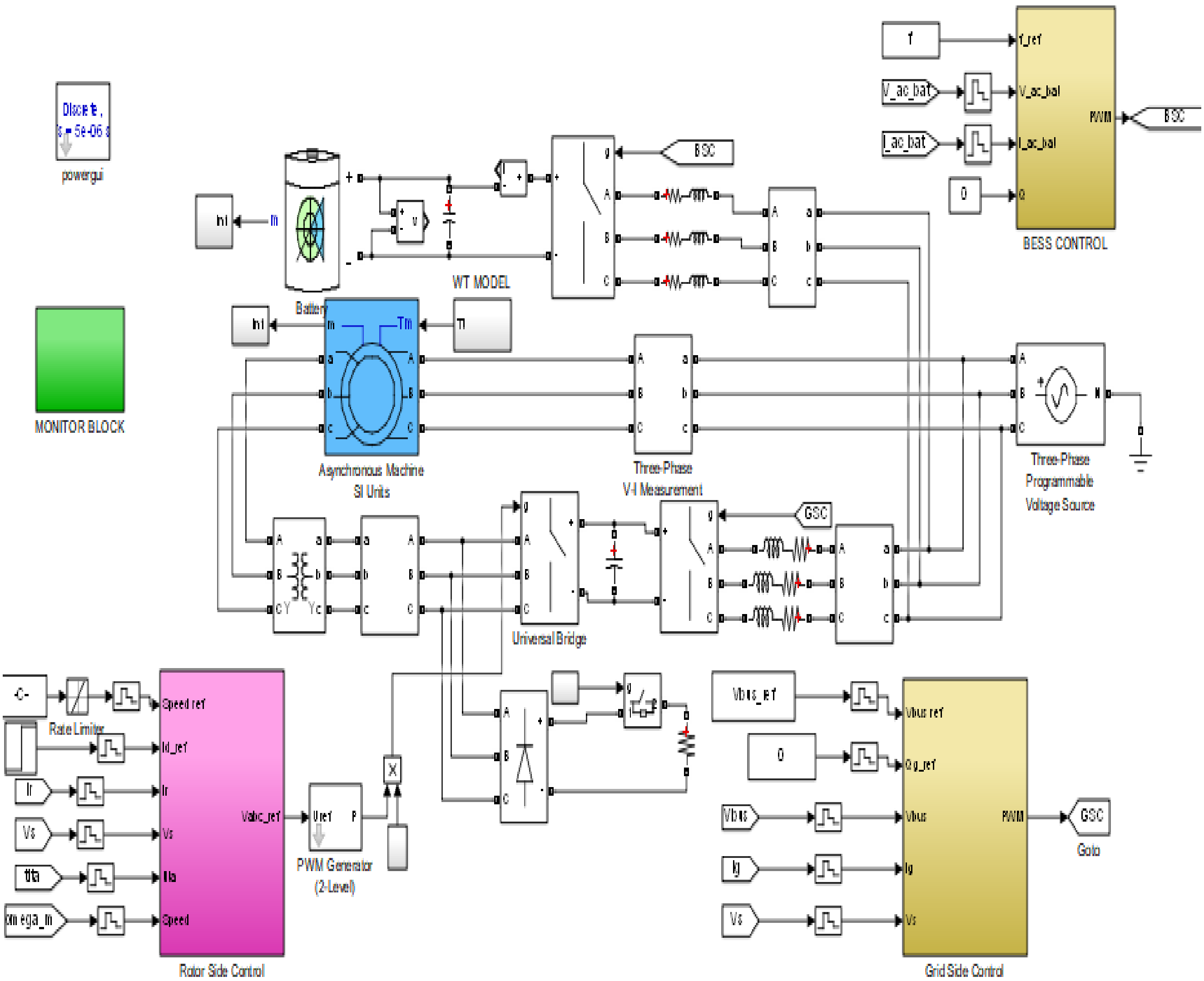

Figure 5.1 The complete Simulink model of the system

5.2.1. Rotor Side Converter Control Model

Figure 5.2 illustrates the RSC control Simulink model during a symmetrical fault condition. The control model is carried out by using reference frame theory which is clearly explained in Appendix B. To reduce the complexity of the model first the three-phase is converted to a two-phase stationary reference frame using Clark transformation and then the two-phase stationery is converted to a two-phase rotating reference frame using Park transformation. As clearly discussed in Chapter Four, the RSC has an inner and outer control loop. The inner control loop is in charge of controlling the currents while the outer control loop controls the speed/torque of the machine. As observed in the model the maximum power point tracking method is used to track the maximum power from the wind and provides the torque reference value. The reference value of torque is then divided by K_{opt} to generate the q-axis rotor current reference.

The actual and reference rotor current values are compared, and the difference is sent to another PI controller, which determines the reference voltage for the q components. The actual value of the d-axis rotor current is compared to the reference value and an error is sent to the PI regulator. The PI controller eliminates the steady-state error and generates a reference voltage for the d-component. The generated d-q reference voltage is converted to a two-phase stationary reference frame and then to a three-phase by using a suitable vector transformation.

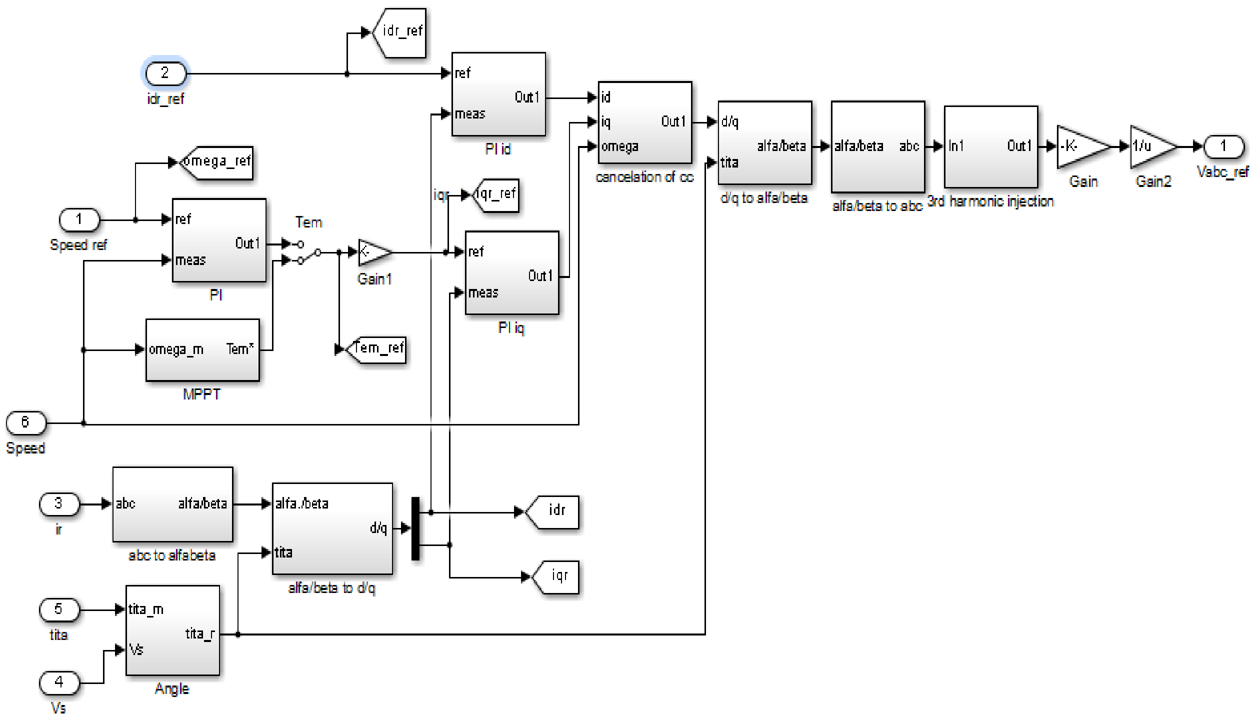

Figure 5.2 RSC control Simulink model

5.2.2. Grid Side Converter Control Model

The GSC is in charge of maintaining the DC-link voltage constant. The GSC has an inner and outer control loop, similar to the RSC, with the inner control loop managing currents and the outer loop controlling DC-link voltage. The actual and reference DC-link voltage values are compared, and the error is sent to the PI regulator, which eliminates the error and provides the d-axis current reference value. The PI controller compares the d-axis and q-axis grid current reference and actual value and provides the d-axis and the q-axis reference voltage. The inverse Park and Clark transformation is used to convert the d-axis and q-axis to three-phase utilizing transformation theory.

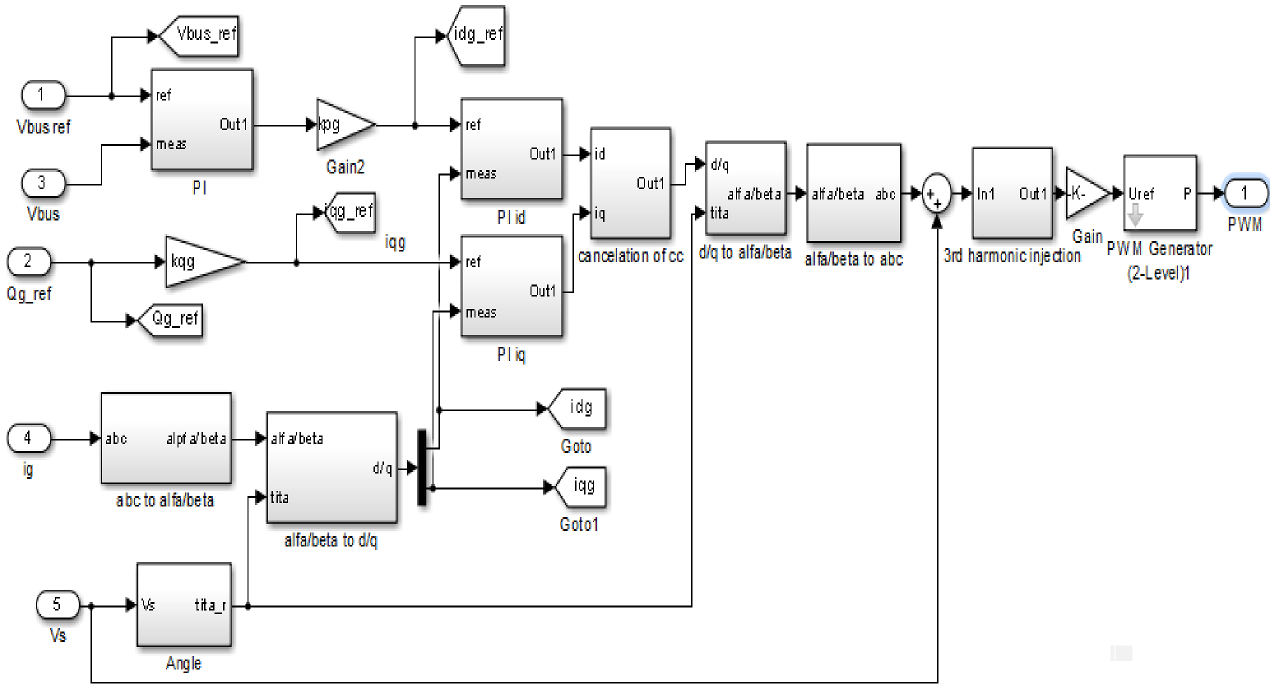

Figure 5.3 GSC control Simulink model

5.2.3. BESS Control Model

In Figure 5.4, the control model for a Battery Energy Storage System is depicted. In section 4.5, the control over each of the model's parameters is discussed in depth.

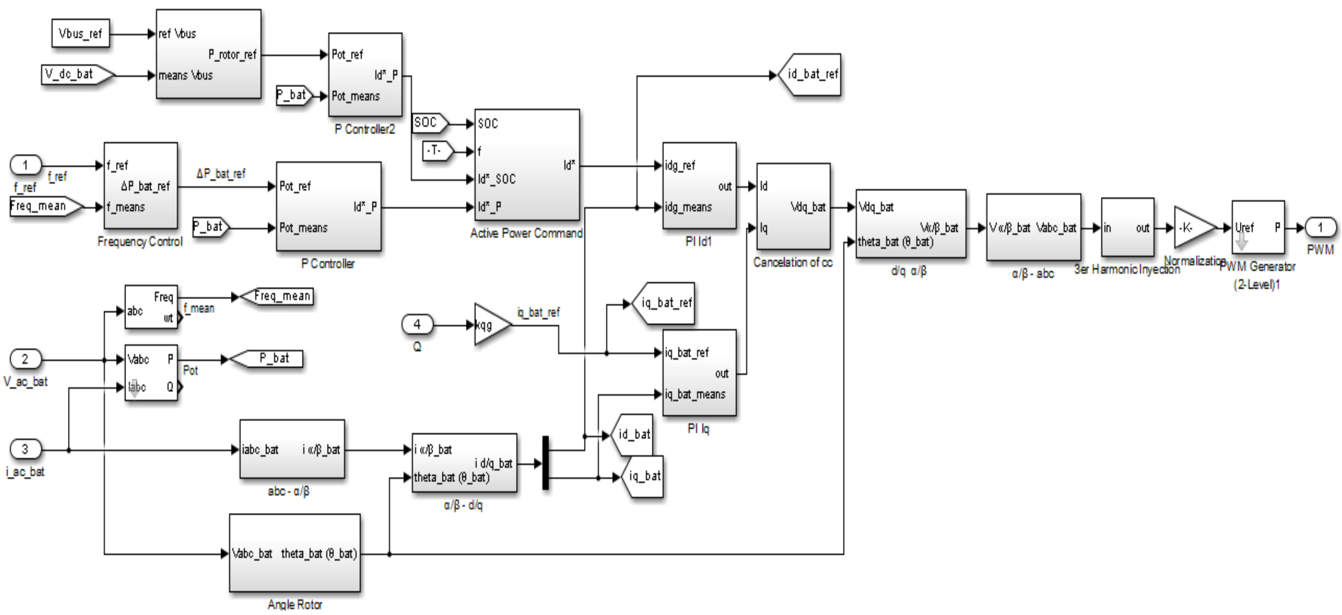

Figure 5.4 BESS control Simulink model

5.2.4. RSC and GSC Control Model During Asymmetrical Fault

During asymmetrical fault analysis, the RSC and GSC control models change slightly from those used in symmetrical fault analysis. The induced voltages in the rotor circuit in the case of an asymmetrical fault are composed of three terms: positive, negative, and zero sequences. The negative natural flux that occurs at the stator during a voltage dip induces harmonic pulsation, torque fluctuation, and saturation in the rotor converter. As a result, a vector control system is used to control the variables of the machine. In symmetrical analysis, only a positive sequence was taken into account while regulating currents, but in asymmetrical analysis, both the positive and negative sequences must be taken into consideration when modeling the control system. Furthermore, to guarantee that each sequence is adequately regulated, it is necessary to manage the negative and positive sequences separately [45]. Figure 5.5 and Figure 5.6 depict the RSC and GSC control models during an asymmetrical fault condition.

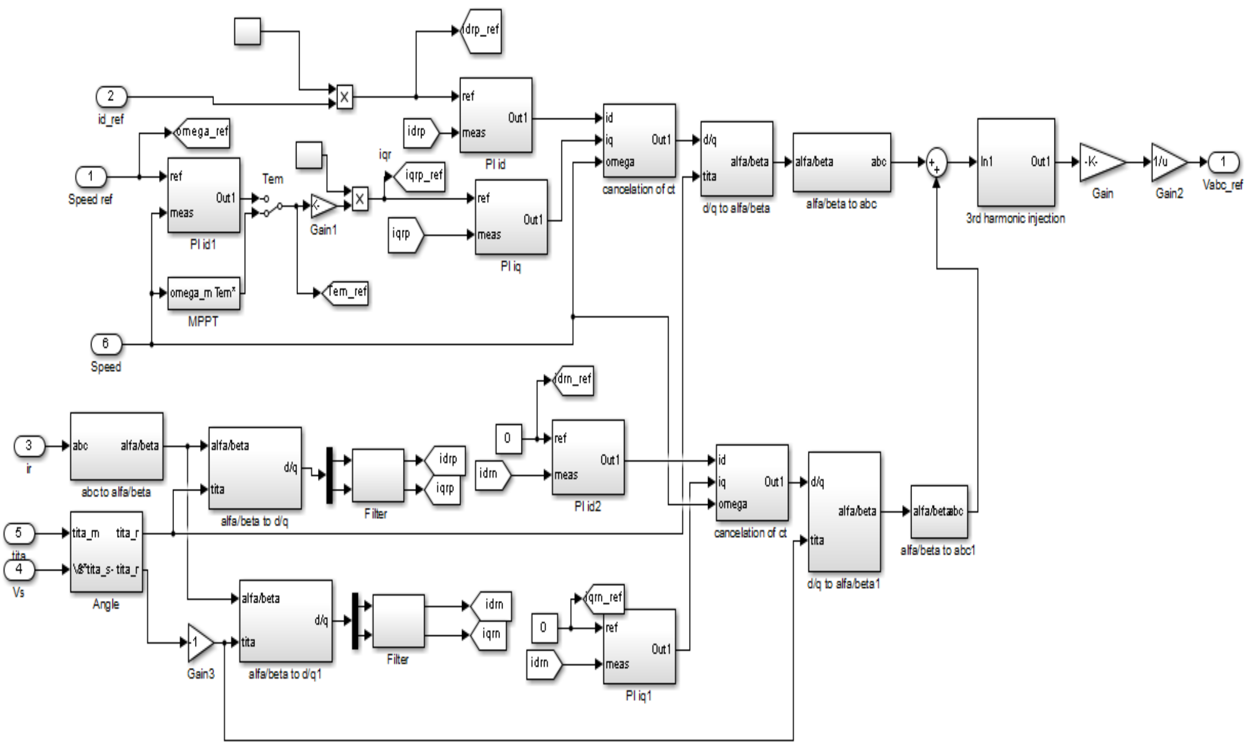

Figure 5.5 RSC control Simulink model

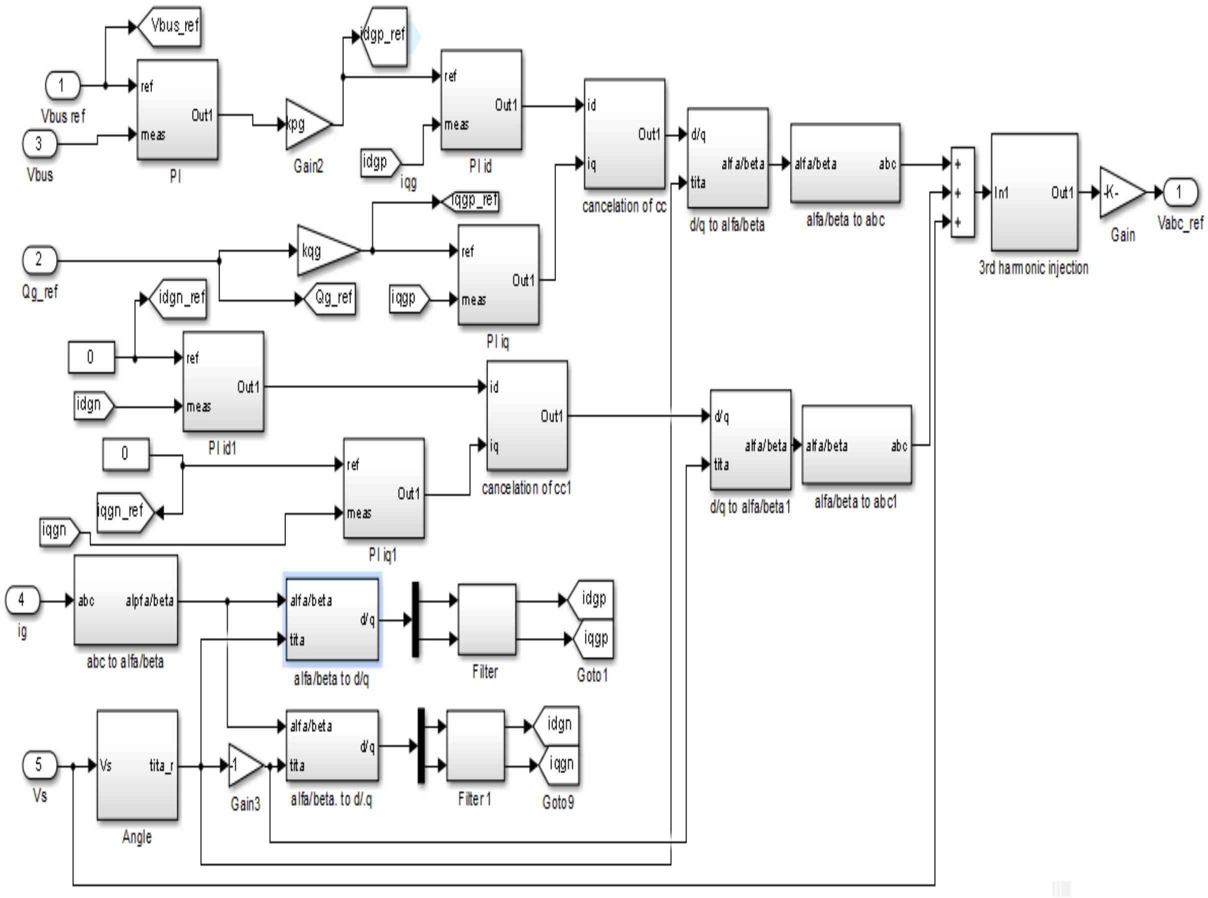

Figure 5.6 GSC control Simulink model

5.3. Under Normal Operating Condition

Under normal operating conditions, the rotor side converter is used to control the speed of the machine, electromagnetic torque, and active and reactive power. The field-oriented regulation of DFIG is implemented in a synchronous rotating d-q reference frame with a direct axis aligned with the stator flux vector. Owing to this alignment, the active power/torque and reactive power are controlled by the quadrature and direct rotor current respectively. Moreover, the direct component of stator voltage and the quadrature component of stator flux are zero. Whereas, the quadrature component of flux and direct component of voltage is constant. The grid side converter, on the other hand, is used to maintain a steady DC-link voltage and to provide reactive power as required by the grid. A vector-control technique with a reference frame aligned along the grid voltage vector position is used in the GSC case, meaning that the direct component of stator voltage is constant and the quadrature component of stator voltage is zero. The d-axis current is used to regulate the DC-link voltage and the q-axis current is used to regulate the reactive power in the PWM voltage source converter [58].

5.3.1. RSC Under Normal Condition

As previously stated, during the steady-state condition, the RSC control is used to regulate the speed and torque of the machine. Moreover, the RSC control of the system is performed with a stator flux-oriented vector control. Figure 5.7 demonstrates that the stator voltage is balanced and operating at a steady-state. Figure 5.8 indicates that the rotor speed is in normal operating condition, and the torque simulation result indicates that the machine is in generator mode. The applied wind speed varies from 8m/s to 10m/s, with the speed increasing to 10m/s after 4 seconds. As the wind speed varies the rotor speed also varies in rpm. This indicates that the rotor speed varies in proportion with the wind speed. When the wind speed increases, the stator, and rotor currents are observed to operate at steady-state and to be synchronized, as shown in Figure 5.9. The variation of rotor current at 4-5 sec occurred due to the variation of speed that is performed at 4 sec. However, this variation is eliminated after 5 sec by the control system and the rotor current becomes balanced. Figure 5.10 indicates a steady rotor current across d-axis and q-axis. The d-axis rotor current has a value of zero since no reactive power is required for compensation (Qs=0). Hence, the machine is operating at a unity power factor. The q-axis rotor current, on the other hand, is controlled following its reference value. As stated in Chapter Four The q-axis rotor current is regulated in proportion to the torque due to the stator flux alignment. The indirect speed control MPPT requires that the torque follow its reference value.

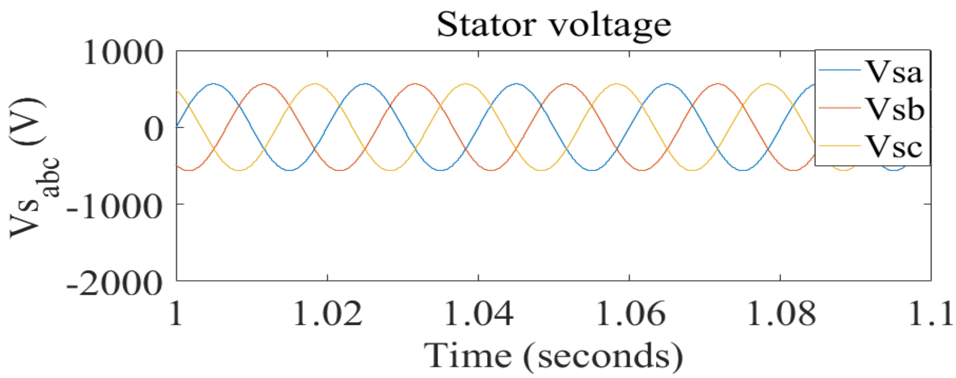

Figure 5.7 Stator voltage

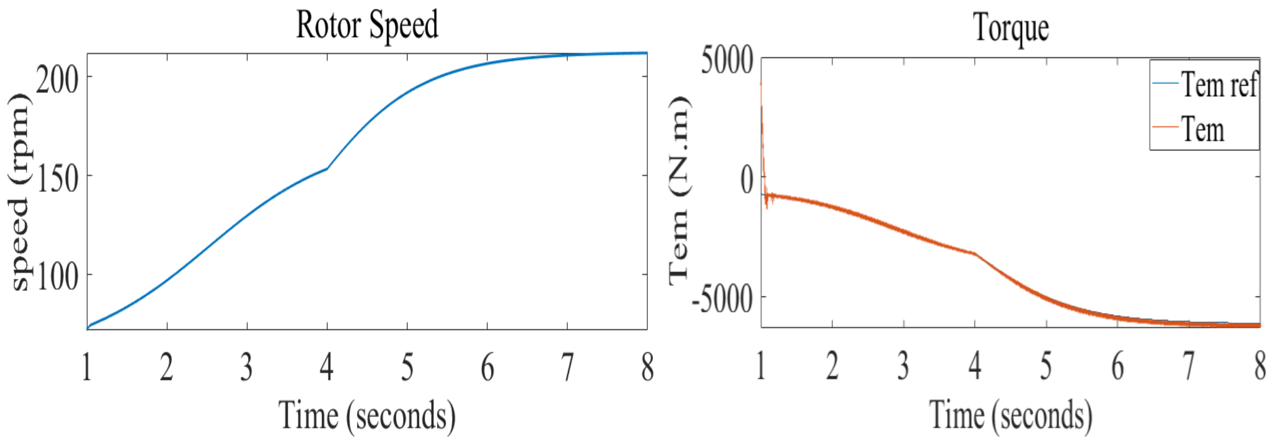

(a) Rotor speed (b) Torque

Figure 5.8 Rotor speed and torque

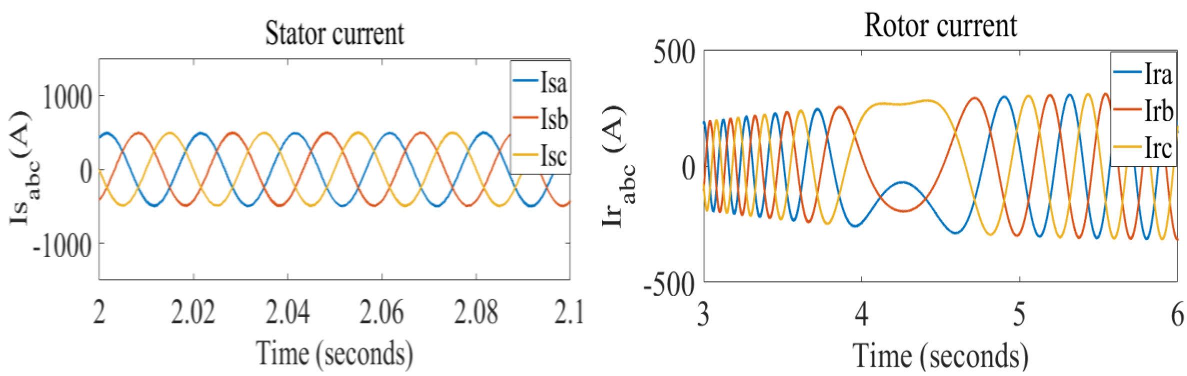

(a) Stator current (b) Rotor current

Figure 5.9 Stator and rotor current

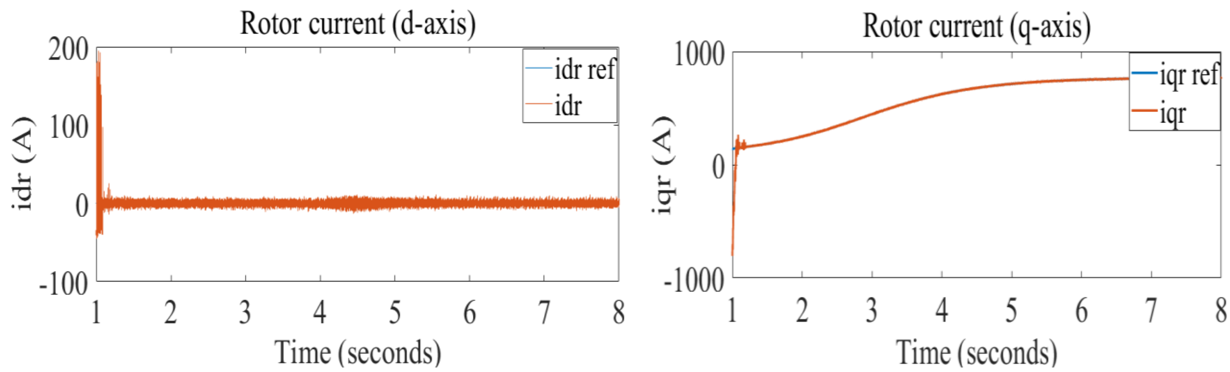

(a) Rotor current (d-axis) (b) Rotor current (q-axis)

Figure 5.10 Rotor current across d-axis and q-axis

5.3.2. GSC Under Normal Condition

The GSC controller is described in detail in Chapter Four. GSC control of the system is performed using voltage-oriented vector control. In this case, the d-axis of the rotating frame is aligned with the grid voltage space vector which means the d-axis grid voltage is constant while the q-axis grid voltage is zero. Figure 5.12 (a) indicates that the nominal values of the grid current are balanced. During normal operation, the DC-link voltage remains constant at 1150 volts, as shown in Figure 5.12 (b). Similarly, in steady-state conditions, as illustrated in Figure 5.13 the grid current across the d-axis and q-axis is held constant at zero.

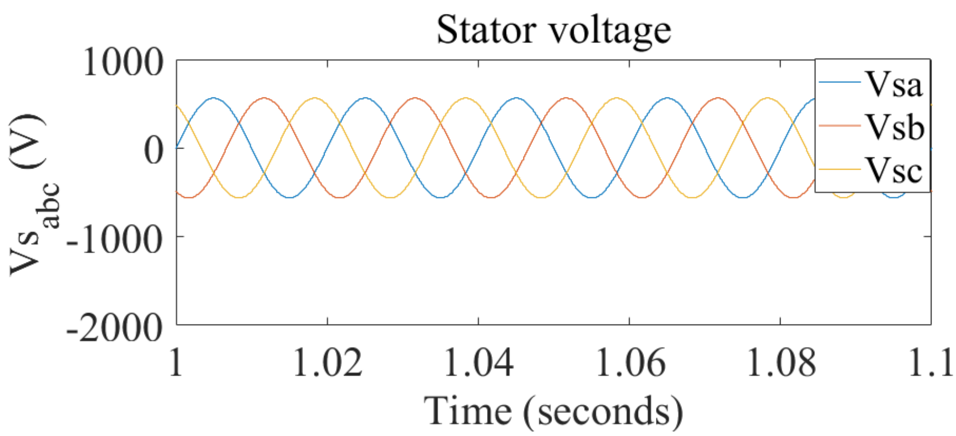

Figure 5.11 Stator voltage

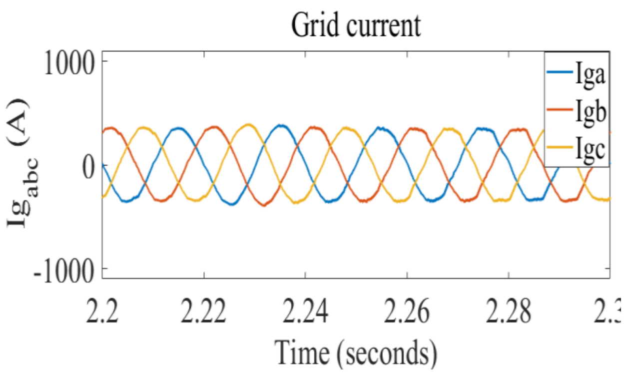

(a) Grid current

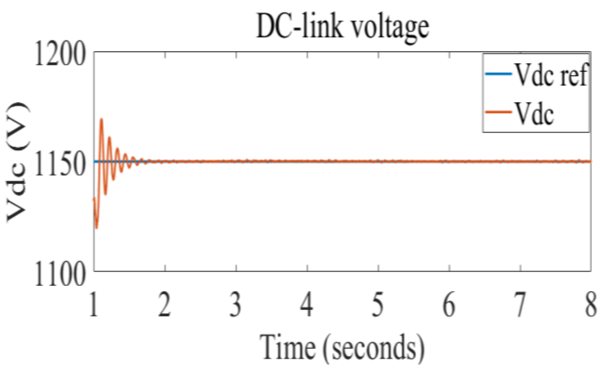

(b) DC-link voltage

Figure 5.12 Grid current and DC-link voltage

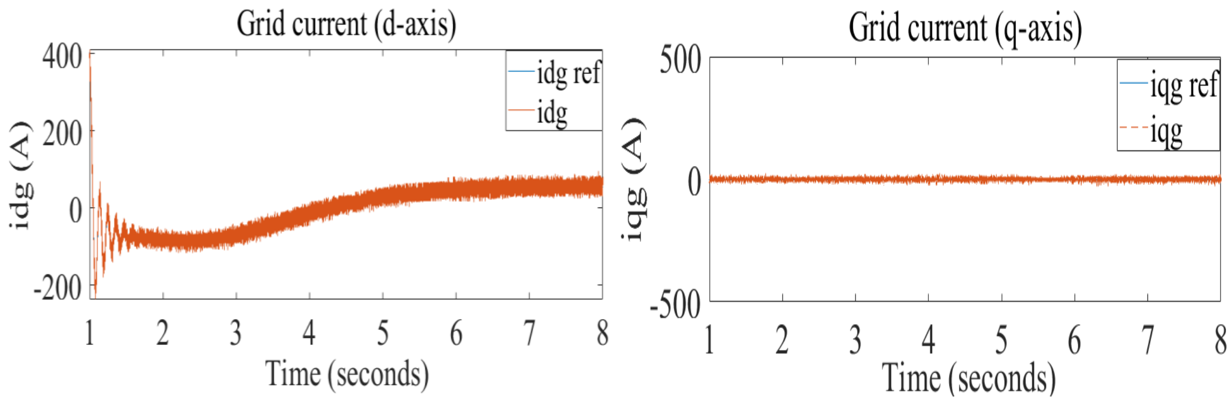

(a) Grid current (d-axis) (b) Grid current (q-axis)

Figure 5.13 Grid current across d-axis and q-axis

5.4. Under Grid Fault Condition

As described in Chapter Three, when a symmetrical fault occurs at a grid terminal, the voltage at the terminal decreases, so do the stator and rotor fluxes of the generator, causing the generator to demagnetize. The electromagnetic torque fluctuates, resulting in mechanical friction on the drive train. Furthermore, the voltage dip induces a high stator current, which contributes to a high rotor current. The high currents cause the voltage in the DC-link to increase which will damage the power converters [50]. Due to the above reasons, this thesis work is carried out to evaluate and examine how the machine performs when a three-phase symmetrical fault is imposed at the grid terminal and how the implemented protection system improves the performance of the machine by riding through the fault. In this section, the performance of a machine during the grid fault with the existing capacitor bank is analyzed.

5.4.1. RSC Under Grid Fault Condition with Existing Capacitor Bank

A dynamic simulation is carried out by imposing a three-phase symmetrical fault at the grid terminal for 150ms to analyze the DFIG based WT without any protection system applied. The duration of fault which causes voltage dip is from 2sec up to 2.15sec as shown in Figure 5.14. This system is analyzed in compliance with the German grid code requirement, which is one of the stingiest requirements, to investigate the fault ride-through capability of a wind farm. The German grid code states that the wind generator shall withstand the fault and stay connected to the grid for a period of 150ms for a voltage dip up to 10% and the wind power plant must restore 90% of the system voltage at 1500ms after the voltage dip [39]. The impact of grid fault on the machine is shown in subsequent figures below.

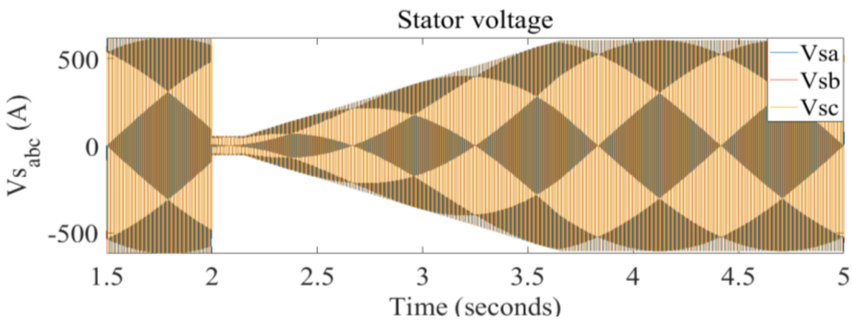

Figure 5.14 Stator voltage

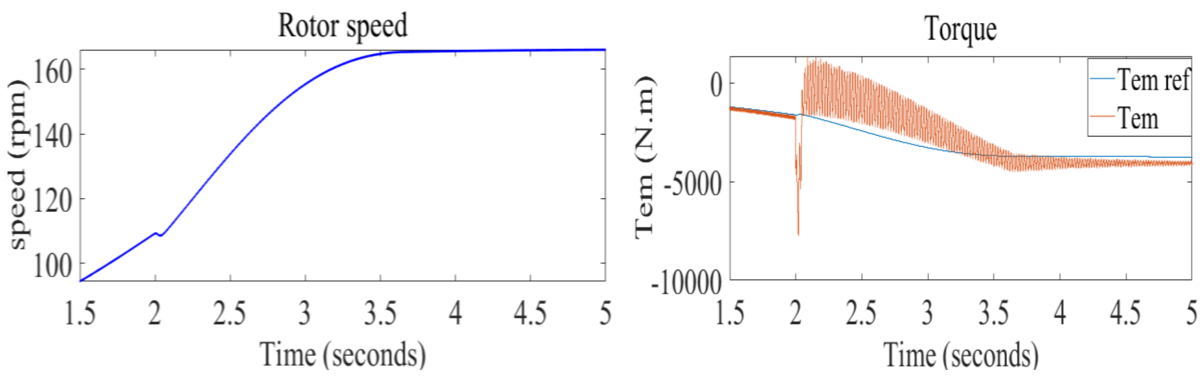

(a) Rotor speed

(b) Torque

Figure 5.15 Rotor speed and torque

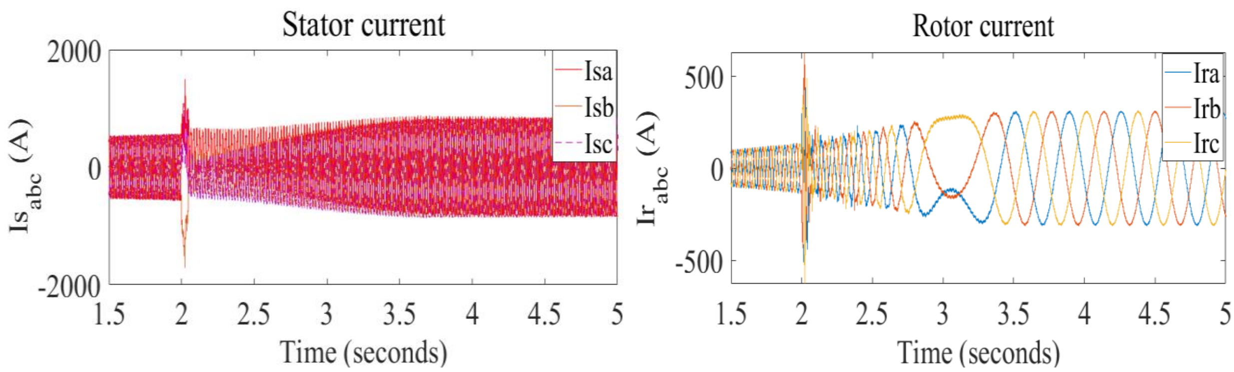

(a) Stator current

(b) Rotor current

Figure 5.16 Stator and rotor current

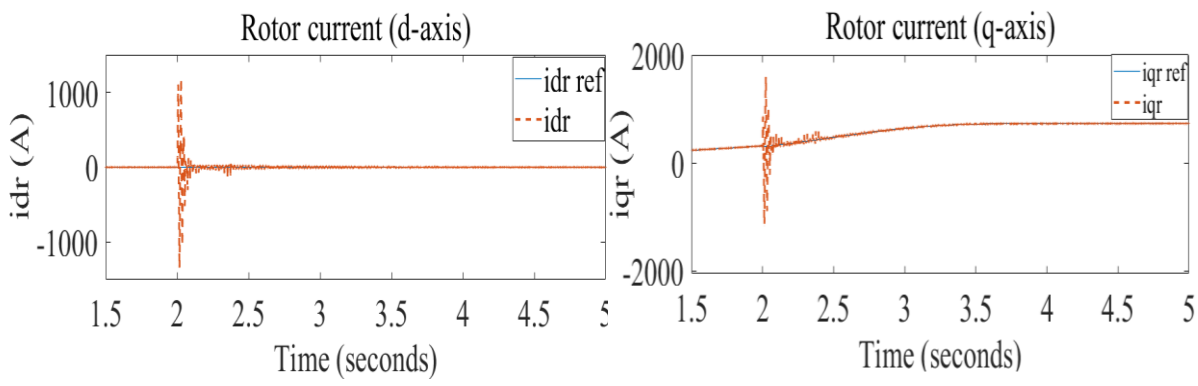

(a) Rotor current (d-axis) (b) Rotor current (q-axis)

Figure 5.17 Rotor current across d-axis and q-axis

When a symmetrical fault occurs, as shown in Figure 5.14, the stator voltage of the DFIG drops to 10% of the nominal voltage at the time of 2 sec and remains there for 150ms. Once the fault is cleared at 2.15 sec, the voltage begins to recover from 2.15 to 3.65 seconds, and after 3.65 seconds, it is seen to return to steady-state activity as the pre-fault period. Figure 5.15 depicts the variation of the rotor speed and electromagnetic torque of the DFIG. The rotor speed varies in response to changes in electromagnetic torque. During a fault state, at 2 seconds, the speed is observed to have a low value, corresponding to a low value of torque. This torque is considerably decreased to zero and fluctuates causing mechanical tension in the gearbox. Figure 5.16 depicts the variation of the stator and rotor currents encountered due to the occurrence of the fault. During the pre-fault period, both the stator and rotor currents are shown to operate well at a steady state. However, after the occurrence of a fault at 2 seconds, these currents are increased to a high value. First, a high stator current occurs, and then, due to the magnetic coupling between the stator and rotor windings, the high stator current causes a high rotor current. The stator and rotor winding magnetically coupled imply that with or without contact the magnetic field generated by the stator winding affects the rotor winding. Figure 5.17 indicates that when a failure occurs, both the rotor currents across the d-axis and the q-axis rise to elevated values. As illustrated in the Figures above, even though the rotor side converter can be utilized to compensate for rotor current variation by increasing the rotor voltage reference, it will eventually lose its controlling ability over the machine due to the DFIG having a power converter with a rotor voltage limit. In other words, the converter supplying the rotor will only provide 30% of the supply voltage, and as a result, the converter reaches its limit rapidly and, as a result, cannot control the generator during a failure [50].

5.4.2. GSC Under Grid Fault Condition with Existing Capacitor Bank

When a grid fault occurs, the voltage drops, inhibiting the GSC from transferring the whole power from the rotor to the grid. As a result, the excess energy charges the DC-link capacitor instantly, leading to DC-link overvoltage. Figure 5.18 elucidates that the stator voltage reduces to 10% of the nominal voltage at 2 sec and recovers from 2.15 to 3.65 after the clearance of fault. Figure 5.19 (a) illustrates how the presence of a fault induces the grid current to rise to a high value, and how the current is observed to be unbalanced as a consequence of the grid faults. Figure 5.19 (b) portrays variation of the DC-link voltage which is seen to operate at 1150V before the fault occurs. However, at 2 sec during the grid fault, the DC-bus voltage is stimulated at a high value of approximately 1350 and this is attributed to the fact that there is a short period of loss of control following a sudden drop in voltage at the grid terminal. This DC-link over-voltage normally results due to overcurrent at the stator and rotor winding of the machine. The grid currents across d-axis and q-axis are shown in Figure 5.20. The d-axis rotor current also increases at 2 seconds.

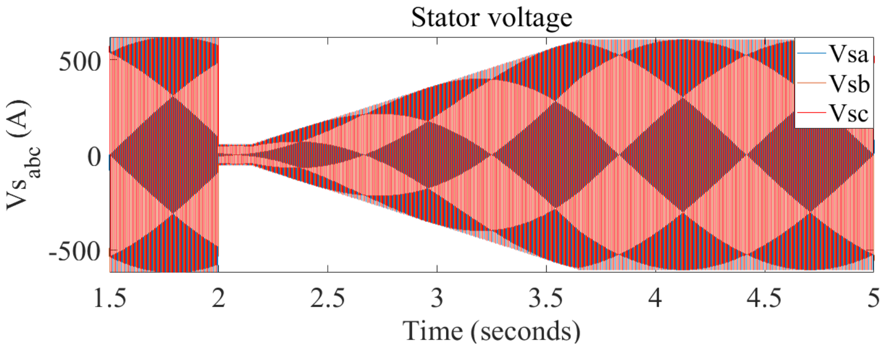

Figure 5.18 Stator voltage

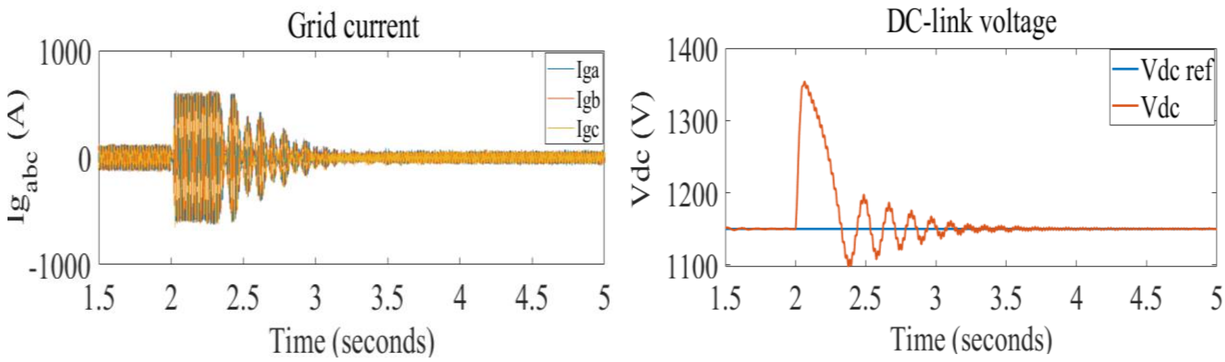

(a) Grid current (b) DC-link voltage

Figure 5.19 Grid current and DC-link voltage

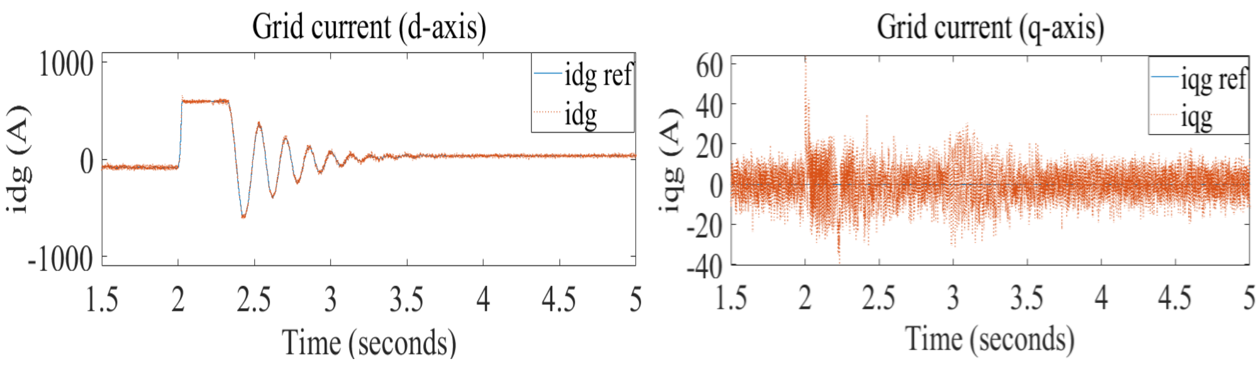

(a) Grid current (d-axis)

(b) Grid current (q-axis)

Figure 5.20 Grid current across d-axis and q-axis

5.5. Under Grid Fault Condition with Crowbar Protection

As already stated above, when a grid fault occurs, the sudden change in stator voltage should be accompanied by the sudden rotor voltage change to prevent a high increase in rotor current. The depth of the grid voltage dip and the type of fault determines the induced rotor voltage. If the depth of the voltage dip is very limited and the required voltage does not exceed the maximum voltage that the rotor converters will generate, the current remains regulated and no risk is posed to the generator or the power converters. However, if the depth of the voltage dip caused by symmetrical fault components is high (0.1pu in this study), the voltage generated at the rotor terminal exceeds the maximum available tension of the converter, as a result, control is lost and over current appears. This high current will escalate as the depth of the dip increases, causing damage to the power converters. As a result, it is reasonable to state that this wind turbine model does not guarantee that the rotor current will remain within acceptable limits without control being lost. To address the above issues and protect the converters from damage, a crowbar protection device is installed at the rotor terminal. As the voltage drops, crowbar protection is triggered, which provides a low resistance path, isolating the RSC and ensuring that all rotor currents pass through it. As a result, it will protect the system from over-currents caused by a lack of control. The performance of DFIG during fault using a crowbar protection system is further discussed below.

5.5.1. RSC Under Grid Fault Condition with Crowbar Protection System

A three-phase symmetrical fault is imposed at the grid terminal at 2 sec to analyze the variation in stator voltage during the fault condition. Figure 5.21 (a) demonstrates the voltage dropping to 0.1pu and remaining at that stage for 150ms. Before the event of the fault, it is evident that the currents are operating normally and the crowbar is not enabled, implying that no current flows through the crowbar resistance. When the voltage dip is detected, the crowbar protection is activated for 100 milliseconds inhibiting the RSC and protecting it from high currents by allowing the current to pass through the resistor. Figure 21 (b, d, f) represents how the high stator and rotor current encountered due to the occurrence of fault circulates through the crowbar. This implies that owing to the crowbar resistance, the power converters are protected against the high currents. Once the voltage dip is directly observed by the DFIG stator, it is also critical to examine the behavior of the stator flux to identify the problems encountered by the voltage dip perturbation. The torque and flux are influenced by the grid fault, as shown in Figure 5.21 (c, e). The flux is observed to decrease to near zero, and so is the torque. This flux, even after the clearance of fault, cannot evolve to its final steady-state quickly. So, when the crowbar is activated, it concurrently accelerates the flux evolution as quickly as possible. The torque is also observed to be influenced by the fault, as shown in Figure 5.21 (c). It is realized that even after the fault has been cleared, the torque does not meet the reference value. This is because torque control is lost when the crowbar is enabled. Once the rotor current reduces and the flux return to its nominal value, and the available converter voltage starts to control the machine, the crowbar is disconnected and RSC is reactivated.

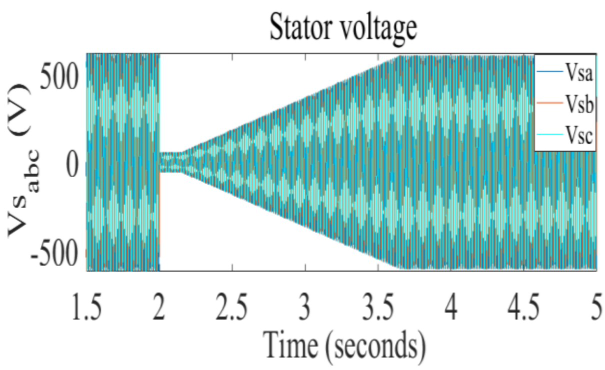

(a) Stator voltage

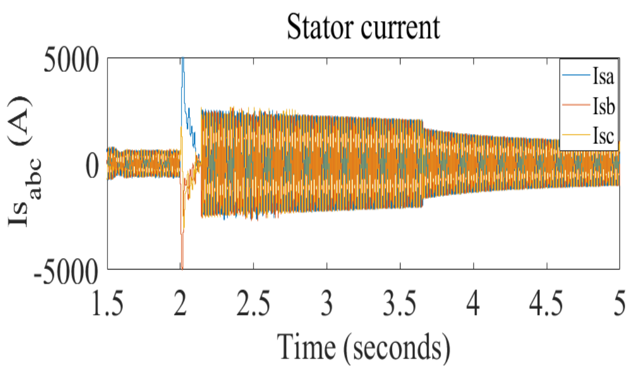

(b) Stator current

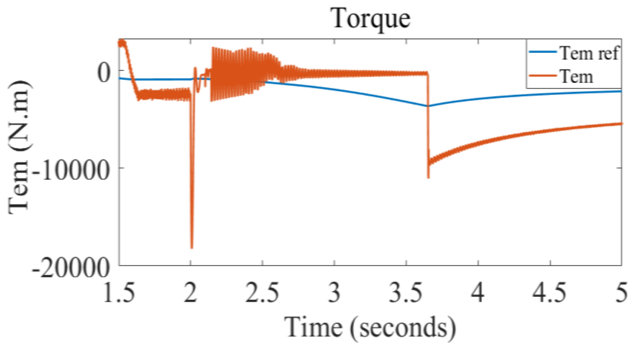

(c) Torque

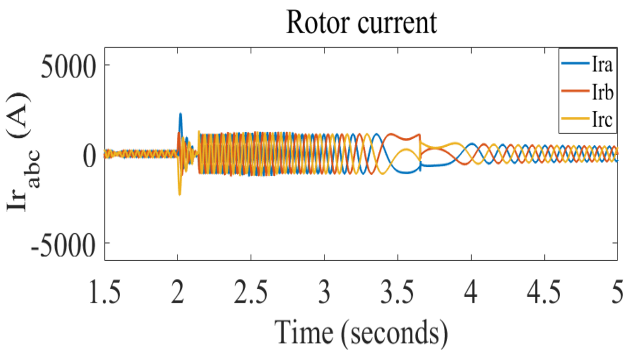

(d) Rotor current

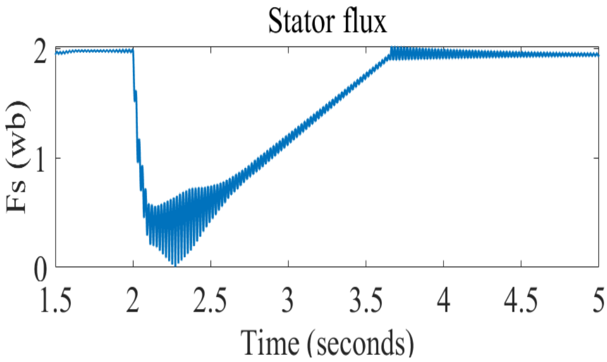

(e) Stator flux

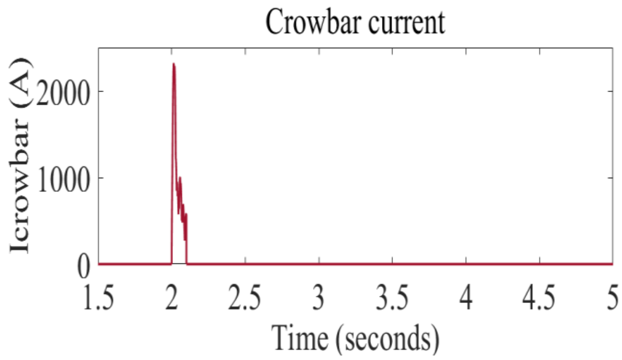

(f) Crowbar current

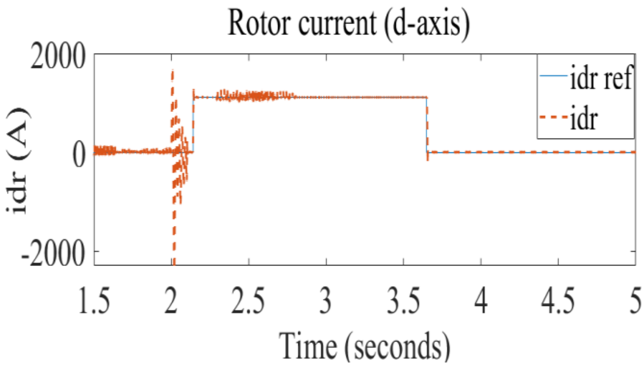

(g) Rotor current (d-axis)

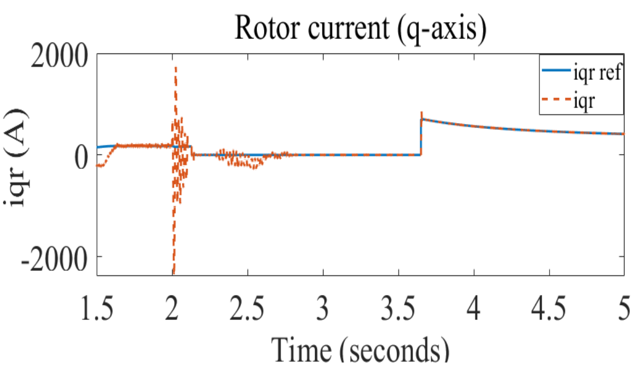

(h) Rotor current (q-axis)

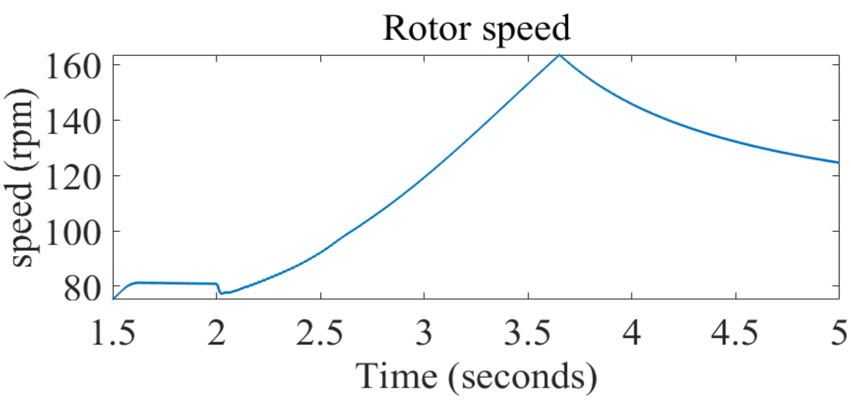

(i) Rotor speed

Figure 5.21 Performance of DFIG with a crowbar at RSC

The currents across the d-axis and q-axis are depicted in Figure 5.21 (g, h). As a dip occurs, as required by grid code, increasing the d-axis rotor current will provide progressively reactive power. However, since the crowbar blocks the RSC during activation, no reactive power can be generated. As a result, it is only after some time (2.14 sec) that reactive power is supplied. Figure 5.21 (i) indicates the speed control being lost. When the crowbar is engaged, it disables the RSC, resulting in a loss of speed control.

5.5.2. GSC Under Grid Fault Condition with Crowbar Protection System

It is discussed in section 5.2.1 that during fault the GSC loses its ability to control the DC-link voltage due to the limited value of rotor voltage that the power converter generates. As already observed in Figure 5.22 (b) the DC-link voltage rises to a high value owing to the voltage dip which leads to loss of control. Thus, in this section the performance of DFIG at the GSC is analyzed by applying a protection mechanism at the time control is lost. Figure 5.22 (b) illustrates how the grid current is maintained constant after the activation of the crowbar. and Figure 5.22 (c) elucidates that while the crowbar is enabled, no energy is transferred to the DC-link capacitor, and hence the DC-link voltage is more likely to decrease. However, after the crowbar is deactivated and the fault is cleared, the DC-link voltage is observed to return to a steady state. The grid currents across d-axis and q-axis, in Figure 5.22 (d, e), remain at its nominal value following its reference value after the fault is completely cleared. Due to the reference frame being oriented along the grid voltage vector, the d-axis grid current is used to regulate the DC-link voltage and the q-axis grid current is used to regulate the reactive power in the PWM voltage source converter. The d-axis grid current is observed to reduce as shown in Figure 5.22 (d) and hence, the DC-link voltage is also reduced.

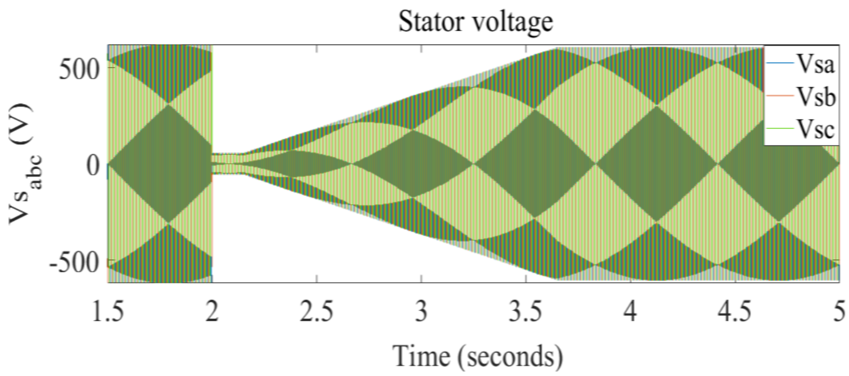

(a) Stator voltage

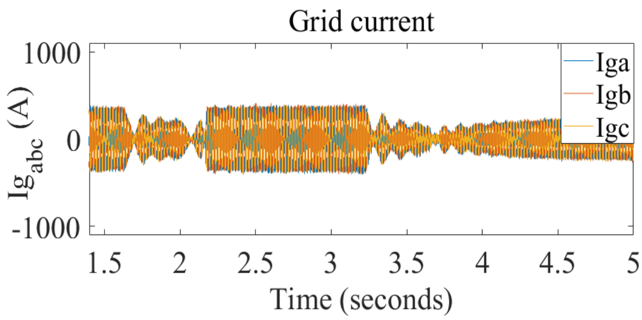

(b) Grid current

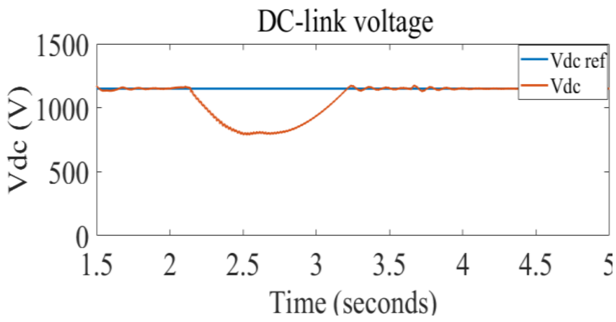

(c) DC-link voltage

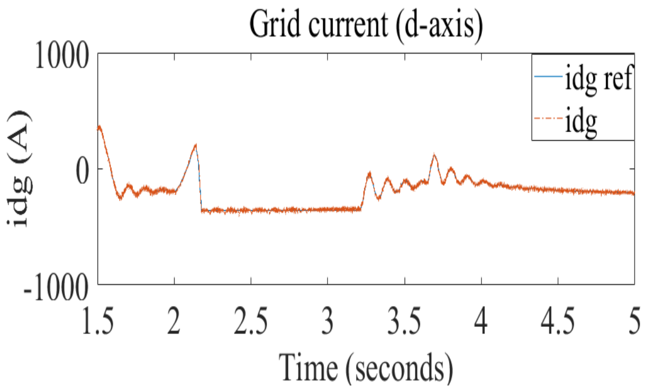

(d) Grid current (d-axis)

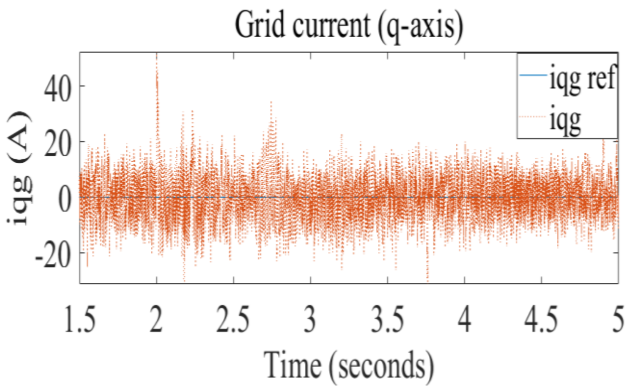

(e) Grid current (q-axis)

Figure 5.22 Performance of DFIG with the crowbar at GSC

5.6. Under Grid Fault Condition with Crowbar Protection Integrated with BESS

Although the crowbar protection system is critical for securing the converters, it has some drawbacks. The negative aspect of the crowbar system is that, while it protects the RSC by ensuring that high currents flow through it, machine control is lost as a consequence of RSC inhibition, and the DFIG acts like a squirrel cage induction generator, only absorbing reactive power from the grid, resulting in grid voltage degradation. Moreover, no torque oscillation damping and reactive power support are achieved on the machine side. As a result, BESS implementation is vital since, in the event of a loss, the stored energy in the battery discharges, powering the GSC.

5.6.1. RSC Under Grid Fault Condition with Crowbar Protection Integrated with BESS

As previously stated, the core concern with the crowbar protection method is that prolonged use of the rotor crowbar induces a lack of machine control. However, by incorporating BESS with Crowbar, the BESS ensures that control over the machine is not lost. As previously illustrated in Figure 5.21 (c, i), when the crowbar is enabled, torque and speed control is lost because the crowbar blocks the RSC. For a certain period, the torque is observed to be zero, and the speed is decreased from its nominal value. However, as seen in Figure 5.23 (c, i), once the BESS is merged with the crowbar protection system, after some time, the speed is observed to return to its normal operation. Following the reference value, the torque is also retained at its nominal value.

Another drawback of the crowbar is that it causes the DFIG to operate as an induction machine, causing stator side magnetization to be drawn. This causes a high-slip reactive power demand from the grid, further degrading the voltage. As displayed in Figure 5.21 (g), raising the direct current provides for reactive power only after the crowbar was disabled. as reactive power cannot be provided while the crowbar is enabled. However, when BESS is employed, as depicted in Figure 5.23 (g), even with crowbar protection stimulated, BESS allows reactive power to be supplied to the grid, which improves the performance of the machine. Figure 5.23 (b, d, f) indicates how the high value of stator and rotor current enters the crowbar.

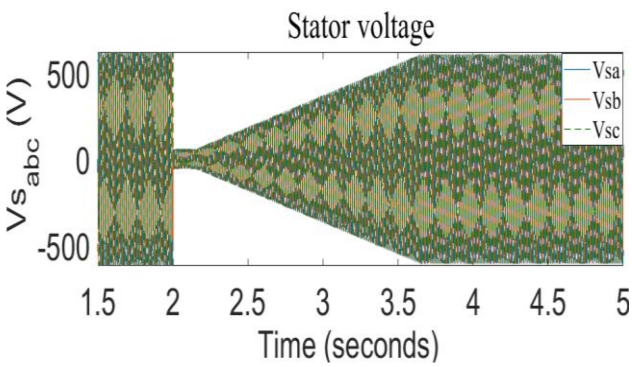

(a) Stator voltage

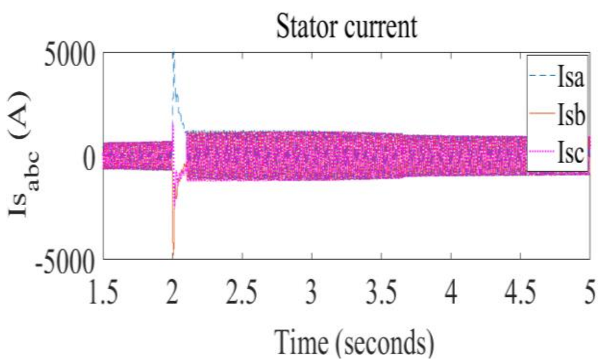

(b) Stator current

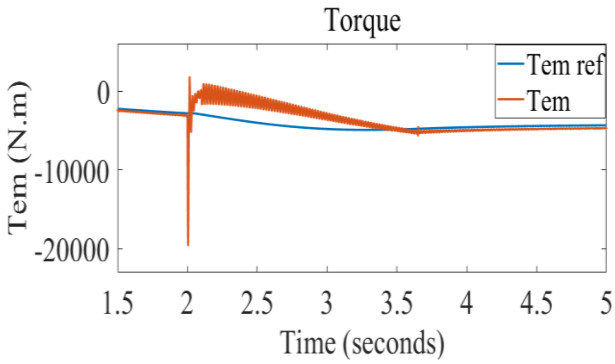

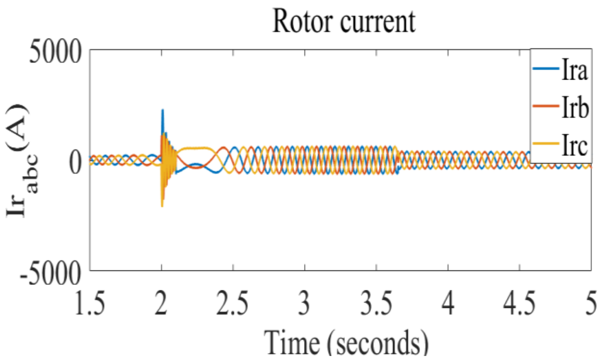

(c) Torque

(d) Rotor current

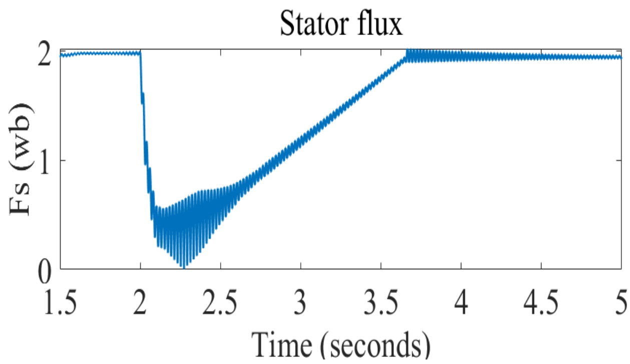

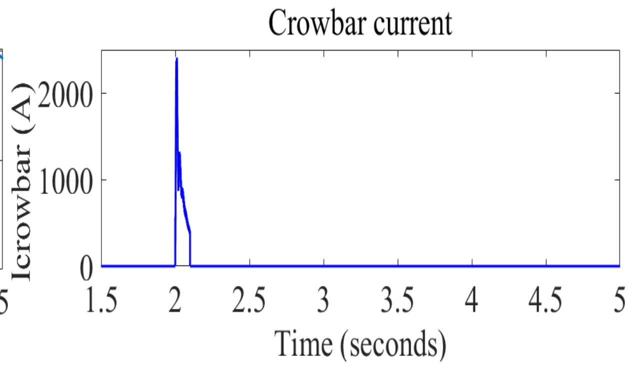

(e) Stator flux

(f) Crowbar current

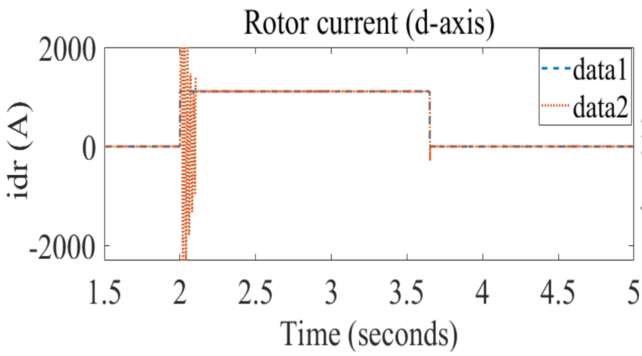

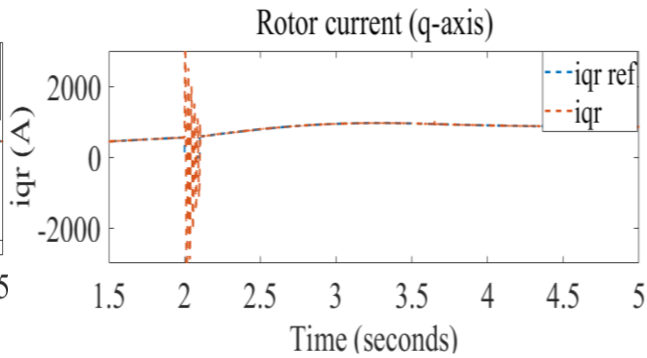

(g) Rotor current (d-axis)

(h) Rotor current (q-axis)

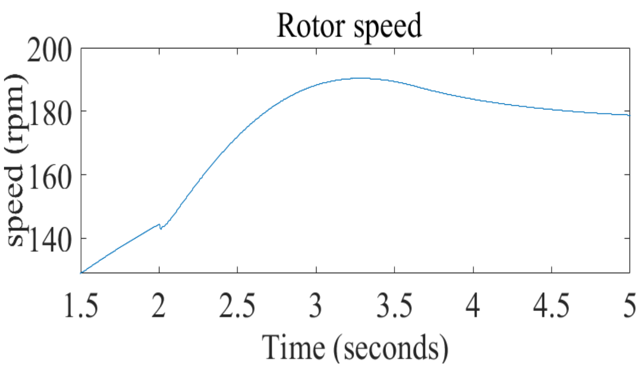

(i) Rotor speed

Figure 5.23 Performance of DFIG with crowbar integrated with BESS at RSC

5.6.2. GSC Under Grid Fault Condition with Crowbar Protection Integrated with BESS

The battery, following a power converter, aids in maintaining a constant DC bus voltage. During an interruption, As the crowbar blocks the RSC and the DC-link voltage is lowered after an interruption, the battery begins to discharge to preserve the voltage at the DC-link constant. Figure 5.22 (c) depicts that the DC-link voltage is reduced as a consequence of the crowbar being activated. However, this issue is solved when the BESS is integrated with the crowbar. Figure 5.24 (c) shows that the DC-link voltage is nearly constant owing to the BESS. In Figure 5.24 (d), the grid current across the d-axis, which is in charge of regulating the DC-link voltage, is also shown to be constant. Figure 5.24 (e) illustrates that the grid current across the q-axis remains stable.

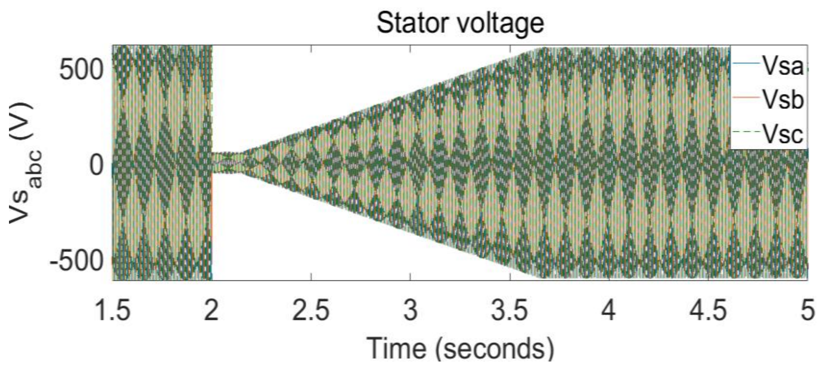

(a) Stator voltage

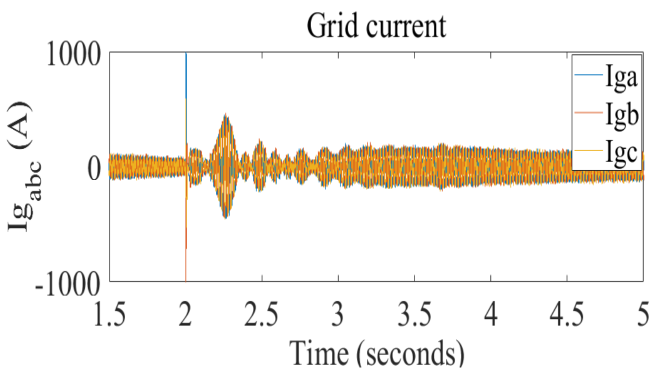

(b) Grid current

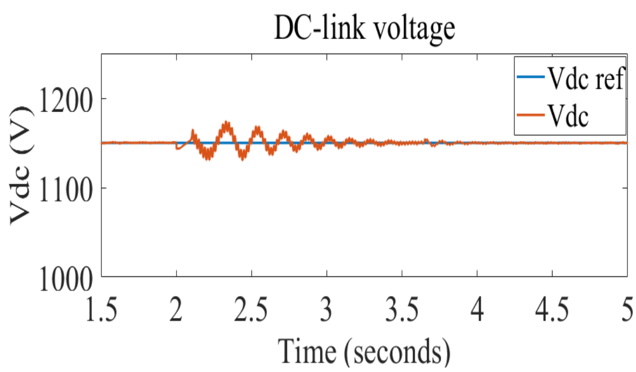

(c) DC-link voltage

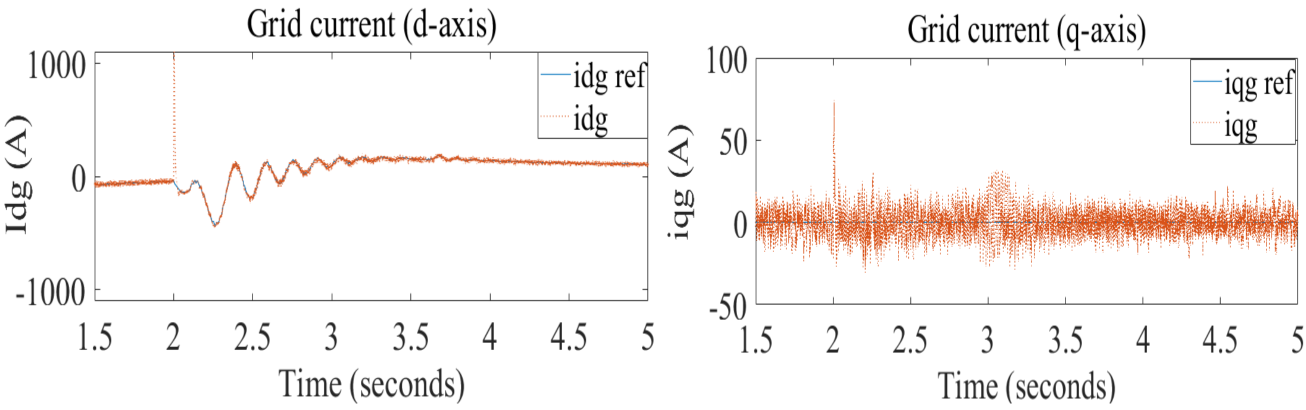

(d) Grid current (d-axis) (e) Grid current (q-axis)

Figure 5.24 Performance of DFIG with crowbar integrated with BESS at GSC

5.7. Comparative Analysis of the Results

This section provides a thorough comparison of various parameters at the RSC and GSC with the existing capacitor bank, crowbar protection mechanism, and crowbar integrated with BESS. Torque, speed, stator and rotor currents, and rotor current at the d-axis are among the parameters used for comparison. At the end of the analysis, a conclusion is drawn based on this comparison.

5.7.1. Comparative Analysis at RSC

Detail comparison of various parameters observed at RSC with the existing capacitor bank, crowbar protection system, and crowbar incorporated with BESS is performed. Figure 5.25 illustrates various parameters at RSC which were used for comparative purposes. A distinct number is assigned to each figure to differentiate it. The parameters with the existing capacitor bank are denoted by ‘1', the parameters with the crowbar protection system are denoted by ‘2', and the parameters with the crowbar integrated with BESS are denoted by ‘3'. Figure 5.25 (a1, a2, and a3) demonstrate the torque value with an existing capacitor bank, crowbar protection, and crowbar integrated with BESS. Subfigure (a1) depicts that when a fault occurs, a high torque pick is noticed and machine control is lost for 2 to 3.5 seconds. High torque fluctuation is seen, and the actual value of torque is also noted to deviate from its reference value. Subfigure (a2) displays that with the crowbar activated, even though the fluctuation of torque is minimized, control over torque is lost, and the torque takes time to follow the reference value even after the crowbar is deactivated. However, in subfigure (a3), the torque fluctuation is lowered to a considerably lower value, and the torque is likewise observed to restore to its nominal level after 3.4 seconds. Subfigures (c1 and d1) depict stator and rotor currents using the existing capacitor bank. High currents, which are likely to damage the power converters are detected at the occurrence of the fault at 2 sec. Subfigures (c2, d2, f2) and (c3, d3. f3) demonstrate that when the crowbar is activated, high currents flow through it. As a result, the converters are shielded from large currents caused by faults. Subfigure (e1) displays the rotor current across a d-axis using the existing capacitor bank. It is observed that when a defect emerges, the machine does not supply any reactive power, thereby further degrading the voltage at the terminal. In subfigure (e2), it is proven that rising rotor current at d-axis supplies reactive power to the grid; however, it is also noted that reactive power is given to the grid only after the crowbar is deactivated (i.e. 2.14sec). With a BESS integrated with a crowbar, as shown in subfigure (e3), the machine is observed to be delivering reactive power the instant the fault occurs at the grid terminal, which is 2 seconds.

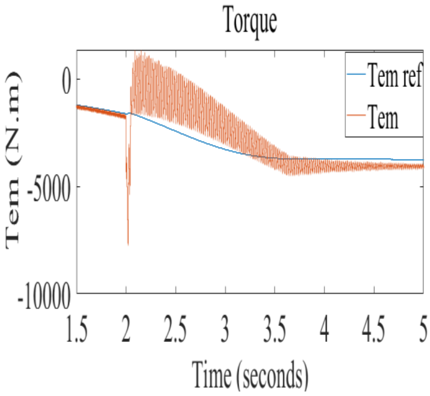

(a1)

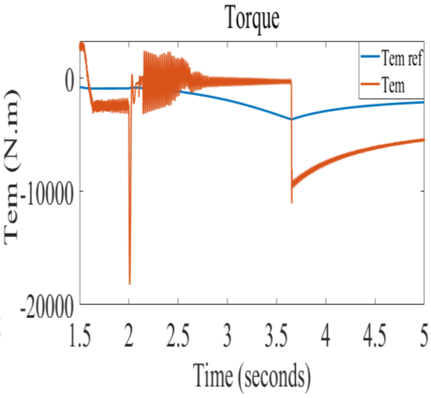

(a2)

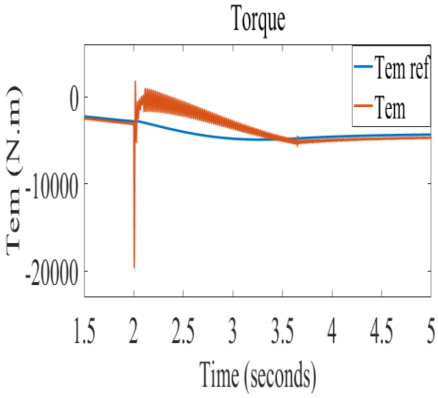

(a3)

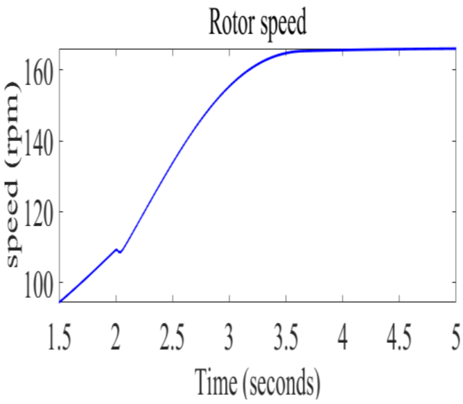

(b1)

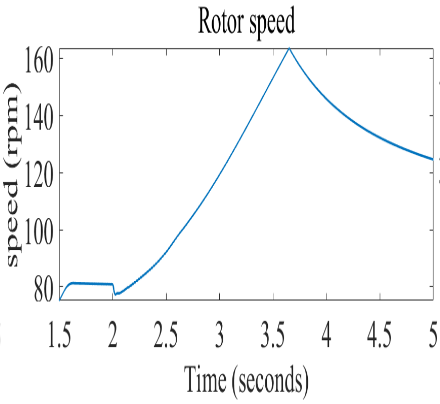

(b2)

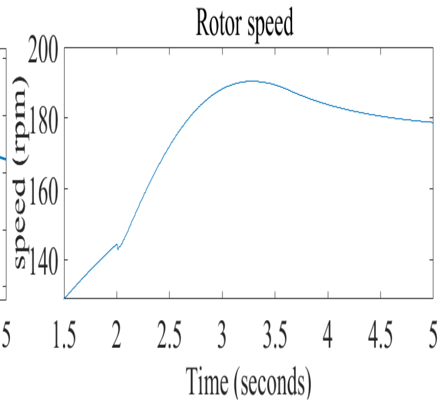

(b3)

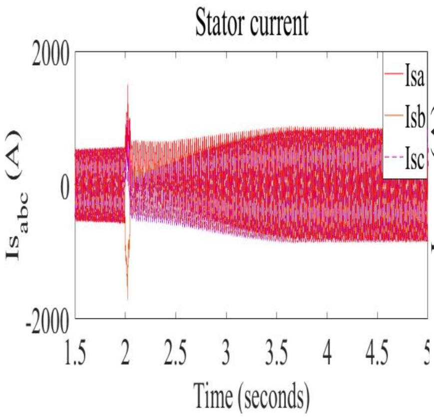

(c1)

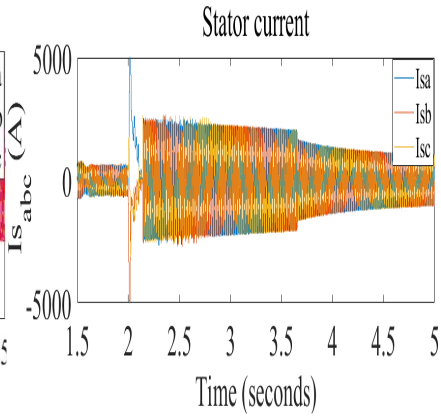

(c2)

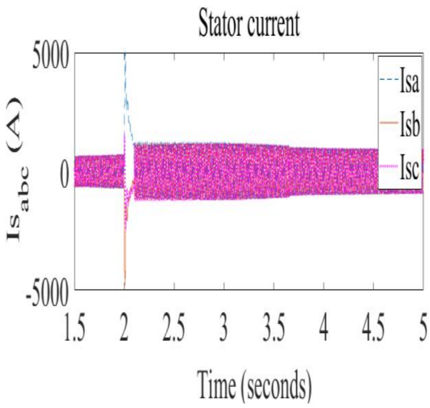

(c3)

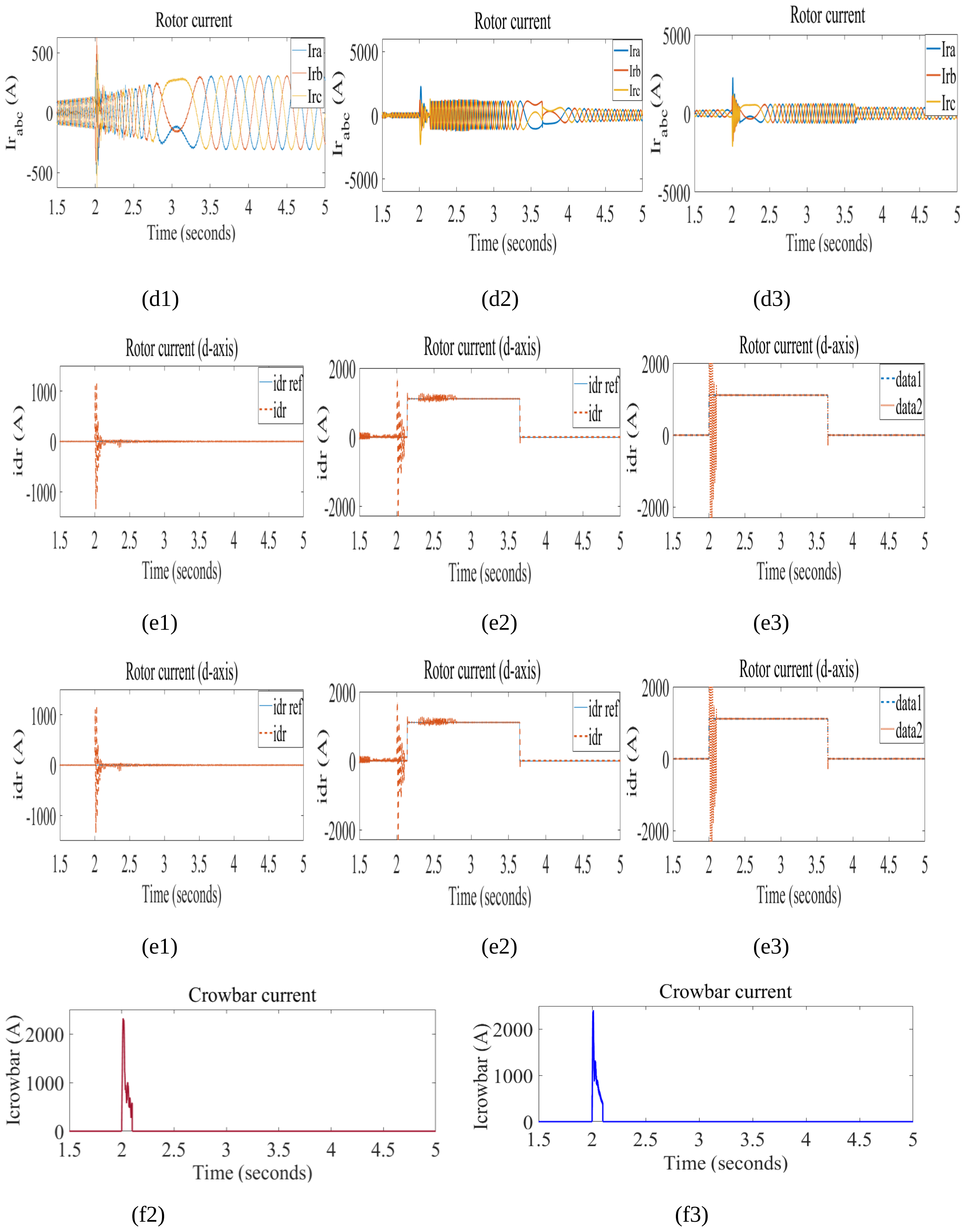

Figure 5.25 Comparative analysis at RSC

5.7.2. Comparative Analysis at GSC

Figure 5.26 depicts a comparison of various parameters at GSC with the existing capacitor bank, crowbar protection system, and crowbar merged with BESS. Subfigures (a1, a2, and a3) demonstrates currents at the grid side converter. It is observed that due to the occurrence of fault this current fluctuates in all three methods. However, after the fault is cleared the system is observed to return to its normal operating condition. In subfigure (a3) the current at the grid terminal returns to normal around 2.6 seconds which is faster restoration than the existing capacitor bank and the crowbar protection system. Subfigures (b1, b2, and b3) depict the DC-link voltage with the existing capacitor bank, crowbar protection system, and crowbar integrated with BESS, respectively. In subfigure (b1), the DC-link voltage is observed to rise to 1350v. This amount of DC-link voltage will damage the power converter if no protection scheme is applied. When the crowbar is utilized in the system, the DC-link voltage drops to a low level as depicted in subfigure (b2). This is because the crowbar prevents all energy from passing through the DC-link capacitor causing the dc-link voltage to drop. In subfigure (b3), the DC-link voltage is shown to remain at its nominal value (1150v) with a small variation. These fluctuations, which are removed after 2.6 sec, are not high enough to harm the power converters. Subfigures (c1, c2, and c3) exhibit the grid currents across the d-axis using the three approaches. The DC-link voltage is controlled by the d-axis grid current. The grid current across the d-axis is observed to increase, as shown in subfigure (c1). As illustrated in subfigure (c2), the d-axis grid current is observed to reduce when the crowbar protection system is applied to the system. Subfigure (c3) depicts the current further lowered and maintained at its nominal value. Thus, with the third method (crowbar integrated with BESS) it is observed that fault ride-through capability is enhanced.

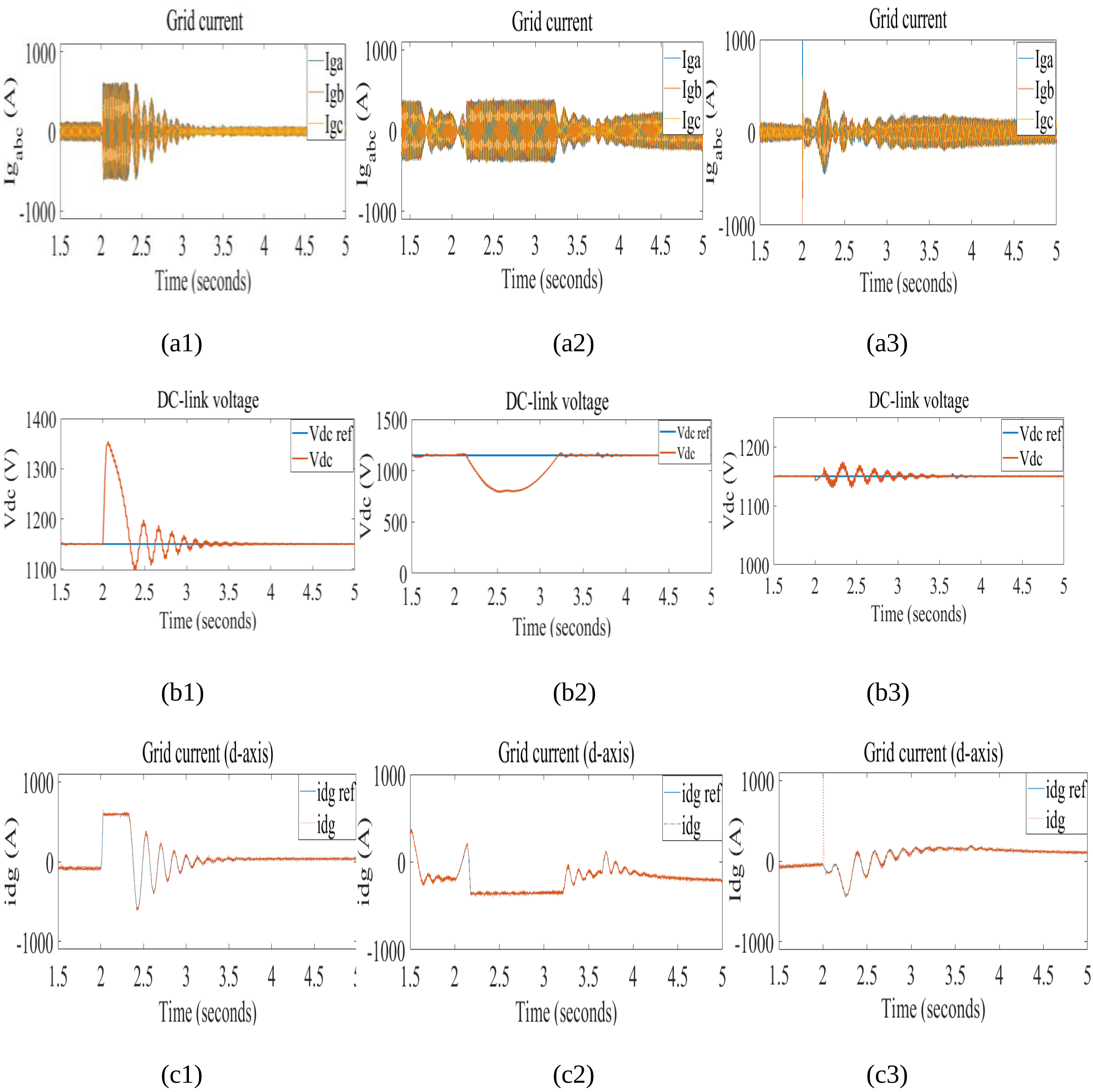

Figure 5.26 Comparative analysis at GSC

Table 5-1 demonstrates a numerical comparison of the results.

Table 5-1 comparative analysis of the result

Parameters	Existing Capacitor bank	Crowbar protection	Crowbar integrated with BESS
DC-link voltage	The DC-link voltage overshoots to 1350v which is a high peak. The settling time is 3.5 seconds	Voltage reduced to 775v and recovers after 3.45seconds	Voltage is maintained at 1150 with few fluctuations. Settles at 2.9 seconds
Grid current across the d-axis	The grid current rises to a higher value (600A) and fluctuates between 600 and -600 and settles down at 3.3seconds	The grid current kept fluctuating between -350 and -200 and even after 4.5 sec it does not settle down to its nominal value.	The fluctuation of grid current reduces and settles down to nominal value (zero) after 2.9 seconds
Rotor current across d-axis	The machine is not providing reactive power to the grid due to the fault, and since no protection system is applied.	Due to the activation of the crowbar, DFIG does not supply reactive power for 140ms. It can only supply after 2.14 seconds.	Reactive power is provided to the grid at 2 seconds until the voltage completely recovers which is 3.65 seconds
Torque and speed	High torque fluctuation is settled down at 3.9 seconds and speed returns to nominal value at 3.5 seconds.	Control over the torque and speed is lost and didn’t return to nominal value after 5 seconds.	Fluctuation of the torque is reduced and the torque control recovers after 3.3 seconds. The speed also recovers after 3.5 seconds.

As a result of the comparison analysis, the suggested protection system outperforms the crowbar and the existing capacitor bank in terms of fault ride-through capability. FRT capability refers to the ability of the generator to stay connected to the grid even when there are faults. In this analysis, the proposed method performs better in riding through the fault and safeguarding the machine from harm. For instance, the settling time for DC-link voltage using simply a crowbar protection system is 3.45 seconds, whereas the settling time utilizing the suggested technique is 2.9 seconds. This implies that the system rides the fault quickly and preserves its nominal value. As a result, the suggested technique outperforms relying just on the crowbar protection mechanism.

5.8. Asymmetrical Fault Analysis

In the case of asymmetrical fault, the induced voltages in the rotor circuit consist of three terms: positive, negative, and zero sequences. When the stator of DFIG is connected to an unbalanced grid, the positive sequence of the grid voltage produces a stator flux with a constant amplitude that rotates at the grid frequency; The negative sequence produces a stator flux with identical characteristics but rotates in the opposite direction; and eventually, the zero-sequence produces no stator flux if the neutral point is excluded. Thus, the overall stator flux is the sum of two opposing fluxes: the positive flux and the negative flux [43]. The negative natural flux that occurs at the stator during a voltage dip induces harmonic pulsation, torque fluctuation, and saturation in the rotor converter. As a result, a vector control system is used to control the variables of the machine. It is essential to govern the negative and positive sequences individually to ensure each sequence is well regulated [45]. In the following sections, a phase-to-phase fault is investigated using the vector control approach to determine the amplitude and frequency of each sequence.

5.8.1. RSC in case of Asymmetrical Fault

DFIG is susceptible to both symmetrical and asymmetrical grid faults. The performance of the machine in the presence of a symmetrical fault has been thoroughly addressed in previous sections. It has been noted that in the case of symmetrical fault, the natural flux is generated in the stator, causing the speed and torque to fluctuate and the currents and dc-link voltage to increase to a higher value. In the asymmetrical event, though, the power and torque fluctuate due to the negative natural flux. Since the negative sequence of flux rotates in the opposite direction of the rotor, depending on its amplitude, it may produce a strong emf in the winding. The magnitude of this emf is determined by the depth of the voltage dip. If the depth of the voltage dip is small, the induced emf will not surpass the maximum voltage of the power converter and therefore will not saturate the rotor converter. To evaluate the performance of DFIG, the LLG fault (B and C phases to ground) is applied at the grid terminal for 1.2 seconds. Figure 5.27 (a) depicts the stator voltage with a voltage dip at 3sec. The voltage dip lasts 1.2 seconds and tends to recover after 4.2 seconds. Figures 5.27 (b and c) demonstrates the rotor speed and torque and how the voltage drop influences these two parameters. The speed variation is due to a brief loss of control caused by a voltage imbalance. In Figure 5.27 (c), the torque is also seen to fluctuate due to the voltage imbalance. This fluctuation has the potential to induce friction and mechanical stress. The amplitude of the torque ripple is determined by the negative flux and current. The negative flux is caused by grid imbalance and is independent of control. The negative current, on the other hand, is highly dependent on the control. After the fault is cleared, the torque and speed are shown to recover due to the zero-reference value of the negative current.

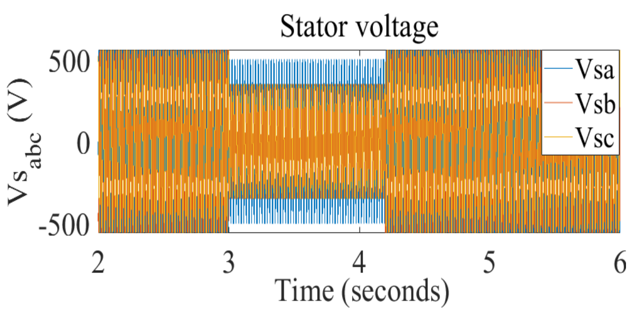

(a) Stator voltage

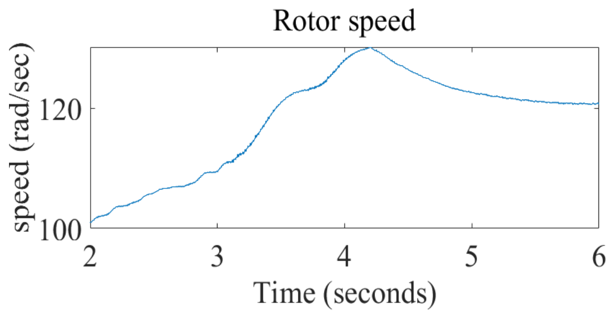

(b) Rotor speed

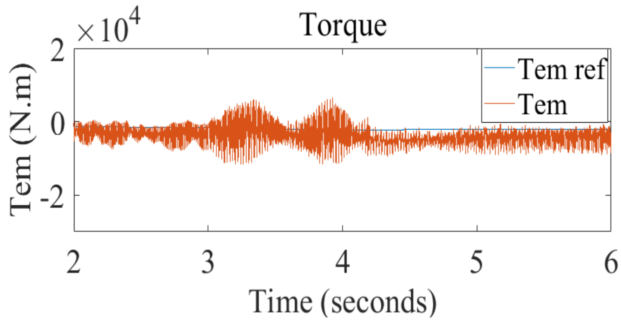

(c) Torque

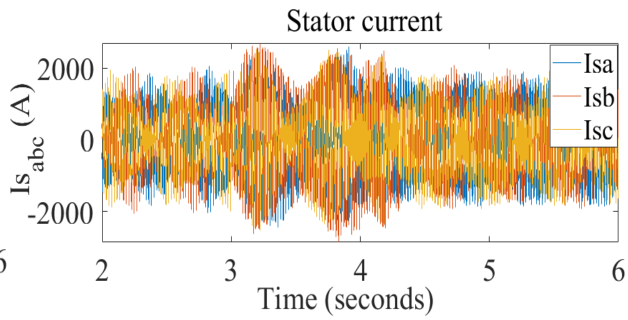

(d) Stator current

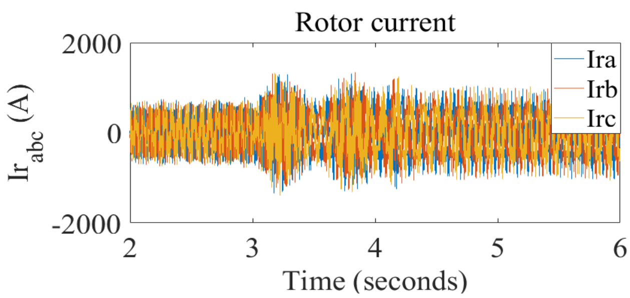

(e) Rotor current

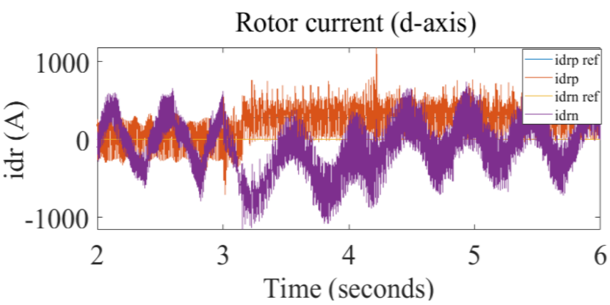

(f) Rotor current (d-axis)

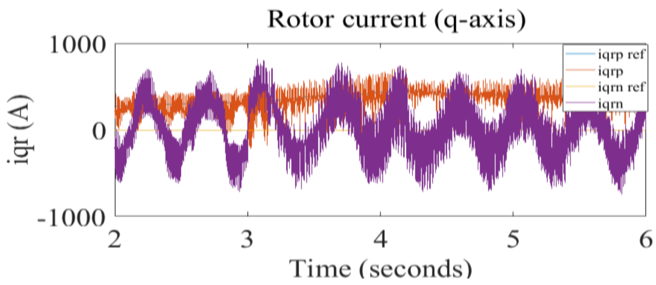

(g) Rotor current (q-axis)

Figure 5.27 Performance of DFIG at RSC

Figure 5.27 (d and e) indicates the stator and rotor currents, respectively. As depicted in Figure 5.27 (a), the voltages in phases 'B' and 'C' have fallen to very low levels. It is observed that the amplitude values of phase ‘A', ‘B', and ‘C' currents undergo a substantial rise during the fault cycle. The rotor current values depend on the rotor voltage and the derivative of the stator flux with time, so the stator disturbance is further transferred to the rotor due to magnetic coupling between the stator and rotor, resulting in high rotor current. In this case, the magnitude of the rotor voltage does not surpass the maximum voltage of the power converter and therefore will not saturate the rotor converter. Thus, by implementing only the controller, the rotor currents can be regulated. Figures 5.27 (f and g) show the positive and negative sequence rotor currents across the d-axis and q-axis, respectively. Since it is undesirable, the negative sequence rotor current across the d-axis and q-axis is set to zero.

5.8.2. GSC in case of Asymmetrical Fault

As previously stated, if a stator-flux-oriented frame is used in the unbalanced case, the natural flux influences the orientation of the reference frame. The behavior under-voltage dip is complicated in this situation. As a result, in this situation, the reference frame will be aligned with the grid voltage, and the phase of the grid voltage will be determined using a phase-locked loop (PLL). The following Figures indicate the performance of the machine during voltage imbalance with the control system applied. The voltage dip is detected at the time of 3 sec and lasts for 1.2 sec. The DC-bus voltage fluctuates during the voltage dip due to the imbalance at the grid terminal as shown in Figure 5.28 (a). However, after 4.2 seconds, the voltage recovers and the system continues operation. Since the negative sequence current has a zero-reference value, the grid current is balanced and symmetric after the fault is cleared as depicted in Figure 5.28 (b).

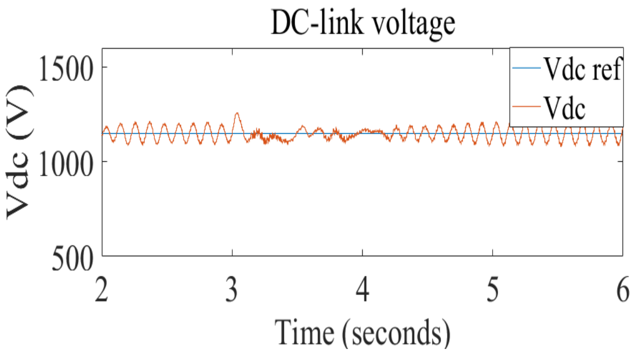

(a) DC-link voltage

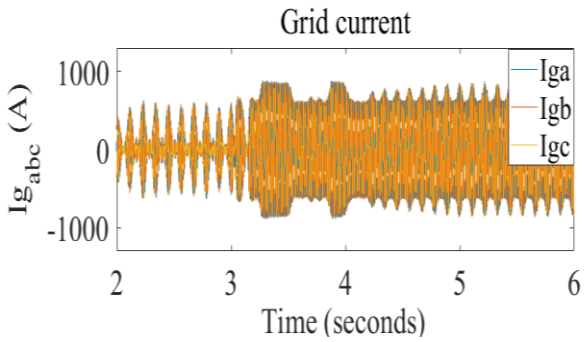

(b) Grid current

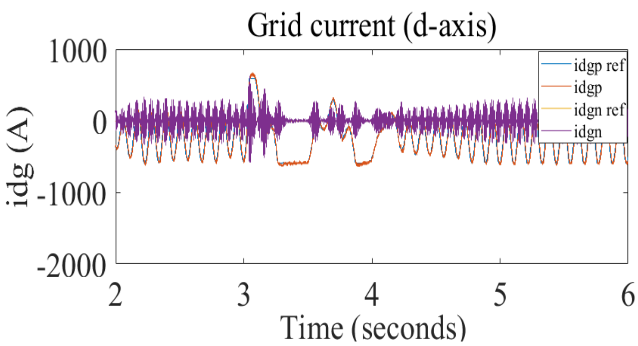

(c) Grid current (d-axis)

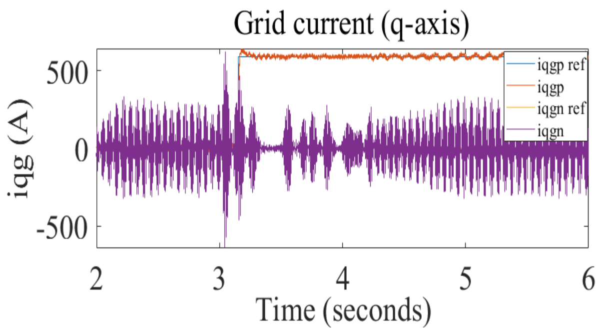

(d) Grid current (q-axis)

Figure 5.28 Performance of DFIG at GSC

As already observed above, in asymmetrical fault analysis since the control can withstand the fault by itself, adding a crowbar protection system or BESS will just rather be the addition of hardware and cost. However, in the case of symmetrical fault, even though it is rare in occurrence, the high current that arises is much more severe to damage the power converter demanding additional protection devices. Moreover, when a three-phase symmetrical fault occurs at the grid terminal, by implementing a protection system, it is possible to observe the massive impact that crowbar and BESS have on the system. Thus, this thesis mainly emphasized three-phase symmetrical fault than the asymmetrical fault.

CHAPTER SIX:

CONCLUSION AND RECOMMENDATION

6.1. Conclusion

Doubly Fed Induction Generator is primarily used in the modern wind power industry due to its high reliability, increased power efficiency, reduced mechanical stress on wind turbines, and low cost. Regardless, this machine is extremely vulnerable to grid faults. A severe grid terminal fault causes reduced stator and rotor flux, increased stator and rotor current, which may influence the converter, DC-link overvoltage, and torque fluctuation, which increases mechanical tension. During this situation, the grid code demands the generator to remain connected to the grid. As a result, this thesis analyzes the performance of the machine in compliance with the German grid code requirement. Moreover, two approaches have been adopted to resolve this issue, as well as to enhance FRT capabilities. The first one is the crowbar protection mechanism. When a grid failure occurs, causing a voltage drop, the crowbar protection system is enabled for a certain amount of time (100ms) from the fault event. At the same time, the RSC is blocked, and all current circulates in the crowbar. According to the simulation results in Chapter Five, the use of a crowbar reduces the stator and rotor currents, as well as the DC-link voltage, which was previously found to be higher, and lessens the electromagnetic fluctuation for a certain period. Thus, the employment of a crowbar protection system could prevent the DFIG from being disconnected from the grid during a fault by reducing the detrimental effects of the grid fault.

The second approach utilized to improve fault ride-through capability was to integrate the crowbar with BESS. This method was shown to improve the performance of the machine over the previous one. As shown in the simulation results, the DC-link voltage is almost stable, the stator and rotor currents are restricted to appropriate levels, and the reactive power is fed to the grid even though the crowbar is enabled and the speed is held at its nominal value. A Comparison among the existing capacitor bank, crowbar protection system, and crowbar integrated with BESS was made and as a consequence, it is concluded that using a crowbar protection system is crucial for protecting the power converters from high currents and for preventing the DFIG from being disconnected from the grid during a fault. However, using a crowbar integrated with BESS improves the performance of the machine and FRT capability over merely using the crowbar. Moreover, the performance of the machine under asymmetrical fault conditions has been evaluated. Under imbalance voltage conditions, high currents, as well as variable torque and speed were observed. However, since the fault was not severe enough to saturate the rotor converters, it was possible to regulate the currents using RSC control.

6.2. Recommendations

In this thesis work, the analysis of DFIG under symmetrical fault was conducted using crowbar systems and crowbar integrated with BESS, so future work should include:

- Analyze the performance of the machine by employing other protection devices for the enhancement of fault ride-through capability.
- Implement alternative control strategies for both RSC and GSC to compare control approaches.
- Examine the performance of the machine for low voltage ride-through using various country grid codes.

Research Fund Acknowledgment

This research project is funded by Adama Science and Technology University under the grant number ASTU/SM-R/174/20, Adama, Ethiopia.

REFERENCES

[1]. Devashish, A. Thakur, S. Panigrahi, and R. R. Behera, “A Review on Wind Energy Conversion System and Enabling Technology,” *2016 International Conference on Electrical Power and Energy Systems (ICEPES)*, 2016.

[2]. A. Ramkumar, “Performance Analysis of Double Fed Induction Generator Based Wind Energy Conversion System”, *Ph.D. Thesis submitted to Kalalingam University*, pp.23-29, 2014.

[3]. Mahmoud Rihan, O. Noureldeen, and B. Hasanin, "Behavior Improvement of Doubly-Fed Induction Generator W3

[4]. ind Farms during Grid Fault Occurrence," *in 17th International Middle East Power Systems Conference*, 2015.

[5]. Rabie Gohar and Servati. F, “Modeling a DFIG-Based Wind Turbine Focusing on DFIG and Aerodynamic Models,” *European Online Journal of Natural and Social Sciences*, vol. 3, no. 3, pp. 744-757, 2014.

[6]. Sherif. O, Zain Elabideen, A. A. Helal, and I. F. El-Arabawy, "Low Voltage Ride Through Capability Techniques for DFIG-Based Wind Turbines," *International Journal of Electrical, Computer, Energetic, Electronic and Communication Engineering*, vol. 10, no 7 pp. 910-918, 2016.

[7]. Z. Rafiee, M. Rafiee, and M. R. Aghamohammadi, "The Voltage Dip and Doubly-Fed Induction Generator with Considering Uncertainty Conditions," *Bulletin of Electrical Engineering and Informatics*, vol. 9, no. 1, pp. 30-38, 2020.

[8]. L. Widanagama, Arachchige, A. Rajapakse, and D. Muthumuni, “Implementation, Comparison and Application of an Average Simulation Model of a Wind Turbine Driven Doubly Fed Induction Generator,” *Energies*, vol. 10, no. 11, pp. 1726, 2017.

[9]. M. K. Döşoğlu, “Enhancement of Dynamic Modeling for LVRT Capability in DFIG-Based Wind Turbines,” *Iranian Journal of Science and Technology, Transactions of Electrical Engineering*, vol. 44, no. 4, pp. 1345–1356, 2020.

[10]. X. Zhang, X. Cao, W. Wang, and C. Yun, “Fault Ride-Through Study of Wind Turbines,” *Journal of Power and Energy Engineering*, vol. 01, no. 05, pp. 25–29, 2013.

[11]. A. F. Abdou, A. Abu-Siada, H. R. Pota, and N. K. Roy, “Improving Fault Ride Through Capability of DFIG During RSC Flashover Fault,” *IEEE International Conference on Smart Energy Grid Engineering (SEGE)*, 2013.

[12]. N. Amutha and B. Kalyan Kumar, “Improving Fault Ride-Through Capability of Wind Generation System Using DVR,” *International Journal of Electrical Power & Energy Systems,* vol. 46, pp. 326–333, 2013.

[13]. S. Tohidi and M. Behnam, “A Comprehensive Review of Low Voltage Ride Through of Doubly Fed Induction Wind Generators,” *Renewable and Sustainable Energy Reviews,* vol. 57, pp. 412–419, 2016.

[14]. Aoran Xu, Liu Zhang, Cailian Gu, and YiZhang, “Crowbar Circuit in Wind Power Grid Low Voltage Ride Through,” *China International Conference on Electricity Distribution (CICED),* 2014.

[15]. X. Wang, H. Zhang, and Q. Zhang, “The Strategy of Doubly-fed Induction Generator Low-Voltage Ride-Through Based an Integrated Protection Circuit,” *IOP Conference Series: Materials Science and Engineering,* vol. 486, pp. 012134, 2019.

[16]. C. M. Rahul Charles, V. Vinod, and A. Jacob, “Field Oriented Control of DFIG Based Wind Energy System Using Battery Energy Storage System,” *Procedia Technology,* vol. 24, pp. 1203–1210, 2016.

[17]. E. J. Novaes Menezes, A. M. Araújo, and N. S. Bouchonneau da Silva, “A Review on Wind Turbine Control and its Associated Methods,” *Journal of Cleaner Production,* vol. 174, pp. 945–953, 2018.

[18]. J. Thongam and M. Ouhrouche, “MPPT Control Methods in Wind Energy Conversion Systems”, *Renewable Energy Systems,* pp. 340-353, 2011.

[19]. I. Yazici and E. K. Yaylaci, “Improving Efficiency of the TSR-MPPT Method for Wind Energy Systems by using an Integral Sliding Mode Voltage Regulator”, *Energy Resources Technology,* vol. 140, no.5, 2018.

[20]. M. Nasiri, J. Milimonfared, and S.H. Fathi, “Modeling, Analysis, and Comparison of TSR and OTC Methods for MPPT and Power Smoothing in Permanent Magnet Synchronous Generator-Based Wind Turbines”, *Energy Conversion and Management,* pp. 892–900, 2014.

[21]. A. Raheem Youssef, Hossam H. H. Mousa, and Essam E. M. Mohamed, “Development of Self-adaptive P&O MPPT Algorithm for Wind Generation Systems with Concentrated Search Area,” *Renewable Energy,* vol. 154, pp. 875–893, 2020.

[22]. Yaxing Ren, L. Liuying, J. Brindley, and L. Jiang " Nonlinear PI Control for Variable Pitch Wind Turbine," *Control Engineering Practice,* vol. 50, pp. 84-94, 2016.

[23]. Seung Ho Hyun and Jialong Wang, "Pitch Angle Control and Wind Speed Prediction Method Using Inverse Input-Output Relation of a Wind Generation System," *Electrical Engineering and Technology*, vol. 8, no. 5, pp. 1040-1048, 2013.

[24]. H. Geng and G. Yang, "Output Power Control for Variable-Speed Variable-Pitch Wind Generation Systems," *IEEE Transactions on Energy Conversion*, vol. 25, no. 2, pp. 494-503, 2010.

[25]. A. V. A. Macêdo and W. S. Mota, "Wind Turbine Pitch Angle Control Using Fuzzy Logic," *Sixth IEEE/PES Transmission and Distribution: Latin America Conference and Exposition (T&D-LA)*, pp. 1-6, 2012.

[26]. Syed Zulqadar Hassan, H. Li, Tariq Kamal, and Gussan Mufti, "An Intelligent Pitch Angle Control of Wind Turbine," *ResearchGate*, 2017.

[27]. Dimple, Danduboyina, and Rao, Yerra Sreenivasa," Direct Power Control of Grid-Connected Double-Fed Induction Generator in Wind Energy Conversion System", *International Journal for Modern Trends in Science and Technology*, pp. 2455-3778, vol. 05, no.08, 2019.

[28]. Ayrir Wiam, Haddi Ali, "Direct Torque Control-Based Power Factor Control of a DFIG," *Energy Procedia*, vol. 162, pp. 296-305, 2019.

[29]. D V N Ananth and G V Nagesh Kumar, "Fault Ride-Through Enhancement using an Enhanced Field-Oriented Control Technique for Converters of Grid Connected DFIG and STATCOM for Different Types of Faults", *ISA Transaction*, vol. 62, pp. 2-18, 2015.

[30]. Amrane Fayssal, Azeddine Chaiba, Badreddine Babes, and Saad Mekhilef, "Design and Implementation of High-Performance Field Oriented Control for Grid-Connected Doubly Fed Induction Generator Via Hysteresis Rotor Current Controller," *Revue Roumaine des Sciences Techniques - Serie Électrotechnique et Énergétique*, vol. 61, no. 4, pp. 319–324, 2016.

[31]. Imane El. K, Mohammed.M, and Badre. B "Power Control Strategies in Wind Turbines using DFIG Generator: Field-oriented Control FOC and Sliding Mode Control," *'WSEAS Transactions on Systems archive*, vol. 18, 2019.

[32]. Djeriri Youcef, Meroufel Abdelkader, Massoum Ahmed, and Boudjema Zinelaabidine. "A Comparative Study between Field-oriented Control Strategy and Direct Power Control Strategy for DFIG," *Journal of Electrical Engineering*, vol. 14, pp. 169-178, 2014.

[33]. Shires A and Kourkoulis V, “Application of Circulation-Controlled Blades for Vertical Axis. Energies*,” Journal of Energies*, vol.6 (8), pp. 1-20, 2013.

[34]. Saad MM and Asmuin N, “Comparison of Horizontal Axis Wind Turbine and Vertical Axis Wind Turbine,” *IOSR Journal of Engineering*, pp. 27-30, 2014.

[35]. B. Pokharel, “Modelling, Control, and Analysis of a Doubly Fed Induction Generator Based Wind Turbine System with Voltage Regulation,” *Master's Thesis,* 2011.

[36]. S. Kumar Senapati, “Modelling and Simulation of a Grid-Connected Doubly Fed Induction Generator for Wind Energy Conversion System”, *Master's Thesis*, 2014.

[37]. Djamila Rekioua, “Wind Power Electric Systems: Modeling, Simulation, and Control”, *Springer*,2014.

[38]. M. Ragheb and A. M., “Wind Turbines Theory - The Betz Equation and Optimal Rotor Tip Speed Ratio,” *Fundamental and Advanced Topics in Wind Power,* 2011

[39]. Molina Marcelo and Mercado Pedro, “Modelling and Control Design of Pitch-Controlled Variable Speed Wind Turbines,” 2011.

[40]. Mansour Mohseni, “Enhanced Control of DFIG-Based Wind Power Plants to Comply with the International Grid Codes,” *Ph.D. Thesis*, 2011.

[41]. O. P. Mahela, N. Gupta, M. Khosravy and N. Patel, "Comprehensive Overview of Low Voltage Ride Through Methods of Grid Integrated Wind Generator," *IEEE Access,* vol. 7, pp. 99299-99326, 2019.

[42]. C. Sourkounis and Pavlos Tourou, “Grid Code Requirements for Wind Power Integration in Europe,” *ResearchGate*, pp. 1-9, 2013.

[43]. Aman Abdulla Tanvir, “Control System for Doubly Fed Induction Generator Based Wind Energy Conversion System,” *Master's Thesis*, 2016.

[44]. Gonzalo Abad, Jesús L, M. Rodríguez, L. Marroyo, and Grzegorz Iwanski “Doubly Fed Induction Machine: Modeling and Control for Wind Energy Generation Applications”, *Wiley-IEEE Press*,2011.

[45]. Dehong Xu, F. Blaabjerg, W.Chen and N.Zhu, “Advanced Control of Double Fed Induction Generator for Wind Power System”, *John Wiley & Sons Ltd, United Kingdom,* 2018.

[46]. Haitham Abu-Rub, Mariusz Malinowski, Kamal Al-Haddad, “Power Electronics for Renewable Energy Systems, Transportation and Industrial Applications”, *John Wiley & Sons Ltd, United Kingdom*, pp. 9-12, 2014.

[47]. BinWu, Yongqiang Lang, Navid Zargari, and Samir Kouro, “Power Conversion and Control of Two Energy System” *John Wiley & Sons, Inc., New Jersey,* 2011.

[48]. Ahmed. F. Zobba and R.Bansal, “Handbook of Renewable Energy Technology & Systems”, *World Scientific,* 2011.

[49]. Mossa, Mohmoud A, “Modeling, Analysis and Enhancement of the performance of a Wind Driven DFIG During Steady-State and Transient Conditions”, *Hamburg, Anchor Academic Publishing*, 2014.

[50]. M. C. Salles, A. P. Grilo, and J. R. Cardoso, “Doubly Fed Induction Generator and Conventional Synchronous Generator-Based Power Plants: Operation During Grid Fault,” *Renewable Energy and Power Quality Journal*, pp. 1318–1322, 2011.

[51]. Jackson John Justo, Francis Mwasilu, and JinWoo Jung, “Doubly-Fed Induction Generator-Based Wind Turbines: A Comprehensive Review of Fault Ride-Through Strategies”, *Renewable and Sustainable Energy Reviews Elsevier,* vol. 45, pp. 447-467, 2015.

[52]. Boyu Qin, Hengyi Li, Xingyue Zhou, Jing Li, and Wansong Liu, "Low-Voltage Ride-Through Techniques in DFIG-Based Wind Turbines: A Review," *Applied Sciences,* vol. 10, p. 2154, 2020.

[53]. M. El-Moursi, P. Kaliannan, R.A. Jerin A, and U. Subramaniam, “A Review on Fault Ride Through Solutions for Improving Transient Stability in DFIG Based Wind Turbines, *IET Renewable Power Generation,* vol.12, pp. 1786 – 1799, 2018.

[54]. Mohammad T. Z. Fard, “Modelling and Control of Wind Farms Integrated with Battery Energy Storage Systems”, *Ph.D. Thesis,* 2017.

[55]. S. O. Amrouche, D. Rekioua, and T. Rekioua, “Overview of Energy Storage in Renewable Energy Systems,” *3rd International Renewable and Sustainable Energy Conference (IRSEC),* 2015.

[56]. Luis. A. G. Gomez, A. P. Grilo, M. B. C. Salles, and A. J. Sguarezi Filho, “Combined Control of DFIG-Based Wind Turbine and Battery Energy Storage System for Frequency Response in Microgrids,” *Energies*, vol. 13, no. 4, p. 894, 2020.

[57]. Ayala. E, Simani. S, Pozo, N. and Muñoz. E “Indirect Speed Control Strategy for Maximum Power Point Tracking of the DFIG Wind Turbine System.,” *Revista Técnica Energía,* Vol. 17, Issue 2, pp. 92-101, 2021.

[58]. Ehsan Dadashnialehi, “Modeling and Control of Variable Speed Wind Turbines”, *Master’s Thesis*, 2012.

[59]. Amer Obaid Kareem "Performance Analysis of Doubly-Fed Induction Generator (DFIG)- Based Wind Turbine with Sensor and Sensorless Vector Control", *Ph.D. Thesis*, 2016.

[60]. Sasmita Behera, Bidyadhar Subudhi, and Bibhuti Bhusan Pati, "Design of PI Controller in Pitch Control of Wind Turbine: A Comparison of PSO and PS Algorithm," *International Journal of Renewable Energy Research (IJRER)*, vol. 6, no. 1, pp. 271–281, 2016.

[61]. U. Datta, "Battery Energy Storage System for Renewable Energy Integrated Power System Stability Enhancement", *Ph.D. Thesis*, 2020.

[62]. J. Manepalli, G. Ratnam, and S. Shaheem, "Modeling, and Dynamic Control of DFIG with Integrated Battery Energy Storage System Through LVRT Behavior," vol. 11, no. 6, pp. 21–28, 2016.

[63]. U. Datta, A. Kalam, and J. Shi, "The Relevance of Large-Scale Battery Energy Storage (BES) Application in Providing Primary Frequency Control with Increased Wind Energy Penetration," *Journal of Energy Storage*, vol. 23, pp. 9–18, 2019.

APPENDIXES

Appendix A

Table A- 1 ADAMA-II WT generator and turbine parameters

Parameters	**Values**
Rated Power	1.5MW
Number of Pole Pairs	2
Rated Stator Line-to-line Voltage	690V
Rotor voltage of open circuit	1650V
Rated Stator Current	1110A
Frequency	50HZ
Rated speed	1800rpm
Speed range	1000-2000rpm
Cut-in speed	3.5m/s
Rated speed	12m/s
Cut-out speed	25m/s
Cpmax.	0.4865
Lambda opt	8.1
Rated Slip	0.2
Transformation Ratio, u	0.42
Rated Mechanical Torque	8.5922 k N-m
Stator Winding Resistance, Rs	0.006243 Ω
Rotor Winding Resistance, R_r	0.011074 Ω
Stator Leakage Inductance, Lls	0.198822mH
Rotor Leakage Inductance, Llr	0.198822mH
Magnetizing Inductance, Lm	3.976mH
Inertia	67
Gearbox ratio	94.7
Blade length	37m
Rotor diameter	77m
DC-link voltage	1150v

PI Control Parameters

The PI control parameters are generated from the chapter 4 derived equation. The proportional-integral gains used to regulate the currents, speed, and dc-link voltage are shown in equations (4.17), (4.23), (4.31), (4.43), and (4.49). Appendix D contains MATLAB code that solves these equations. The PI controller values are thus acquired from the workspace in MATLAB when the code is executed. Table A-2 shows the values of the various PI controller parameters.

Table A- 2 PI control parameters

Parameters	**Values**
Kp_ir	2.2037
Kp_ig	0.3642
Kp_wn	5360
Ki_wn	21440
Kp_vdc	-1000
Ki_vdc	-300000
Kpg	0.0012
Kqg	-0.0012
Cbus	0.08
Rg	0.00002
Lg	0.000485
Cbus_BESS	0.015
Rg_BESS	0.0002
Lg_BESS	0.0006

Appendix B

Reference Frame Theory

The mathematical modeling of the three-phase machine appears to be very complex as the flux linkage, the induced voltage, and the currents vary significantly as the electrical circuit is in relative motion. Thus, space vector notation is crucial to derive models and obtain differential equations that concisely describe their behavior than using the classic three-phase representation.

The transformation of balanced three-phase quantity into balanced two-phase (α,β) quadrature quantity is called Clark transformation [43].

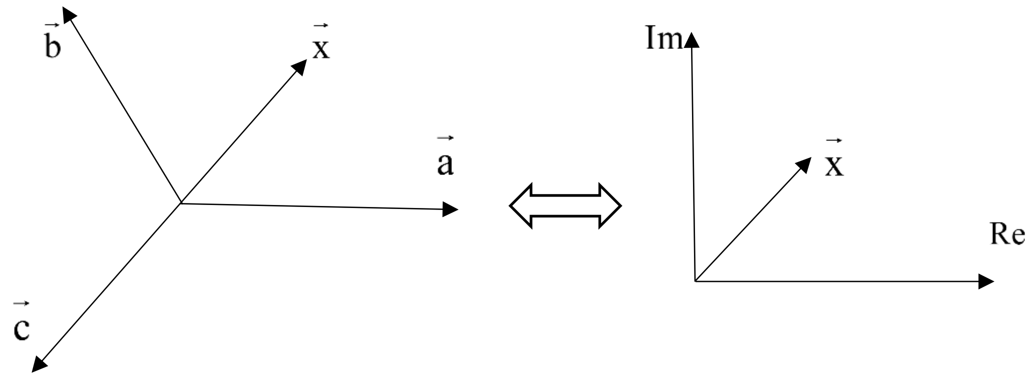

Figure B. 1 Space vector representation in stationary α, β axes[43]

The mathematical representation of this transformation is given as:

$$\vec{x} = x_\alpha + jx_\beta = \frac{2}{3}(x_a + ax_b + a^2 x_c) \quad \text{(B.1)}$$

Where,

$$a = e^{j(2\pi/3)}$$

From abc magnitude, the α,β components of the space vector can be calculated as follows:

$$x_\alpha = \text{Re}\{\vec{x}\} = \frac{2}{3}(x_a - \frac{1}{2}x_b - \frac{1}{2}x_c) \quad \text{(B.2)}$$

$$x_\beta = \text{Im}\{\vec{x}\} = \frac{1}{\sqrt{3}}(x_b - x_c) \quad \text{(B.3)}$$

The above expression can be written in the form of a matrix as follows

$$\begin{bmatrix} x_\alpha \\ x_\beta \end{bmatrix} = \frac{2}{3}\begin{pmatrix} 1 & -1/2 & -1/2 \\ 0 & \sqrt{3}/2 & -\sqrt{3}/2 \end{pmatrix} \cdot \begin{bmatrix} x_a \\ x_b \\ x_c \end{bmatrix} \tag{B.4}$$

Inverse Clark transformation

By taking $x_\alpha = x_a$ into consideration, it is possible to solve x_b and x_c in terms of x_α and x_β in which case the inverse Clark transformation can be obtained [43]. The inverse Clark transformation is given as:

$$\begin{bmatrix} x_a \\ x_b \\ x_c \end{bmatrix} = \begin{bmatrix} 1 & 0 \\ -1/2 & \sqrt{3}/2 \\ -1/2 & -\sqrt{3}/2 \end{bmatrix} \cdot \begin{bmatrix} x_\alpha \\ x_\beta \end{bmatrix} \tag{B.5}$$

Remark:

- The amplitude of x_α and x_β is equal to the amplitude of x_a, x_b and x_c due to 2/3 being the coefficient in the transformation.
- x_α and x_β are sinusoidal varying magnitudes.
- x_α and x_β are 90^0 phase-shifted.

Park Transformation

This transformation converts vectors in a balanced two-phase orthogonal stationary system into an orthogonal rotating reference frame [43].

The following expression is used for the transformation of $\alpha\beta$ coordinates to d-q coordinates

$$\vec{x} = \begin{bmatrix} x_d \\ x_q \end{bmatrix} = \begin{bmatrix} \cos\theta_m & -\sin\theta_m \\ \sin\theta_m & \cos\theta_m \end{bmatrix} \cdot \begin{bmatrix} x_\alpha \\ x_\beta \end{bmatrix} \tag{B.6}$$

Where, θ_m is the electrical angular position of the shaft and given as:

$$\theta_m = \int \omega_m dt \tag{B.7}$$

The inverse park transformation (from DQ to $\alpha\beta$) is expressed as:

$$\vec{x} = \begin{bmatrix} x_\alpha \\ x_\beta \end{bmatrix} = \begin{bmatrix} \cos\theta_m & \sin\theta_m \\ -\sin\theta_m & \cos\theta_m \end{bmatrix} \cdot \begin{bmatrix} x_d \\ x_q \end{bmatrix} \tag{B.8}$$

Appendix C

The Transfer Function Derivation for the Inner and Outer Control Loop

The transfer function for inner loop control for RSC

Inner loop control is used for controlling the d-axis and q-axis rotor currents and the transfer function of the rotor current of the d-q axis is derived as follow [57-58]:

$$i_{dr}^{error} = i_{dr}^{*} - i_{dr} \tag{C.1}$$

From equation 4.14 it is possible to obtain the actual rotor current

$$i_{dr} = (K_{pI} + \frac{K_{iI}}{s})\left(\frac{1}{R_r + \sigma s L_r}\right)\left(i_{dr}^{*} - i_{dr}\right) \tag{C.2}$$

Multiplying the gain parameters and the function by the actual and reference current

$$i_{dr} = (K_{pI} + \frac{K_{iI}}{s})\left(\frac{1}{R_r + \sigma s L_r}\right) i_{dr}^{*} - (K_{pI} + \frac{K_{iI}}{s})\left(\frac{1}{R_r + \sigma s L_r}\right) i_{dr} \tag{C.3}$$

Rewriting the above equation in a simpler form

$$i_{dr}\left[1 + (K_{pI} + \frac{K_{iI}}{s})\left(\frac{1}{R_r + \sigma s L_r}\right)\right] = (K_{pI} + \frac{K_{iI}}{s})\left(\frac{1}{R_r + \sigma s L_r}\right) i_{dr}^{*} \tag{C.4}$$

The transfer function, at last, is obtained by dividing the actual rotor current to the reference rotor current

$$\frac{i_{dr}}{i_{dr}^{*}} = \left(\frac{sK_{pI} + K_{iI}}{s\left(R_r + \sigma s L_r\right)}\right) \cdot \left(\frac{s\left(R_r + \sigma s L_r\right)}{s^2 \sigma L_r + s(R_r + K_{pI}) + K_{iI}}\right) \tag{C.5}$$

Finally, we obtain

$$\frac{i_{dr}}{i_{dr}^{*}} = \frac{i_{qr}}{i_{qr}^{*}}\left(\frac{sK_{pI} + K_{iI}}{s^2 + \frac{s(R_r + K_{pI})}{\sigma L_r} + \frac{K_{iI}}{\sigma L_r}}\right) \tag{C.6}$$

The transfer function of both the direct and quadrature component of the rotor current is the same.

Outer loop control transfer function

Similarly, the transfer function for the outer loop meaning transfer function of the speed is derived as:

From equation 4.19 it is possible to obtain the transfer function

$$\frac{Js}{p}\frac{d}{dt}\omega_r = (T_m - T_e) = K_{p\omega r} + \frac{K_{i\omega r}}{s}(\omega_r^* - \omega_r) \tag{C.7}$$

$$\omega_{dr}^{error} = \omega_{dr}^* - \omega_{dr} \tag{C.8}$$

$$\omega_m = (K_{p\omega_m} + \frac{K_{i\omega_m}}{s})\left(\frac{p}{Js}\right)\left(\omega_m^* - \omega_m\right)$$

Multiplying the gain parameters by the actual and reference speed

$$\omega_m = \left((K_{p\omega_m} + \frac{K_{i\omega_m}}{s})\left(\frac{p}{Js}\right)\right)\omega_m^* - \left((K_{p\omega_m} + \frac{K_{i\omega_m}}{s})\left(\frac{p}{Js}\right)\right)\omega_m \tag{C.9}$$

Adding the two actual speed we get

$$\omega_m\left[1 + \frac{(sK_{p\omega_m} + K_{i\omega_m})p}{sJs}\right] = \left[\frac{(sK_{p\omega_m} + K_{i\omega_m})p}{sJs}\right]\omega_m^* \tag{C.10}$$

Dividing the actual speed with the reference speed we obtain the transfer function.

$$\frac{\omega_m}{\omega_m^*} = \left[\frac{(sK_{p\omega_m} + K_{i\omega_m})p}{sJs}\right]\cdot\left[\frac{sJs}{s^2J + psK_{p\omega_m} + pK_{i\omega_m}}\right] \tag{C.11}$$

Rewriting the above equation in a simple manner the final equation is obtained.

$$\frac{\omega_m}{\omega_m^*} = \left[\frac{sK_{p\omega_m} + K_{i\omega_m}}{(J/p)s^2 + sK_{p\omega_m} + K_{i\omega_m}}\right] \tag{C.12}$$

The derivation of the inner and out loop control transfer function for GSC is similar to that of the RSC.

Appendix D

MATLAB Code

The MATLAB code, crucial to run the entire model, is displayed below

```
close all
clear all
clc

f = 50;                          %%stator frequency in (HZ)
Ps = 1.5e6;                      %%Rated stator power(w)
n= 1500;                         %%Rated rotational speed (rev/min)
Vs = 690;                        %%Rated stator voltage(v)
Is = 1110;                       %%Rated stator current (A)
Tem = 8592;                      %%Rated torque (N.m)
p=2;                             %%Pole pair
u = 0.42;                        %%Stator/rotor turns ratio
Vr = 1650;                       %%Rated rotor voltage
smax = 0.2;                      %%Maximum slip
Vr_stator =(Vr*smax) *u;         %%Rated rotor voltage referred to stator(v)
Rs = 0.006243;                   %%Stator resistance (ohm)
Lsi = 0.198822e-3;               %%Leakage inductance (stator and rotor) (H)
Lm= 3.976e-3;                    %%Magnetizing inductance (H)
Rr= 0.011074;                    %%Rotor resistance refers to the stator(ohm)
Ls= Lm + Lsi;                    %%Stator inductance(H)
Lr= Lm + Lsi;                    %%Rotor inductance(H)
Vbus_ref = 1150;                 %%Dc de bus voltage
Fs= Vs*sqrt(2/3)/(2*pi*f);       %%Stator flux(aprox.) (wb)

J=67;                            %%inertia
D= 1e-3;                         %%Damping
fsw = 4e3;                       %%Switching frequency (HZ)
Ts = 1/fsw/50;                   %%sample time(s)

%Three blade wind turbine model
```

```
N=94.7;                          %%Gearbox ratio
R =37;                           %%Length of the blade
ro=1.225;                        %%Air density

%Cp and Ct curve

beta=0;                          %%pitch angle
cont=1;
  for lambda=0.1:0.01:14
      lambdai(cont)=(1./((1./(lambda+0.08.*beta)-(0.035./(beta^3+1)))));
      Cp(cont)=0.5176.*(116./lambdai(cont)-0.4.*beta-5).*(exp(-
21./lambdai(cont)))+0.0068.*lambdai(cont);
      Ct(cont)=Cp(cont)/lambda;
      cont=cont+1;
  end
  tab_lambda=(0.1:0.01:14);

  %Kopt for MPPT

  Cp_max = 0.46;
  lambda_opt=8.1;
  Kopt = ((0.5*ro*pi*(R^5)*Cp_max)/(lambda_opt^3));
  figure(1)
  plot(tab_lambda,Cp,'linewidth',1.5)
  xlabel('lambda','fontsize',12)
  ylabel('Cp','fontsize',12)

 %Power curve in the function of wind speed

  P = 1.0e+06*[0,0,0.021,0.0849,0.1973,0.3638,0.5949,0.9008,1.2400....
    ,1.3990,1.48900,1.4999,1.50000,1.50000,1.50000,1.50000,1.50000,1. 50000...
    1.50000,1.50000,1.50000,1.5000,1.5000,1.5000,1.5000,0,0,0];

 V = [1.0000,2.0000,3.0000,4.0000,5.0000,6.0000,7.0000,8.0000...
    9.0000,10.0000,11.0000,12.0000,13.0000,14.0000,15.0000,16.0000,17.0000...
```

```
18.0000,19.0000,20.0000,21.0000,22.0000,23.0000,24.0000,25.0000,26.0000,27.0000,28.
0000];
 figure (2)
 plot (V, P,'linewidth',1.5)
 grid
 xlabel ('Wind speed(m/s)','fontsize',12)
 ylabel ('Power (MW)','fontsize',12)

 %%%Rotor Side Converter
 %%PI regulator
 sigma = 1-Lm^2/(Ls*Lr);
 tau_i =(sigma*Lr)/Rr;
 tau_n = 0.05/4;
 wni = 100*(1/tau_i);
 wnn = 1/tau_n;
 kp_id = (2*wni*sigma*Lr)-Rr;
 kp_iq = kp_id;
 ki_id = (wni^2)*Lr*sigma;
 ki_iq = ki_id;
 kp_n = (2*wnn*J)/p;
 ki_n = ((wnn^2)*J)/p;

 %%%%Grid Side Converter
 Cbus=80e-3;                     %DC bus capacitance
 Rg=20e-6;                       %Grid side filter's resistance
 Lg=483e-6;                      %Grid side filter's indutance
 kpg=1/ (1.5*Vs*sqrt (2/3));
 kqg =-kpg;
 %PI regulators
 tau_ig = Lg/Rg;
 wnig = 60*2*pi;

 kp_idg = (2*wnig*Lg)-Rg;
 kp_iqg = kp_idg;
```

```
ki_idg = (wnig^2) *Lg;
ki_iqg = ki_idg;
kp_v =(2*wnig*Cbus);
ki_v = (wnig^2) *Cbus;
Rcrowbar= 0.011074;                %%Crowbar Resistance

 %Battery Energy Storage System
Cbus_bess = 15e-3;                 %% DC bus capacitance
Rg_bess = 20e-5;                   %% Grid side filter? resistance 1
Lg_bess = 600e-6;                  %% Grid side filter? inductance 1e-3
kp_v =(2*wnig*Cbus);
ki_v = (wnig^2) *Cbus;
Vdc_bat_ref= 1150;
```

Published with MATLAB® R2015a